

Skeletal Isomerization of Butane by Sulfated Zirconia Catalysts
– A Branched Field –

von
Diplom-Chemikerin
Barbara S. Klose
aus München

der Fakultät II – Mathematik und Naturwissenschaften –
der Technischen Universität Berlin
zur Erlangung des akademischen Grades
Doktorin der Naturwissenschaften
– Dr. rer. nat. –
vorgelegte und von dieser
genehmigte Dissertation

Promotionsausschuß:

Vorsitzender: Professor Dr. M. Lerch, TU Berlin
Berichter/Gutachter: Professor Dr. R. Schlögl, Fritz-Haber-Institut der MPG, Berlin
Berichter/Gutachter: Professor Dr. R. Schomäcker, TU Berlin

Tag der wissenschaftlichen Aussprache: 06. 12. 2005

Berlin 2005
D 83

Die vorliegende Arbeit wurde in der Zeit von Februar 2002 bis September 2005 in der Abteilung Anorganische Chemie am Fritz-Haber-Institut der Max-Planck-Gesellschaft in Berlin und in zwei Aufenthalten am N.D.-Zelinsky-Institut für Organische Chemie in Moskau angefertigt. Bei allen, die mich in dieser Zeit unterstützt und so zum Gelingen beigetragen haben, möchte ich mich herzlich bedanken.

Zunächst möchte ich den beiden Gutachtern dieser Arbeit danken, Professor Robert Schlögl für die interessante Themenstellung und seine Unterstützung durch hilfreiche Anmerkungen und Diskussionen – trotz mehrmaliger Umbauphasen fand ich in seiner Abteilung ideale Voraussetzungen für meine Arbeit –, und Professor Reinhard Schomäcker für seine freundliche Aufnahme in den Kreis seiner Reaktionstechnikörer und die Übernahme des Zweitgutachtens.

Professor Martin Lerch danke ich, daß er sich so schnell bereit erklärt hat, den Vorsitz des Promotionsausschusses zu übernehmen.

Mein besonderer Dank gilt auch Friederike Jentoft für die gute Zusammenarbeit, Motivation und Förderung durch ihre stete Diskussionsbereitschaft und konstruktive Kritik, die sorgfältige Anleitung zu wissenschaftlichem Arbeiten und ihre zahlreichen Anregungen weit über die Chemie hinaus.

Я хочу поблагодарить профессора Владимира Казанского за многочисленные интересные и полезные дискуссии, а также за предоставленную возможность выполнить ряд экспериментов в его лаборатории. Я признательна Ирине Субботиной, Наталье Соколовой, Александру Серых и Евгению Пидько за помощь в экспериментах. Им всем я обязана своим интересом к русскому языку, литературе и искусству России.

Herzlichen Dank an Jutta Kröhnert (praktische und ideelle Unterstützung), Gisela Lorenz (ausdauerndes Rühren bei der Probenimprägnierung, BET-Messungen sowie Hinweis auf die herrlichen Sonnen- und Mondauf- und -untergänge im 3. Stock des F-Gebäudes), Rolf Jentoft (TG/DSC-Experimente, Aufnahme und Analyse der Röntgenspektren, Reaktorplanung und ein immer offenes Ohr), Frank Girgsdies und Edith Kitzelmann (XRD-Messungen), Nadja Maksimova, Oleksandr Broshnik und Anja Hofmann (BET-Messungen), Annette Trunschke (zeitweilige und dabei angenehme Tischnachbarin, IR Kenntnisse), Bernd Kubias, Manfred Swoboda, Peter Tesky und Sven Hanisch (Reaktorplanung und Fertigung der Einzelteile), Georg Heyne, Peter Zilske (†), Heinz Junkes und Mike Wesemann (elektronische Temperatúrauslesung), die Bibliothekarinnen Uta Siebeky, Katrin Quetting und Maren Dissmann sowie an die „Spaß-AG“.

Auch Personen außerhalb der beiden benannten Einrichtungen waren mir durch ihre Bereitschaft zur fachlichen Diskussion eine große Hilfe. Von diesen möchte ich insbesondere Professor Johannes Lercher (TU München), Professor François Garin (ULP Strasbourg/CNRS), Cornelia Breitkopf (Universität Leipzig) und Alexander Hofmann (HU Berlin) herzlich danken.

Darüber hinaus danke ich meinen Mitdoktoranden für gemeinsame Unternehmungen am und außerhalb des Instituts, vor allen Guido Ketteler, Alexandra Szizybalski, Olga Kirilenko, Eva Rödel, Benjamin Kniep, Jens-Oliver Müller, Mark Willinger, Yevgeniy Temko, Stefan Knobl, Julia Wienold und Raimund Horn.

Den jetzigen und ehemaligen Mitgliedern der Arbeitsgruppe „Funktionale Charakterisierung“ (einst „Säure-Base-Katalyse“) einschließlich Professor Sophia Klokishner sowie allen anderen Mitarbeitern des Fritz-Haber-Institutes, die mir mit Rat und Tat zur Seite standen, danke ich für das angenehme Arbeitsklima und die schöne Zeit.

Unter meinen Freunden danke ich allen voran Simon Schubert für seine Liebe und die Verbesserung meiner Rechtschreibung und Opernkenntnisse. Meinen Geschwistern und insbesondere meinen Eltern, denen ich diese Arbeit widme, bin ich für die bedingungslose und unablässige Unterstützung von ganzem Herzen dankbar.

Meinen Eltern

vorgelegt von Barbara S. Klose

Kurzzusammenfassung

In dieser Arbeit wurde der Einfluß von Handhabe und Lagerung auf Struktur und *n*-Butan-Isomerisierungsaktivität von sulfatierten Zirconiumdioxidkatalysatoren untersucht (SZ sowie FeSZ und MnSZ mit je 0.5 und 2.0 Gew% Metallgehalt), welche mit einem kommerziellen Ausgangsmaterial präpariert worden waren (Calcinierung bei 823 oder 923 K). Darüber hinaus wurden Beweise für die oxidative Dehydrierung (ODH) als erstem Schritt in der Aktivierung von *n*-Butan geliefert, welche zur Bildung von Carbeniumionen als reaktiven Intermediaten führt.

Die Katalysatoren wurden charakterisiert durch ihre BET-Oberfläche, mittels Röntgenbeugung (XRD), Röntgenabsorptionsspektroskopie (XAS), Thermogravimetrie (TG) und dynamischer Wärmestrom-Differenz-Kalorimetrie (DSC) mit *on-line* Massenspektrometrie, des weiteren durch Fouriertransformations-Infrarotspektroskopie in Transmission (FTIR) und diffuser Reflexion (DRIFTS) durch Adsorption von Sonden oder *on-line* gaschromatographisch *in situ* am arbeitenden Katalysator. Die katalytischen Tests wurden bei 323–378 K (1 oder 5 Vol% *n*-Butan in N₂, Atmosphärendruck) nach Aktivierung bei 723–773 K in IR-Zellen oder in Festbettreaktoren durchgeführt. Zur Steigerung der Kapazität wurde ein Apparat entworfen, der drei simultane katalytische Reaktortests im Labormaßstab ermöglicht. Eine Wirbelschicht aus Sand diente raschem Aufheizen und Abkühlen, ein Micro-GC der schnellen Trennung und Quantifizierung von Edukt (*n*-Butan) und Produkt (Isobutan).

Es wurde gezeigt, daß SZ-Katalysatoren sensible Materialien sind, die strukturelle Veränderungen sowie einen Aktivitätsverlust erfahren, wenn sie mechanischem Streß wie Pressen oder Mahlen ausgesetzt sind, Behandlungen die üblicherweise zur Probenvorbereitung benutzt werden. Des weiteren wiesen die Katalysatoren Änderungen in Struktur und Aktivität mit der Lagerungsdauer (bis zu 9 Monaten) auf, wobei diese Vorgänge durch Sättigung mit Wasser und das Fehlen von Sauerstoff in der Atmosphäre beschleunigt werden. Lagerung von MnSZ in einem Laborschrank ist der Aufbewahrung in einer Glovebox vorzuziehen. Das Wissen über die Empfindlichkeit von SZ-Materialien ist eine wichtige Grundvoraussetzung zum Erstellen gültiger Struktur-Aktivitäts-Beziehungen.

Im Verlauf der *n*-Butan-Isomerisierung wird auf SZ-Katalysatoren Wasser gebildet. Während der Induktionsphase steigt die Isomerisierungsgeschwindigkeit linear mit der Menge an gebildetem Wasser an. Da die Carbeniumionenintermediate in der Induktionsperiode gebildet werden, deutet eine gleichzeitige Wasserbildung auf ODH als verantwortliche Reaktion hin. Bei hohen Temperaturen (573 K) ist Sulfat erwiesenermaßen das Oxidationsmittel in der Totaloxidation von *n*-Butan unter Bildung von CO₂, H₂O und H₂S. Bei tieferen Temperaturen (373 K) ist nach der Isomerisierung von *n*-Butan mit gleichzeitiger Wasserbildung eine Abnahme der Sulfatbanden zu beobachten (IR), was darauf hinweist, daß Sulfat auch in diesem Prozeß als Oxidationsmittel dient. In Gegenwart von Mn ist die Isomerisierungsgeschwindigkeit bei gleicher Wassermenge größer; die intrinsische Turnover-Frequenz pro Carbeniumion wird von 10⁻⁶ s⁻¹ in SZ auf 10⁻⁴ s⁻¹ erhöht. Bisher war man davon ausgegangen, daß Promotoren wie Fe und Mn die Initiierung der Reaktion erleichtern, hier konnte ein Effekt eines Promotors auf die eigentliche Isomerisierung gezeigt werden.

*Skeletal Isomerization of Butane by Sulfated Zirconia Catalysts
A Branched Field*

by Barbara S. Klose

Abstract

This thesis investigated the influence of handling and storage on the structure of sulfated zirconia catalysts (SZ as well as FeSZ and MnSZ containing 0.5 or 2.0 wt% metal each) prepared from a commercial precursor (calcination at 823 or 923 K) as well as their activity in *n*-butane isomerization. Proofs for oxidative dehydrogenation (ODH) as initial step in activation of *n*-butane leading to formation of a carbenium ion as reactive intermediate are presented.

The catalysts were characterized by BET surface area analysis, X-ray diffraction (XRD), X-ray absorption spectroscopy (XAS), thermogravimetric measurements (TG) combined with differential scanning calorimetry (DSC) and on-line mass spectrometry (MS), as well as Fourier transform infrared spectroscopy in transmission (FTIR) and diffuse reflectance (DRIFTS) by adsorption of probe molecules and combined with on-line gas chromatography (GC) *in situ* on the operating catalyst. Catalytic tests were performed at 323–378 K (1 or 5 vol% *n*-butane in N₂, atmospheric pressure) after activation at 723–773 K in IR cells or in fixed bed reactors. To enhance the capacity and allow simultaneous tests of catalytic performance, an apparatus enabling three parallel catalytic reactor tests on laboratory scale was designed, using a fluidized sand bed for rapid heating and cooling and a Micro-GC for fast separation and quantification of reactant (*n*-butane) and product (isobutane).

It could be shown that sulfated zirconia catalysts are sensitive materials that undergo structural changes combined with a loss in activity when subjected to mechanical stress like pressing or milling, treatments that are commonly used to prepare samples for different measurements. Furthermore, the catalysts undergo changes in structure and activity with time of storage (up to 9 months), whereby water saturation as well as the absence of oxygen in the atmosphere enhance their velocity. Keeping MnSZ in a laboratory cupboard turned out to be preferable to storage in a glovebox. The knowledge about the sensitivity of sulfated zirconia materials is a vital prerequisite for making valid structure–activity relationships.

It could be shown that during *n*-butane-isomerization water is formed on sulfated zirconia catalysts and that the rate during the induction period of rising conversion is linearly correlated to the amount of water. Since the carbenium ion intermediates are built up during the induction period, the simultaneous formation of water points towards ODH as the responsible reaction. Sulfate is proven to be the oxidizing agent in total oxidation of *n*-butane at high temperatures (573 K) under formation of CO₂, water and H₂S. After isomerization of *n*-butane at lower temperatures (373 K) with concomitant water formation, a decrease of the sulfate IR bands is observed, indicating sulfate to be the oxidizing agent also in this process. In the presence of manganese, the rate is higher for the same amount of water; the intrinsic turnover frequency per carbenium ion is increased from 10⁻⁶ s⁻¹ in SZ to 10⁻⁴ s⁻¹. So far it has been believed that promoters such as iron or manganese facilitate the reaction initiation; here an effect of a promoter on the isomerization itself is proven.

Table of Abbreviations

a	amorphous
α	absorptance / absorption factor
c	cubic, speed of light, concentration
cus	coordinatively unsaturated
Δ	difference
d	diameter, distance
d_{in}	inner diameter
d_{out}	outer diameter
DRIFT(S)	Diffuse Reflectance Infrared Fourier Transform (Spectroscopy)
DSC	Differential Scanning Calorimetry
ε	apparent crystallite size, decadic extinction coefficient
eq.	equivalent(s)
FeSZ	iron-promoted sulfated zirconia
FT	Fourier transform
FWHM	full width at half maximum
HTZ	high temperature cell (<i>Hochtemperaturzelle</i>)
IR	infrared
k	absorption coefficient
K	equilibrium constant, (form) factor
κ	Napierian extinction coefficient
l	length
L	crystallite thickness
λ	wavelength
lg	\log_{10}
ln	\log_e
m	monoclinic, mass
max	maximum
MFC	mass flow controller
MnSZ	manganese-promoted sulfated zirconia
MS	mass spectrometry
IN	set of natural numbers
ν	frequency

p	pressure
P	power
psi	pounds per square inch
PTFE	polytetrafluorethylene
ρ	reflectance / reflection factor
RDF	radial distribution function
s	scattering coefficient
SZ	sulfated zirconia
SZH	sulfate-doped hydrous zirconia
t	tetragonal
T	temperature
τ	transmittance / transmission factor
TG	thermogravimetry
TOS	time on stream
V_{mol}	molar volume
vol%	volume percent
vs.	versus
w	flow velocity
wt%	weight percent
Z	zirconia (ZrO_2)
ZH	hydrous zirconia

Table of Contents

1.	Introduction	1
2.	Literature Overview about Sulfated Zirconia-Based Catalysts	3
2.1	Structure of the Zirconia Bulk	3
2.2	Structure of Sulfate	4
2.3	Acidity and Acid Sites	5
2.4	Promoted Sulfated Zirconia	7
2.5	<i>n</i> -Alkane Isomerization Mechanisms	8
2.6	Deactivation	9
2.7	Strategy	10
3.	Synthesis and Characterization of Sulfated Zirconia-Based Catalysts	11
3.1	Synthesis of Zirconia and Sulfated Zirconia-Based Catalysts	11
3.2	Analysis of the Phase Composition in Zirconia-Based Catalysts by XRD	12
3.2.1	X-ray diffraction (XRD)	12
3.2.2	Sample Preparation and Data Analysis	14
3.3	Analysis of amount and thermal stability of the sulfate by TG-DSC	15
3.3.1	Motivation	15
3.3.2	Thermogravimetry (TG) and Differential Scanning Calorimetry (DSC)	15
3.3.3	Results	16
3.3.4	Discussion	18
3.3.5	Summary	21
3.4	Interpretation of the IR Spectra of SZ and Promoted SZ	21
3.4.1	Infrared Spectroscopy in Transmission and in Diffuse Reflectance	21
3.4.2	Results	23
3.4.3	Discussion	25
3.4.4	Summary	28
4.	Design of a Three-Channel Fixed Bed Reactor	30
4.1	Motivation	30
4.2	System Requirements	31
4.3	Design and Experimental Details	31
4.3.1	Reactors	31
4.3.2	Reactor Heating	32
4.3.3	Experimental Set-Up	33
4.3.4	Product Analysis	34
4.4	Test Results	35
4.4.1	Gas Distribution	35
4.4.2	Heating and Cooling	36
4.4.3	Gas Phase Analysis	37
4.5	Summary and Outlook	38

5.	Handling of Sulfated Zirconia-Based Catalysts.....	39
5.1	Influence of Mechanical Stress on Sulfated Zirconia-Based Catalysts.....	39
5.1.1	Motivation.....	39
5.1.2	Results.....	40
5.1.2.1	Structure.....	40
5.1.2.2	Surface Area.....	43
5.1.2.3	Catalytic Performance.....	44
5.1.2.4	DRIFT Spectroscopy and TG.....	45
5.1.3	Discussion.....	47
5.1.3.1	Structural Changes Induced by Pressing.....	47
5.1.3.2	Milling.....	47
5.1.4	Summary.....	49
5.2	Storage and Aging of Sulfated Zirconia-Based Catalysts.....	50
5.2.1	Motivation.....	50
5.2.2	Results.....	50
5.2.2.1	Color, Moisture, and Structural Changes upon Aging.....	50
5.2.2.2	Changes in Catalytic Performance with Aging Time.....	52
5.2.3	Discussion.....	54
5.2.4	Conclusions and Outlook.....	55
6.	Sites of Sulfated Zirconia-Based Catalysts.....	56
6.1	Quasi <i>in situ</i> <i>n</i> -butane isomerization and CO adsorption on FeSZ.....	56
6.1.1	Motivation.....	56
6.1.2	Results.....	56
6.1.3	Discussion.....	58
6.1.4	Summary.....	60
6.2	Adsorption of hydrogen and <i>n</i> -butane on SZ and Fe- or Mn-promoted SZ.....	60
6.2.1	Results.....	61
6.2.1.1	Catalyst characterization.....	61
6.2.1.2	Low temperature adsorption of hydrogen.....	62
6.2.1.3	Reaction with hydrogen at elevated temperatures.....	62
6.2.1.4	Adsorption of <i>n</i> -butane at room temperature.....	63
6.2.1.5	Interaction with <i>n</i> -butane at elevated temperatures.....	64
6.2.2	Discussion.....	66
6.2.2.1	Lewis and Brønsted acid strength.....	66
6.2.2.2	Interaction of SZ and MnSZ with hydrogen.....	68
6.2.2.3	Interaction of SZ and promoted SZ with <i>n</i> -butane.....	70
6.2.2.4	Effect of Promoters.....	72
6.2.3	Conclusions.....	73

7.	<i>n</i> -Butane Isomerization on Sulfated Zirconia-Based Catalysts.....	75
7.1	Introduction	75
7.2	Results	76
7.2.1	Activation in N ₂ and <i>n</i> -butane isomerization	76
7.2.2	Activation and regeneration of MnSZ in N ₂ and O ₂	78
7.3	Discussion	80
7.3.1	Estimation of water content after activation	80
7.3.2	Activation and catalytic performance	81
7.3.3	IR spectra during <i>n</i> -butane isomerization	82
7.3.4	Regeneration.....	87
7.4	Conclusions	88
8.	Conclusions and Outlook	90
8.1	Prerequisites for Successful Structure–Activity Correlations	90
8.2	Initial Step in Skeletal Isomerization of <i>n</i> -Butane	91
8.3	Outlook.....	94
9.	Experimental	96
9.1	Materials.....	96
9.2	Preparation	96
9.3	Calcination	97
9.4	BET Surface Analysis	97
9.5	Thermogravimetry (TG) and Differential Scanning Calorimetry (DSC).....	98
9.6	X-Ray Diffraction (XRD) and X-Ray Absorption Spectroscopy (XAS).....	98
9.7	Pressing and Milling.....	98
9.8	Infrared Spectroscopy in Transmission and in Diffuse Reflectance	98
9.9	Catalytic tests	100
10.	Literature	102

Curriculum Vitae

Publications

1. Introduction

About 85–90 % —and this number is increasing— of all chemical products are made in catalytic processes.¹ The term “catalysis” was coined 1835 by Jöns Jakob Berzelius in analogy to “analysis”.² A catalyst changes the kinetics of a thermodynamically possible reaction by opening a new reaction pathway with lower activation energy. Thus, the catalyst speeds up the chemical reaction so that it proceeds at lower temperature and pressure. Once initiated, the catalytic process is undergone repeatedly since the catalyst is restored in its original state in the end of the catalytic cycle. Because of experimental uncertainties, the number of product molecules formed per surface site on a heterogeneous catalyst has to exceed 100 to distinguish a catalytic from a stoichiometric reaction.³ Most substances that are called a catalyst are only a “precatalyst” (Präkatalysator), a precursor that transforms into the catalytically active species under certain activation treatment, which can also be exposure to the reaction conditions.

Without catalysis there would be no worldwide mobility, as catalysts are necessary for synthesis of fuels. A catalytic process which has caused much interest in petrochemistry since it was first reported in literature 43 years ago by Holm and Bailey⁴ is the skeletal isomerization of *n*-alkanes catalyzed by sulfated zirconia-based catalysts. Branched alkanes are used as fuel components that improve the combustion properties because of their high octane numbers. Isobutane, which has a research octane number of 100.4,⁵ is not added directly to gasoline but used for the production of alkylate or —after dehydrogenation— the synthesis of ethers like methyl *t*-butyl ether (MTBE). In the end of the 1970ies, Hino and Arata showed that sulfated zirconia catalyzes skeletal isomerization of *n*-butane already at room temperature.^{6,7} Under standard conditions (298 K), the reaction enthalpy, entropy, and Gibbs free energy for *n*-butane isomerization are as follows: $\Delta_r H^\circ = -7 \text{ kJ mol}^{-1}$, $\Delta_r S^\circ = 15 \text{ J K}^{-1} \text{ mol}^{-1}$, $\Delta_r G^\circ = -2.3 \text{ kJ mol}^{-1}$.⁸ Low temperatures are, thus, most desirable for this type of reaction, since the equilibrium is shifted towards the desired product (branched alkane). In the thermodynamic equilibrium, 45 % isobutane are present at 453 K, at 311 K even 75 % of butane is isomerized.⁹ Other catalysts for *n*-alkane isomerization are strong liquid acids, such as HF/SbF₅,⁵ which are corrosive and difficult to handle, and chlorided alumina or zeolites as solid acids that allow to profit from the easier separation of the product from the catalyst in heterogeneous catalysis and to avoid the use of hazardous mineral acids. Chlorided alumina was used already in 1941 for the first commercial *n*-butane isomerization unit in the United States.¹⁰ This catalyst is operated at quite low temperatures between 393 K and 453 K, but chloride is lost and has to be added constantly. The zeolite-based processes are

more environmentally friendly but require higher temperatures of 533 K. The technical catalyst based on sulfated zirconia is active at low temperatures (353 K) and contains Pt among several other promoters to increase the rate and avoid deactivation.

After more than 25 years of research, the mechanism of the industrially important skeletal isomerization on sulfated zirconia is still not understood in detail and no convincing structure–activity relationship has evolved. The aim of this thesis is to reveal influences of storage and handling on sulfated zirconia catalysts and to elucidate the mode of operation of these catalysts as well as the role of the promoters in the process of isomerization with help of catalytic tests and infrared spectroscopy. To increase the number of tests, a reactor system should be designed for advanced through-put.

The thesis is structured as follows: The fundamental knowledge on sulfated zirconia is summarized in Chapter 2 ending with the presentation of the work strategy. The synthesis of the catalysts and methods for their characterization are described in Chapter 3 presenting some first results about the amount and thermal stability of the sulfate (Chapter 3.3) and the infrared spectra of the activated catalysts (Chapter 3.4). In Chapter 4, the design and test results of a three-channel fixed bed reactor for parallel catalyst testing are presented. Chapter 5 deals with the handling of sulfated zirconia-based catalysts investigating their sensitivity towards mechanical stress and long-time storage under different conditions. In Chapter 6, infrared spectroscopy is used for probing the sites on sulfated zirconia-based catalysts by quasi *in situ* CO adsorption and observing the interactions of H₂ and the reactant, *n*-butane, with the catalysts. In Chapter 7, the processes during activation, reaction and deactivation are monitored *in situ* by infrared spectroscopy, and regeneration procedures are evaluated. The conclusions about the *n*-butane isomerization on sulfated zirconia are summarized in models for activation and the initiation of the catalytic cycle in Chapter 8.

2. Literature Overview about Sulfated Zirconia-Based Catalysts

Due to their catalytic power in alkane isomerization, catalysts based on sulfated zirconia (“SZ”) have been subjected to intensive research in the last 25 years. Numerous overviews have been written about the catalysts themselves as well as the catalyzed reactions.^{11–27}

2.1 Structure of the Zirconia Bulk

Zirconia appears in three polymorphs under atmospheric pressure: monoclinic, tetragonal, and cubic zirconia; at high pressures orthorhombic phases are formed.²⁸ The room temperature stable monoclinic α -phase ($m\text{-ZrO}_2$) is transformed into the tetragonal β -phase ($t\text{-ZrO}_2$) at 1373 K and into the cubic γ -phase ($c\text{-ZrO}_2$) at 2573 K.²⁹ In $t\text{-ZrO}_2$ as in $c\text{-ZrO}_2$ the coordination number of Zr is eight, while the O ions are fourfold coordinated. Due to lower symmetry in $m\text{-ZrO}_2$, Zr is only heptacoordinated, so that two kinds of O ions exist, which are either trigonal planar or tetrahedrally surrounded by Zr.

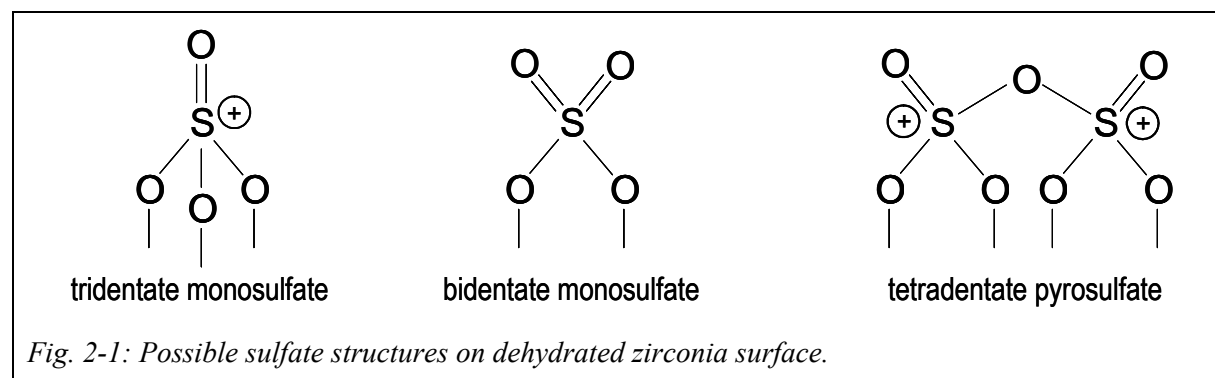
However, at room temperature zirconia has not necessarily to be monoclinic, other phases can be stabilized or exist as metastable phases. Ali et al.³⁰ investigated the zirconia phases during the calcination of amorphous zirconium hydroxide using *in situ* XRD. They found that the hydroxide remained amorphous up to 573 K, crystallized into a metastable $c\text{-ZrO}_2$ rich phase at 673 K that transformed into a $t\text{-ZrO}_2$ rich phase upon heating to 873 K, and finally underwent a transition to a $m\text{-ZrO}_2$ containing phase mixture at 1073 K; upon cooling to room temperature the $m\text{-ZrO}_2$ fraction increased. A rise of the final $m\text{-ZrO}_2$ amount with increasing calcination temperature has been generally observed.^{30,31} Garvie attributed the phase change $t\text{-ZrO}_2 \rightarrow m\text{-ZrO}_2$ during calcination to a crystallite size effect: Due to the higher surface energy in comparison with $m\text{-ZrO}_2$, formation of the tetragonal phase is favored until a critical crystallite size of ca. 30 nm is reached, at which the difference in the bulk energies compensates the difference in surface energies.^{32,33} Bouvier et al. used the size effect to prepare nanocrystalline zirconia that was tetragonal and contained less than 1 wt% $m\text{-ZrO}_2$; upon high pressure (8–30 GPa) $c\text{-ZrO}_2$ was obtained.³⁴ Explanations that have been proposed for the stabilization of $t\text{-ZrO}_2$ at low temperatures other than particle size are oxygen vacancies,³⁵ Zr vacancies close to OH^- ions that occupy O sites,³⁶ and pressure induced strain, which was assumed to be dependent on the degree of polycondensation.³⁷

Metastable phases are also formed in the presence of anionic or cationic impurities, e.g. $t\text{-ZrO}_2$ and $c\text{-ZrO}_2$ are stabilized by metal oxides that are incorporated into zirconia in form of a solid solution.^{38,39} Addition of sulfate to zirconia prior to calcination results in stabilization of the tetragonal phase.^{15,40} As for pure zirconia, the $m\text{-ZrO}_2$ fraction increases with

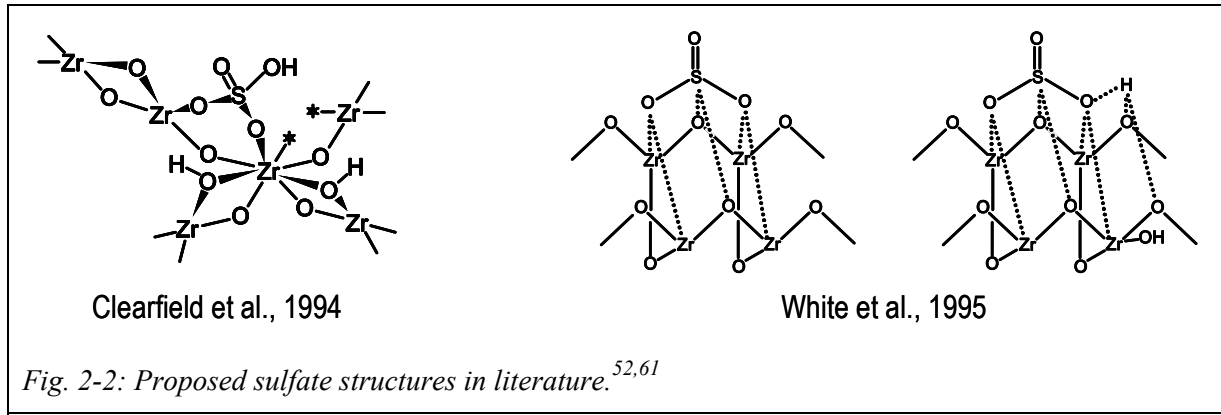
calcination temperature, but the decrease in surface area is decelerated and the $t\text{-ZrO}_2 \rightarrow m\text{-ZrO}_2$ phase transformation shifted to higher calcination temperatures.^{41,42} For many years it was believed that the tetragonal phase is necessary for the catalytic activity of sulfated zirconia in *n*-butane isomerization;⁴³ more recent work revealed that monoclinic and cubic SZ can also be active in this reaction.^{44–46}

2.2 Structure of Sulfate

By doping with sulfate, zirconia is transformed into a catalyst for skeletal isomerization. Activity is, thus, related to the structure of sulfate, which has been investigated intensively. Many models have been proposed explaining the strong acidity of the materials and assuming that the sulfate is located at the surface.^{15,27} In several published structure models, SO_4^{2-} is connected to zirconia via three oxygen bridges (tridentate),^{47,48} or via two oxygen bridges (bidentate) either chelating one Zr cation^{11,13,49} or bridging two Zr cations;^{50–52} a nearly C_{3v} symmetric monodentate species corresponding to adsorbed SO_3 that is transformed into adsorbed sulfuric acid upon water addition has also been proposed.⁵³ Pyrosulfate species, $\text{S}_2\text{O}_7^{2-}$, have been suggested to exist at higher sulfate coverage.^{48,54} If SZ is not totally dehydrated, hydrated states of sulfate will be present.⁵⁴ Hydroxyl groups might be attached to S or Zr,^{55–58} but OH bridging S and Zr has been proposed as well.^{59,60} In Fig. 2-1, the most prominent structures of dehydrated sulfate species are presented.



Clearfield et al. proposed a bidentate adsorbed bisulfate species in vicinity of two coordinatively unsaturated (cus) Zr sites, which are created by dehydration at 573 K and act as Lewis sites, to be responsible for superacidity (Fig. 2-2, left).⁵² White et al. suggested a penta-coordinated sulfur resulting from adsorption of SO_3 in a way that one oxygen atom remains double-bonded, the other two oxygen atoms are bridging two zirconium atoms each, and the sulfur is bridging two oxygen atoms from the zirconia lattice (Fig. 2-2, right).⁶¹



The occurrence of numerous models allows assuming a coexistence of different sulfate structures, which are flexible and strongly dependent on coverage and the degree of hydration. In 2004 DFT calculations on the surface structure of tetragonal SZ have been published by Hofmann and Sauer for different loadings of H₂O and SO₃ (or H₂SO₄); evaluation of the relative stability of the species—including H₂O, [H⁺,OH⁻], SO₃, [H⁺,HSO₄⁻], [2H⁺,SO₄²⁻], [H⁺,HS₂O₇⁻], and [2H⁺,S₂O₇²⁻]⁶²—by statistical thermodynamics for different temperatures and pressures showed that only mono- and pyrosulfates, but no more highly condensed sulfates may occur.⁶²

2.3 Acidity and Acid Sites

SZ was first believed to be superacidic because of its ability to isomerize saturated hydrocarbons,⁶ a reaction that in liquid phase is catalyzed by superacids like FSO₃H-SbF₅ or HF-SbF₅ as described by Olah et al.⁶³ Superacidity was mentioned for the first time by Hall and Conant in 1927.⁶⁴ According to Gillespie, superacids are defined as acids exceeding the strength of 100 % sulfuric acid and, thus, possessing a Hammett acidity function of $H_0 < -11.9$.⁶⁵ Indeed, for SZ $H_0 < -16.04$ was found, so that the material was claimed to be superacidic.⁷ However, Hammett's indicator technique was established for protic acids in liquid phase, assuming equilibrium between a Hammett base *B*—typically an aromatic indicator compound showing a color change upon protonation—and its conjugate acid BH^+ with the acid constant K_{BH^+} .⁶⁶ From the concentrations *c* of the different species, the acidity function H_0 is defined as:

$$H_0 = -\lg K_{BH^+} - \lg \frac{c_{BH^+}}{c_B} = pK_{BH^+} + \lg \frac{c_B}{c_{BH^+}} \quad (\text{Eq. 2-1})$$

Due to size and aromatic nature of the indicators, interactions between Hammett bases and solids acids might have other reasons than acidity. Accordingly, the validity of this method for acid strength determination of solid catalysts was questioned.¹⁵

At the surfaces of oxides, generally, two different types of acid sites may be present: Brønsted sites consisting of hydron-donating OH groups and Lewis sites created by cus metal ions (of zirconium or promoters in zirconia based materials). The acidity is then characterized by type, number, and strength of the acid sites. These quantities are determined by adsorption of probe molecules. To obtain information about the type of sites, the adsorbed species or changes of the adsorbent due to interaction with the adsorbate are monitored using techniques such as IR and NMR.⁶⁷ Amount and strength of the sites are accessible by temperature programmed desorption (TPD) experiments or by calorimetry combined with barometric-volumetric measurements, so that differential heats of adsorption may be determined. Typical probe molecules for acid sites are small molecules of different basic strength such as pyridine and CO.

Since first proposed as probe for solid acids in 1963,⁶⁸ pyridine has become one of the most commonly used probes, because Brønsted and Lewis sites can be determined simultaneously and be distinguished due to appearance of certain bands in the IR spectra. However, adsorption of pyridine results in a shift of the S=O stretching vibration, suggesting a change of the electronic structure of the sulfate.⁶⁹ Sikabwe et al. found a decreased thermal stability of sulfate in the presence of pyridine for promoted SZ, leading to oxidation indicated by SO₂ and CO₂ production during TPD.⁷⁰ Srinivasan et al. confirmed oxidation of pyridine during TPD on SZ, PtSZ, and FeMnSZ, claiming that the oxygen is supplied mostly by the sulfate but also by the metal oxide lattice.⁷¹ Morterra and Cerrato observed that only the Brønsted acidity was detected correctly, while the acidity of the Lewis sites was overestimated to a degree that depends on the surface concentration of sulfates.⁷²

Another widely used probe is CO. When adsorbed at room temperature only the strongly acidic Lewis sites are probed, while at low temperature (77 K) also weak interactions with Brønsted sites are detected. CO adsorption is usually combined with IR spectroscopy, by which the perturbation of the CO stretching vibration due to adsorption is monitored. The shift of the corresponding IR band from the gas phase position at 2143 cm⁻¹ is used as measure for acid strength. Brønsted sites are identified by a shift of surface OH groups. In spite of numerous investigations with CO adsorption, the activity of SZ at low temperatures and the role of the promoters could not be explained. The number of Lewis sites detected with CO is strongly dependent on the degree of hydration; it grows with increasing temperatures of activation or calcination.^{60,73} This is explainable by a water-induced transformation of Lewis into Brønsted sites, which has been observed before.⁵⁰ Brønsted acid sites⁷⁴ as well as Lewis acid sites⁷⁵ or a combination of both⁴¹ have been suggested to be responsible for activity.

Many groups could not detect superacidic sites on SZ; instead the acidity was found to be in the same range as that of strong zeolites. Kustov et al. concluded this from the IR shifts of the hydroxyl groups upon benzene adsorption that amounted to 200 cm^{-1} for SZ and were, thus, larger than the shifts of silanol groups ($120\text{--}140\text{ cm}^{-1}$) but smaller than those in HX ($240\text{--}260\text{ cm}^{-1}$), HY ($280\text{--}320\text{ cm}^{-1}$) or HZSM-5 (350 cm^{-1}).⁵⁵ Smaller OH shifts than in acidic zeolites were also observed after CO adsorption on SZ under saturation conditions.⁷⁶ Using acetonitrile adsorption monitored by $^1\text{H-NMR}$ and FTIR spectroscopy, Adeeva et al. detected a Brønsted acidity similar to that of HY but smaller than that in H-ZSM-5.⁷⁷ Based on their results from low temperature ($77\text{--}373\text{ K}$) benzene conversion on SZ, Ghenciu and Fărcașiu explained the activation of saturated alkanes on SZ by a high one-electron oxidation ability.⁷⁸ However, in the recent literature SZ is still called superacidic by part of the community.^{26,79,80}

2.4 Promoted Sulfated Zirconia

Main group metals such as Al^{81,82} and Ga,⁸³ transition metals like Pt,^{84–86} especially first row transition metals^{87,88} in cationic form act as promoters in skeletal isomerization reactions. Among them, iron and manganese were most intensely studied, in combination^{18,70,71,77,81,87,89–111} and as single promoters,^{14,88,94,97,101,108,112} whereby some authors could not find a promoting effect for manganese^{90,94,101} or a combination of both promoters.¹¹³

The increase of isomerization activity by addition of promoters to SZ was first explained by an increase in acidity of the catalyst, according to the idea of an acid-catalyzed reaction.^{89,93} This had to be dismissed, since the experiments that led to this conclusion were proved to be misleading,^{70,71,91} and several groups detected similar or even decreased acid strength upon addition of Pt, Ni, Fe or Mn.^{77,94,114} Instead, a redox function in the reaction initiation (see Chapter 2.5) has been attributed to the promoters,^{98,99,102,105} and, as evidence, a more active material after activation in oxidizing atmosphere than after activation in inert gas has been put forth by Wan et al.⁹⁹ and by Song and Kydd¹⁰⁵ for mixed FeMn-promoted catalysts. It could be shown that manganese and iron are at least in part incorporated into the zirconia lattice,³⁹ but it is not clear if and how they participate in the alkane activation and reaction.

2.5 *n*-Alkane Isomerization Mechanisms

The catalytic cycle of *n*-alkane isomerization on SZ is believed to proceed via adsorbed carbenium ions, as it was suggested by Nentitzescu and Cantuniani for wet aluminum chloride in 1933.¹¹⁵ Discussion is ongoing about two points, (i) the reaction initiation, i.e. the activation of the alkane leading to formation of the carbenium ion, and (ii) the isomerization itself. Fig. 2-3 presents the suggested steps for the reaction mechanism of *n*-butane isomerization.

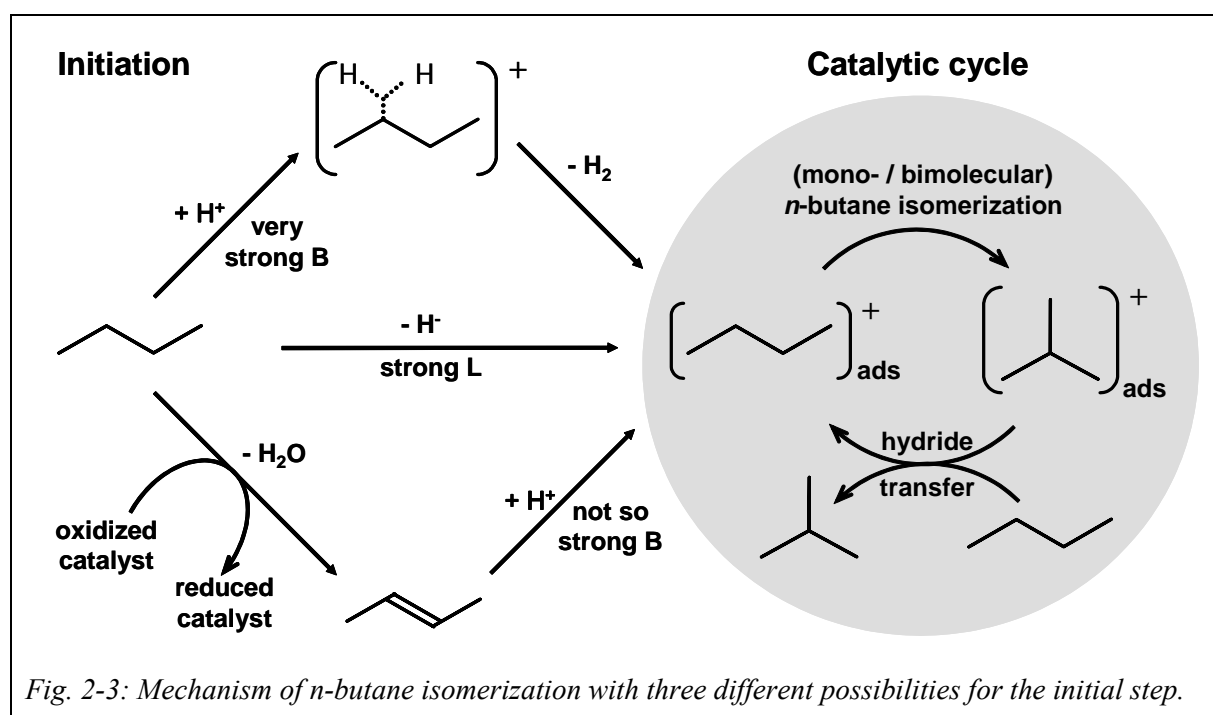


Fig. 2-3: Mechanism of *n*-butane isomerization with three different possibilities for the initial step.

So far, no universally acknowledged picture of the initial step for the reaction mechanism and the nature of the active sites has evolved. Three possibilities have been proposed for formation of the first carbenium ions: (i) protonation of the alkane by very strong Brønsted acid sites via an alkanium (carbonium) ion-like transition state,¹¹⁶ (ii) hydride abstraction by strong Lewis acid sites,¹¹⁷ or (iii) oxidative or non-oxidative dehydrogenation of the alkane with H_2O or H_2 as byproducts followed by protonation of the resulting alkene by moderately strong Brønsted acid sites.^{118,119} The first two mechanisms are in analogy with alkane isomerization in liquid superacids;^{63,120} the third one is supported by the fact that addition of butene to the feed resulted in higher *n*-butane conversion.^{98,121–123} Using alkene-purified feed on SZ, Hong et al. were able to detect H_2 evolution during *n*-butane isomerization,¹¹⁹ while Li et al. observed water formation *in situ* by infrared spectroscopy.¹²⁴ Since promoters were not found to increase the acidity, they are believed to further the oxidative dehydrogenation (ODH) pathway; as evidence served the presence of Fe^{2+} in the deactivated catalyst¹²⁵ and a

higher conversion after activation in air instead of He.⁹⁹ However, these different mechanisms and the involved sites are still controversially discussed.^{113,126,127}

The induction period that is observed for SZ-based catalysts until the maximum activity is reached has been attributed to the accumulation of carbenium ions.^{102,103} Their isomerization is performed in two steps, (i) the skeletal rearrangement to the isoproduct followed by (ii) a hydride transfer from incoming reactant molecules to the isomerized carbenium ions, so that the isoalkane is desorbed while new carbenium ions are created.¹²⁰ For the isomerization in step (i), two different pathways are discussed, a monomolecular (intramolecular) or bimolecular (intermolecular) mechanism. Since the monomolecular isomerization is proceeding via a protonated cyclopropane complex, it is believed to occur for C_nH_{2n+2} with $n \geq 5$, but has been questioned in case of *n*-butane because of the necessary formation of a primary carbenium ion, which is about 105 kJ mol^{-1} less stable than a secondary one.¹²⁰ Instead, a bimolecular mechanism, also known as “conjunct polymerization”,^{128,129} has been proposed involving a C_8 intermediate formed from the *n*-butane carbenium ion and butene, which is either present as impurity in the feed or formed via (oxidative) dehydrogenation of *n*-butane.¹¹⁹ Mass spectrometric investigations showed that reaction of double ^{13}C -labeled *n*-butane on SZ at 403 K led to a binomial distribution of 1–4 labeled atoms in the product supporting a bimolecular mechanism,¹³⁰ while at 523 K the monomolecular mechanism seemed to be favored.¹³¹ Suzuki and Okuhara proved an increasing contribution of the monomolecular mechanism with increasing temperature.¹³²

2.6 Deactivation

Usually, at higher conversions, deactivation of sulfated zirconia-based catalysts is observed. To sustain high activity, this phenomenon has to be prevented and was, thus, studied intensively. Several reasons have been proposed for the deactivation of SZ: (i) coke formation,^{19,41,118,133–144} which has been excluded by other authors,¹⁴⁵ (ii) sulfur loss as H_2S ,^{133,136} (iii) reduction of Zr^{4+} ,¹¹⁸ (iv) a $t\text{-ZrO}_2 \rightarrow m\text{-ZrO}_2$ phase transformation,^{136,146} or (v) poisoning by water.¹³⁴ For promoted SZ, deactivation has been explained by reduction of the promoter for Fe-containing SZ by Millet et al.¹²⁵ However, Yamamoto et al. reported that the valence of Fe was unaffected by *n*-butane.¹⁰⁸ Mn reacted upon exposure to butane,¹⁰⁸ but not in a way that could be correlated to the catalytic performance as evidenced by *in situ* XAS.^{147,148} This makes clear the importance of *in situ* studies. However, most investigations were carried out *ex situ* comparing the catalyst state before and after reaction, without monitoring it in the active state.

2.7 Strategy

As shown above, it is known that sulfated zirconia is able to isomerize small alkanes like *n*-butane at low temperatures via adsorbed carbenium ions, and that its activity can be further enhanced by addition of metal cationic promoters. However, the nature of the active sites is still controversially discussed, the reaction mechanism as well as the role of the promoters therein is not fully understood, and a structure–activity relationship is missing so far. Thus, in this thesis several starting points were chosen:

- (1) The mechanism of *n*-butane isomerization is still under debate, especially the reaction initiation and the isomerization itself. This thesis concentrates on the first point, the investigation of butane activation resulting in reactive carbenium ion intermediates. At low temperatures and *n*-butane partial pressures, sulfated zirconia catalysts undergo an induction period. Diffuse reflectance IR spectroscopy was used *in situ*, during batch and flow experiments, to investigate changes of the catalyst's functional groups during this period and to detect possible by-products, resulting from different initiation pathways. To understand the chemical behavior of the catalysts and the role of the promoters for the catalytic process, interactions of the reactant with the catalyst were studied at different temperatures in the absence and presence of manganese and iron as promoters. *In situ* catalytic tests were performed to investigate regeneration and the influence of different activation pretreatments.
- (2) SZ catalysts are essentially metastable, as they consist mainly of the tetragonal zirconia phase. In this thesis, the phase stabilizing effects of promoters and sulfate on the defective crystal structure were systematically investigated, the latter exposed to mechanical stress and hydrothermal conditions as well as to water- and oxygen-depleted atmosphere. Knowing the influence of these treatments on the solids allows in turn the generation of structurally different samples from the same parent material. Such catalysts are ideally suited to establish structure–activity relationships, which is the ultimate goal in understanding catalysis, since from these relations a rational catalyst design is possible. A correlation between solid state chemistry and reactivity is thus another focus of this thesis. These two points are closely linked. The structure of the catalyst determines the nature of the sites and their interactions with reactant and products, which via the kinetics can influence the mechanism of the reaction initiation and the resulting catalytic activity.

3. Synthesis and Characterization of Sulfated Zirconia-Based Catalysts

3.1 Synthesis of Zirconia and Sulfated Zirconia-Based Catalysts

The synthesized compounds used for this thesis were pure zirconia (“Z”) as reference compound, sulfated zirconia (“SZ”), and sulfated zirconia promoted with 0.5 or 2.0 wt% iron (“FeSZ”) or manganese (“MnSZ”). Zirconium hydroxide (“ZH”) and sulfated zirconium hydroxide (“SZH”) served as precursors (both *MEL Chemicals*). According to the manufacturer, SZH contains (NH₄)₂SO₄ equal to an SO₃ content of 5–6 wt% on the ZrO₂ content of 70–80 %. Before further processing, the material was dried for 21 h at 383 K and cooled to room temperature in a desiccator. The desired amount of iron or manganese was introduced via the “incipient wetness” method: Fe(III) or Mn(II) nitrates were dissolved in just as much water as necessary to wet the used amount of SZH, and the obtained solution was added dropwise under vigorous stirring to the powder. The solution concentration was chosen such that the final promoter content —estimated on the basis of TG measurements showing that 74 % of the precursor remained after thermal treatment as “sulfated zirconia”—was 0.5 or 2.0 wt% metal. The resulting powder (“FeSZH” or “MnSZH”) was dried at room temperature before calcination at 923 K. ZH and SZH were calcined at a lower temperature (823 K) to achieve a higher fraction of tetragonal phase in the product. The temperatures were selected according to recommendations in the literature; good performance is reported for promoted sulfated zirconia after calcination at 923 K and for unpromoted sulfated zirconia after calcination at 823 K.^{105,149} In Tab. 3-1, the colors of all samples before and after calcination are summarized as well as their denotation as used in this thesis; the promoter content in wt% appears as one-decimal number in front of the sample name.

Tab. 3-1: Colors and nomenclature of the samples synthesized for this thesis

uncalcined sample	color before calcination	calcined sample	color after calcination
ZH	white	Z	white
SZH	white	SZ	white
0.5FeSZH	light yellow	0.5FeSZ	light orange
2.0FeSZH	ochre	2.0FeSZ	orange
0.5MnSZH	pale pink / tan	0.5MnSZ	light bluish grey
2.0MnSZH	pale brown	2.0MnSZ	bluish grey

Calcination was performed in 20–25 g portions in a boat of 2 mm thick quartz with a volume of 17.1 ml (see Fig. 3-1). The sample bed temperature was monitored by a

thermocouple positioned in the middle of the bed. During heating to the desired calcination temperature, an exothermal reaction occurs leading to an overshoot of the bed temperature. The so called “glow” phenomenon was reported in 1812 by Berzelius for antimonates and antimonites,¹⁵⁰ and observed by Davy when he heated hydrated zirconia.¹⁵¹ The temperature release is dependent on the calcined amount as well as its packing.¹⁵⁰ Due to the small heat conductivity of the catalyst powders, temperatures above the desired calcination temperature may be reached during calcination of larger and more compactly packed amounts. The activity of the catalyst samples in *n*-butane isomerization increases with the size of the quartz boat.¹⁵² Thus, the largest boat was used to obtain most active samples. Fig. 3-2 shows the glow phenomenon during calcination; it is observed first for pure zirconia, then for sulfated zirconia, and finally for the promoted samples, except 0.5MnSZH. For all other samples, the maximum oven temperature of 823 K or 923 K is exceeded during the glow.

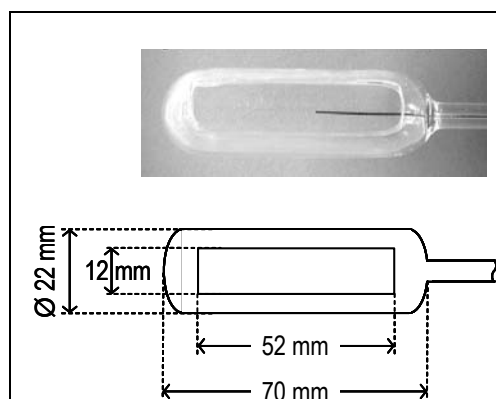


Fig. 3-1: Image and drawing of the 17.1 ml quartz boat for calcination.

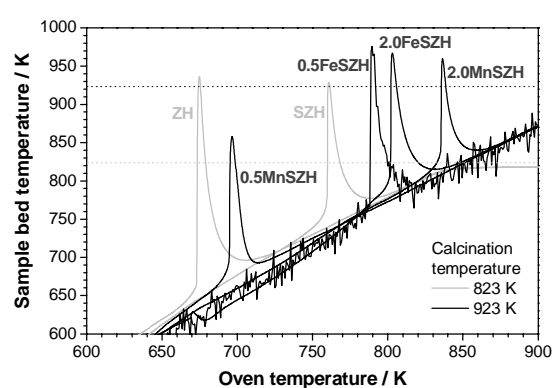


Fig. 3-2: Glow phenomenon during calcination (3 K/min, 200 ml/min synthetic air).

3.2 Analysis of the Phase Composition in Zirconia-Based Catalysts by XRD

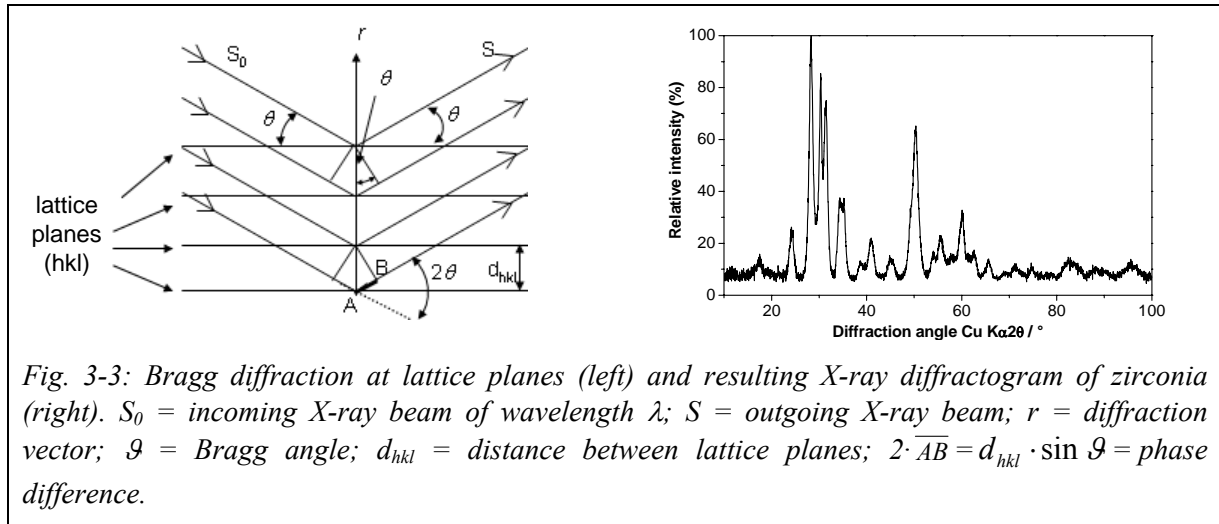
As described in Chapter 2.1, zirconia exists in different crystalline phases. To determine the phase composition of the catalyst powders, they were analyzed by X-ray diffraction (XRD) either in transmission or in reflection (Bragg–Brentano) geometry. In the following the principles of X-ray powder diffraction and the data analysis are described; results are presented and discussed in subsequent chapters.

3.2.1 X-ray diffraction (XRD)

The lattice planes in a crystal are designated as (*hkl*) and characterized by the Miller indices, *h*, *k*, and *l*, which are the reciprocals of the intersections between the lattice plane and

the three crystallographic axes that span the unit cell of the crystal.¹⁵³ The incident X-ray beam (S_0) and the lattice planes have to be oriented in a certain angle (ϑ) to allow diffraction (Fig. 3-3, left). Beams reflected at parallel lattice planes in the distance (d_{hkl}) interfere constructively and give an intensity maximum, which occurs as peak in the X-ray diffractogram, if their path difference, $2 \cdot \overline{AB}$, is an integer of the wavelength (λ). This condition is described by Bragg's law:¹⁵⁴

$$n \cdot \lambda = 2 \cdot d_{hkl} \cdot \sin \vartheta \quad \text{with } n \in \mathbb{N} \quad \text{Eq. 3-1}$$



The X-ray diffractogram (Fig. 3-3, right) is the pattern obtained by plotting the intensity of the diffraction lines versus the angle 2ϑ . In powder samples with randomly oriented crystallites, the same amount of crystallites has the right orientation for diffraction for all lattice planes. If, instead, a certain orientation is preferred the intensity of some reflections is lowered or increased. Information about the lattice parameters is available from the peak position. The sharpness of the diffraction lines is determined from their intensity together with their breadth (β), which is either described by the full width at half maximum (FWHM) or the integral breadth (β_i), i.e. the peak area divided by the peak height. Apart from instrumental broadening, β is increased with decreasing crystallite size and nonuniform strain due to lattice imperfections. If the broadening is caused by small crystallite size alone, the apparent crystallite size (ε) is related to the FWHM of one peak via the Scherrer equation, whereby ε is correlated to the volume weighted thickness of the crystallite (L) by a form factor ($1.0 > K > 0.89$), which is 0.94 for cubic crystallites:^{155,156}

$$FWHM = \frac{\lambda}{\varepsilon \cdot \cos \vartheta} = \frac{\lambda \cdot K}{L \cdot \cos \vartheta} \quad \text{Eq. 3-2}$$

A multi-peak method for determination of both size and strain is the so called Williamson–Hall analysis.¹⁵⁷ Here, the integral breadth is separated into particle size broadening and strain broadening. By plotting $\beta_i \cos \vartheta$ versus $\sin \vartheta$ the apparent crystallite size and the strain (ξ) are extracted from the intercept and the slope via Eq. 3-4:

$$\beta_i = \beta_{size} + \beta_{strain} = \frac{\lambda}{\varepsilon \cdot \cos \vartheta} + 2 \cdot \xi \cdot \tan \vartheta \quad \text{Eq. 3-3}$$

$$\beta_i \cdot \cos \vartheta = \frac{\lambda}{\varepsilon} + 2 \cdot \xi \cdot \sin \vartheta \quad \text{Eq. 3-4}$$

3.2.2 Sample Preparation and Data Analysis

Prior to the X-ray diffraction analysis, the loose powders were usually mixed 1:1 by weight with sieved α -Al₂O₃ (corundum) as standard. This was achieved by gently shaking to avoid mechanical stress (see Chapter 5.1). For measurements in transmission geometry a thin layer of powder was fixed between two foils (Mylar) with help of X-ray amorphous grease; for measurements in reflection geometry a cup of certain size was filled with the sample. The resulting diffractograms were normalized to the intensity of the 113 reflection of corundum at 43.3°. The phase composition of zirconia in the catalysts was then determined by fitting the diffractograms using PowderCell v2.4 by Kraus and Nolze.ⁱ First only the peaks of the standard were fitted with a Gaussian line profile to the structure of corundum (ICSD 31548)ⁱⁱ excluding the 2ϑ regions with many reflections of ZrO₂ (<15°, 26°–34°, 47°–52°, 58°–65°, 79°–87°) to obtain the zeroshift; then the lattice parameters and scaling factors for monoclinic (m-ZrO₂) and tetragonal zirconia (t-ZrO₂) were determined by fitting with a Lorentzian line profile to the structures of m-ZrO₂ (ICSD 18190) and t-ZrO₂ (ICSD 68589). The scaling factors give information about the ratio between m-ZrO₂ and t-ZrO₂. The mass absorption coefficients of m-ZrO₂ ($\mu_i = 1.2068$) and the matrix ($\mu_m = 0.7763$) were determined from a calibration for mechanical mixtures of pure m-ZrO₂ with α -Al₂O₃, by fitting the plot of the theoretical mass fraction of m-ZrO₂ (c_i^{theo}) versus experimental mass fraction determined by PowderCell (c_i^{exp}). The fraction of m-ZrO₂ in the samples was calculated using the equation obtained by the fit:

$$c_i^{theo} = \frac{c_i^{exp} \cdot \mu_i}{c_i^{exp} \cdot (\mu_i - \mu_m) + \mu_m} \quad \text{Eq. 3-5}$$

ⁱ W. Kraus, G. Nolze, Federal Institute for Materials Research and Testing, Rudower Chaussee 5, 12489 Berlin, Germany (http://users.omskreg.ru/~kolosov/bam/a_v/v_1/powder/e_cell.htm; accessed 06.07.2005).

ⁱⁱ Inorganic Crystal Structure Database (ICSD), maintained by the Fachinformationszentrum (FIZ) Karlsruhe (<http://icsd.fkf.mpg.de>; accessed 06.07.2005).

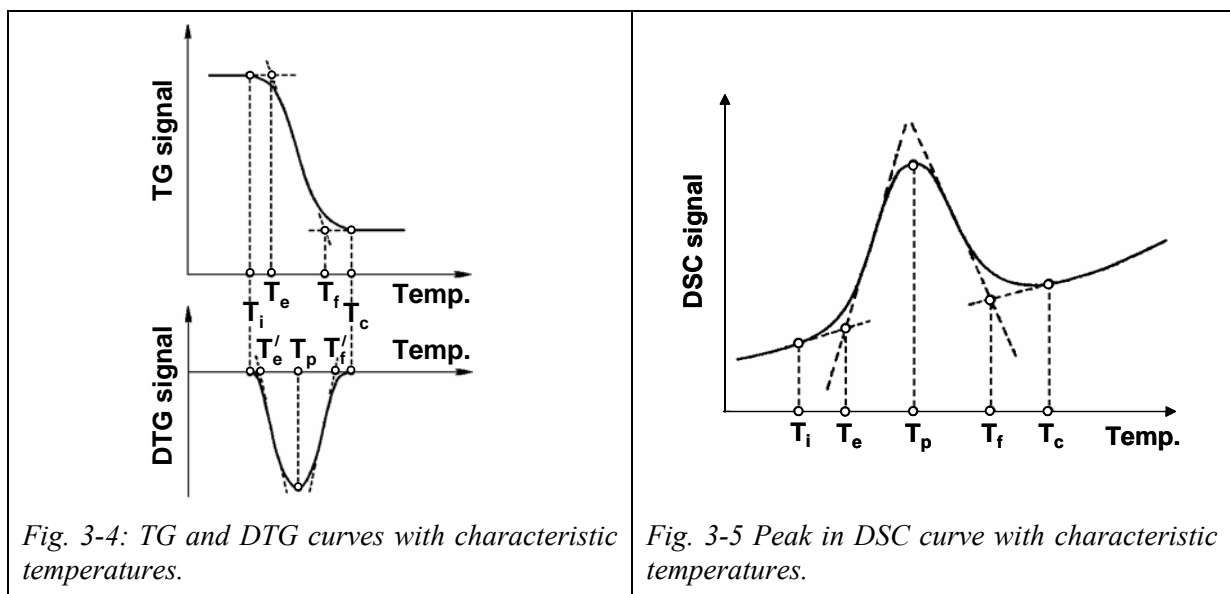
3.3 Analysis of amount and thermal stability of the sulfate by TG-DSC

3.3.1 Motivation

The sulfate content of hydrous sulfated zirconia, the SZ precursor, is 5–6 wt% SO_3 according to the producer. During calcination for 3 h at 723–923 K, the sulfate content is known to decrease with increasing calcination temperature.¹⁵⁸ To determine the actual amount of and the effect of the promoters on the sulfate in the crystalline oxides after calcination at 823 (SZ, 2.0MnSZ) or 923 K (Fe or Mn promoted SZ), experiments were performed on the catalysts in combination with differential scanning calorimetry. Before presenting the results, the principles of TG and DSC methods are summarized.

3.3.2 Thermogravimetry (TG) and Differential Scanning Calorimetry (DSC)

TG and DSC belong to the field of thermal analysis.¹⁵⁹ In TG, mass changes are measured with temperature or time. The measured quantity is the mass change with respect to the initial mass in %. The speed of mass changes is envisioned by the first derivative of the TG curve with time, the so called DTG curve. From these curves characteristic temperatures are determined: T_i and T_c are the temperatures of the first and the last visible mass change, T_e/T_e' and T_f/T_f' are the extrapolated start- and end-temperatures that are defined by the intersection of inflection point tangent and baseline, T_p is the temperature of the peak maximum (Fig. 3-4). Experiments are carried out either with constant heating rate, with stepwise temperature changes, or isothermal. To remove gaseous reaction products, the sample is purged with inert gas (Ar); analysis of the gas phase is achieved by online mass spectrometry (MS).



Modification of figures from Hemminger and Cammenga¹⁵⁹ pp. 93, 131

In DSC, the difference in heat flow to the sample and a reference is measured with temperature. If heat is generated or consumed by an exo- or endothermic reaction of the sample, the heat flow from the sample will be larger or smaller than the heat flow from the reference and the temperature difference between sample and reference (ΔT_{SR}) that is proportional to the heat flow (Φ_r), i.e. the amount of heat (q_r) per time generated by reaction, will deviate from zero.

$$\Phi_r = \frac{dq_r}{dt} = K \cdot \Delta T_{SR} \quad \text{Eq. 3-6}$$

A calibration, in which a known amount of heat is released in the sample, is necessary to determine the factor K and allow for calculation of the heat flow. The characteristic temperatures of reaction begin (T_i , extrapolated T_e) and end (T_c , extrapolated T_f) and of the peak maximum (T_p) are determined in the same way from the DSC curve as from the TG curve as shown in Fig. 3-5.

The temperatures of the first and the last visible deviation from the baseline, T_i and T_c , are difficult to identify. Thus, the extrapolated start- and end-temperatures (T_e and T_f) were used for calculation of the temperature intervals that are needed to determine a weight loss. Events (weight loss, endo- and exothermic processes) were characterized by T_p . For thermal analysis a three-step procedure was used, the samples were first heated to 1373 K at 10 K/min, kept isothermal for 30 min, and then cooled to 473 K at 10 K/min. During the measurements the samples were purged with Ar (20 ml/min) and the gas phase was analyzed by mass spectrometry (MS). The mass spectrometer was calibrated for O_2 so that the moles of O_2 could be calculated from the integral of mass 32 by multiplication with 93. At simultaneous occurrence of SO_2 and O_2 , first the amount of O_2 was obtained from the MS data, and then the amount of SO_2 was calculated from total weight loss minus the determined mass of O_2 .

3.3.3 Results

The TG profiles are characterized by three steps of weight loss: (i) An endothermic loss of 2.2–4.6 wt% at about 370 K, (ii) a nearly heat-neutral 3.9–4.6 wt% loss at about 1080 K, and (iii) a very small exothermic weight loss of only about 0.1–0.2 wt%, which occurs for SZ after the isothermal period in the cooling phase at 980 K (Fig. 3-6), for 2.0MnSZ already towards the end of the heating phase at 1200 K. 0.5MnSZ and 2.0FeSZ show a similar behavior, which is between that of SZ and 2.0MnSZ, since the third weight loss is detected at the beginning of the isothermal section. In Fig. 3-7 the time and temperature of the third weight loss are shown for promoted and unpromoted SZ.

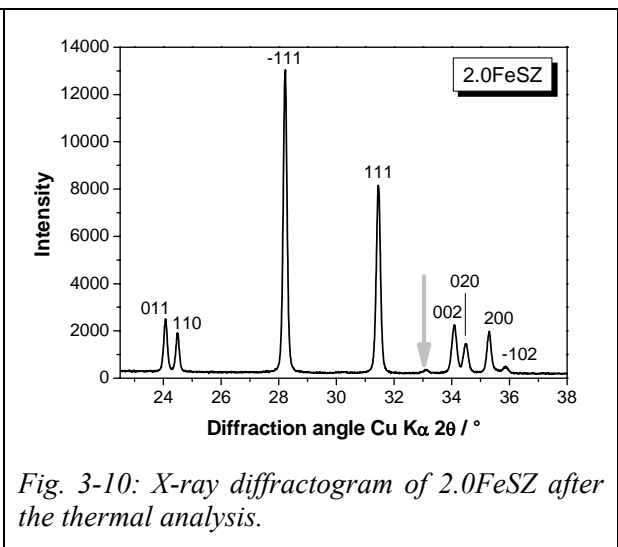
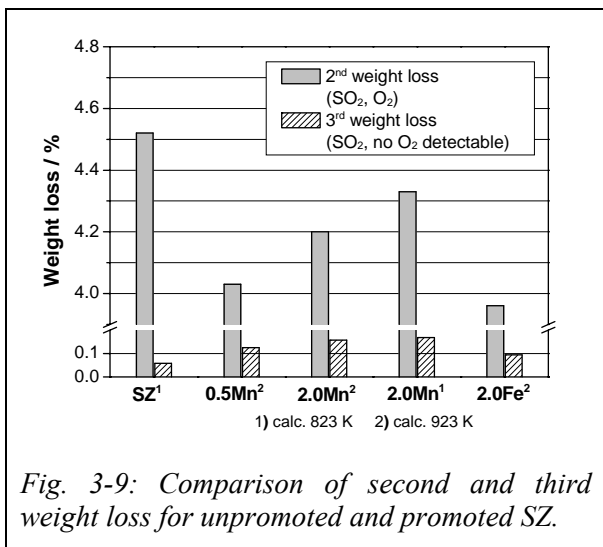
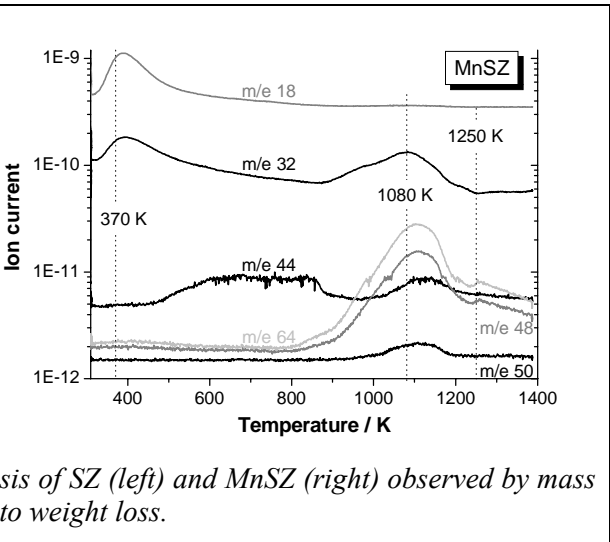
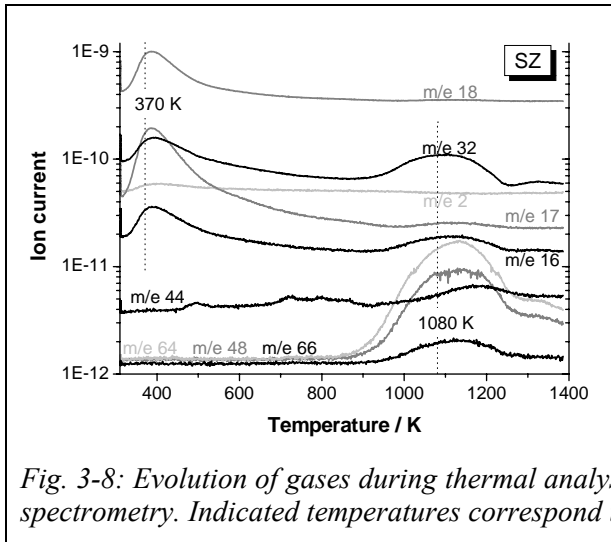
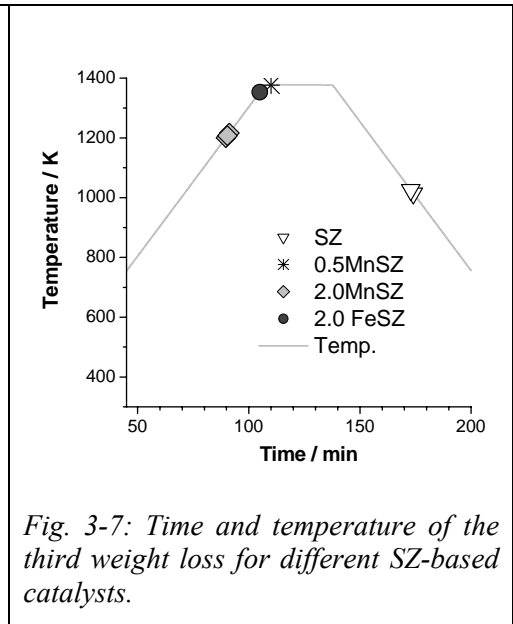
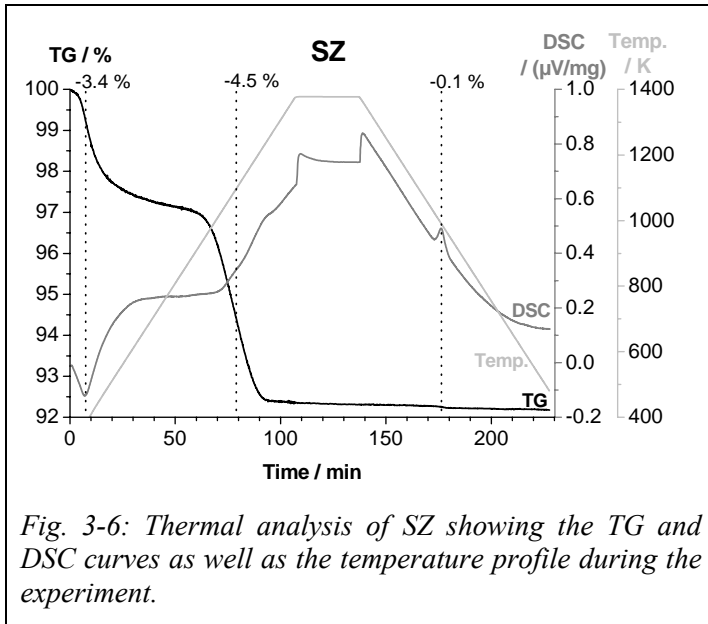


Fig. 3-6: Thermal analysis of SZ showing the TG and DSC curves as well as the temperature profile during the experiment.

Fig. 3-7: Time and temperature of the third weight loss for different SZ-based catalysts.

Fig. 3-8: Evolution of gases during thermal analysis of SZ (left) and MnSZ (right) observed by mass spectrometry. Indicated temperatures correspond to weight loss.

Fig. 3-9: Comparison of second and third weight loss for unpromoted and promoted SZ.

Fig. 3-10: X-ray diffractogram of 2.0FeSZ after the thermal analysis.

Selected masses measured during the TG experiment are shown in Fig. 3-8. During the first weight loss water evolves (m/e 18— H_2O^+ , m/e 17— OH^+ , m/e 16— O^+). The detection of oxygen (m/e 32, 34— O_2^+ , m/e 16, 18— O^+) and hydrogen (m/e 2— H_2^+) is an artifact, water is decomposed in the mass spectrometer. Between the first and the second weight loss CO_2 (m/e 44) is desorbed from the catalysts. During the second weight loss SO_2 (m/e 64, 66— SO_2^+ , m/e 48, 50— SO^+) and O_2 (m/e 32, 16) evolve; the ratio of SO_2 and O_2 is ca. 2:1. The third weight loss coincides with the detection of SO_2 in the off-gas (no O_2). The second weight loss is larger for SZ and MnSZ calcined at 823 K than for promoted samples calcined at 100 K higher temperature; the third weight loss is about twice as large for promoted samples as for unpromoted SZ (Fig. 3-9). All samples are monoclinic after the thermal treatment. In the diffractogram of 2.0FeSZ an additional peak is visible at an angle of 33.1° (Fig. 3-10).

3.3.4 Discussion

The first weight loss is due to dehydration, which is confirmed by the temperature, the water evolution, and the fact that the process consumes heat. Evolution of water has been observed before, for uncalcined SZ at 373–737 K and for calcined SZ at 363–373 K.^{40,137} The different catalysts were stored in a laboratory cupboard after calcination; their water content as determined from the first weight loss varies without any trend.

The second weight loss is observed at temperatures above the calcination temperature, which was 823 K or 923 K, and corresponds to a loss of SO_2 and O_2 . It is dependent on the sulfate content, since it is larger for samples that have been calcined at the lower temperature, which —according to Corma et al.¹⁵⁸— contain a higher amount of sulfate. Evolution of sulfur oxides has been observed above 723 K for uncalcined SZ,^{40,160} for calcined SZ the maximum of SO_2 evolution has been found at 1073 K.¹³⁷ In the mass spectrum of SO_2 the peak at m/e 64 is the most intense one; relative to this, the intensity at m/e 48 should be 50 %. For all measured catalysts the integral intensity at m/e 48 is 54–57 % of that at m/e 64. The real value is probably even smaller and near the expected 50 %, taking into account the artifact in the curves at an ion current of about 9 pA (see Fig. 3-8), which is caused by switching the sensitivity range of the instrument. The observed SO is thus considered as a fragment of SO_2 . The contribution of the S^+ fragment of SO_2 (10 % of the SO_2^+ peak) to the signal at m/e 32 is negligible and the assignment of this peak to O_2 correct. The simultaneous detection of O_2 and SO_2 hints a release of sulfur as SO_3 that decomposes into SO_2 and O_2 . This has been proposed by Srinivasan et al., who considered direct liberation of O_2 from the solid to be unlikely.⁴⁰ At higher temperatures SO_3 is instable; only below 673–873 K

oxidation of SO_2 to SO_3 is observed.²⁹ The decomposition of SO_3 is endothermic; at standard conditions and 298.15 K the enthalpy is only 99.0 kJ/mol.¹⁶¹ If all sulfur oxides are SO_2 , as assumed, the ratio of SO_2 and O_2 (2 eq. SO_2 and 1 eq. O_2) is the same as in SO_3 . Thermodynamics and the molar ratio of the two components are in favor of the assumption that sulfur is released as SO_3 .

Srinivasan et al.⁴⁰ did observe two regions of weight loss when they heated the samples to 1073 K, the first attributed to loss of water and the second to evolution of sulfur. In their experiments a larger amount of O_2 was detected during the early period of SO_2 liberation than during the later periods. This is also observed here from the peak shapes in Fig. 3-8. For mass 32 the maximum occurs earlier than for mass 64. Evolution of CO_2 has a maximum shortly after that of SO_2 . It is rather unlikely for CO_2 to be still adsorbed at temperatures of about 1000 K. Instead CO_2 could evolve from carbonates. However, SZ materials are very acidic and do not form stable carbonates as shown by the IR spectra of the calcined catalysts after activation at 723–773 K (see Chapter 3.4). Thus, at higher temperatures oxygen from the decomposed sulfur oxides might react with carbon on the samples to give CO_2 , which is then detected instead of O_2 . The order of the maximum evolution of gases (O_2 – SO_2 – CO_2) is in favor of this hypothesis.

The third weight loss is accompanied by an exothermic event. Since the initially tetragonal samples are all monoclinic after the TG experiment, the exotherm is ascribed to a phase change, the transition of t- ZrO_2 to m- ZrO_2 . Addition of sulfate is known to stabilize the metastable tetragonal phase of zirconia during calcination.^{160,15} Li et al. observed a reduction of the tetragonal phase combined with the appearance of a monoclinic phase in SZ, if part of the sulfate was removed by washing with water.¹⁶² During the phase change, sulfur is released, but in a less oxidized state than at the previous weight loss, since no O_2 is detected. Manganese and iron might segregate and the restrained oxygen might be consumed healing up the defects in the zirconia bulk. This is in line with the higher weight loss for samples with increased manganese content. Manganese is incorporated into the zirconia lattice and generating oxygen defects due to its lower valence compared to Zr^{4+} . The smaller effect for iron is associated to incomplete incorporation. For the promoted SZ samples, the decomposition temperatures of sulfate are above 1200 K; for SZ the event occurs at 980 K but after holding the sample for 30 min at 1373 K. Thus, a minority of the total sulfate is thermally very stable and, obviously, more so in absence of the promoters. The crystallite size, which is determined via a Williamson–Hall plot from the line width in the diffractograms of the monoclinic samples (e.g. Fig. 3-10) assuming an instrumental

broadening of 0.010, amounts to 800 nm, while the strain is quasi zero. Before the experiment the crystallite size was only 20 nm in the then tetragonal catalysts. Since sulfate is known to stabilize high surface areas during calcination,^{41,42} the sintering does probably start as soon as sulfate is decomposed.

The additional peak in the diffractogram of FeSZ after the TG experiment results from iron oxide, Fe₂O₃, confirming the segregation of iron. The overlap is best for cubic Fe₂O₃, which has a reflection at 32.9772°, or trigonal Fe₂O₃, hematite, which has a reflection at 33.1531°. ⁱⁱⁱ The most intense peak in the diffractogram of trigonal Fe₂O₃ is located at 24.1384° and thus overlapping with those of monoclinic zirconia at 24.07° and 24.46°. Since no intensity is found in the diffractogram at 18.8659° and 23.1562°, where the most intense reflections of cubic Fe₂O₃ are located, the additional peak can be assigned to hematite. A similar separation of zirconia and manganese oxide in MnSZ is not detected. However, the tendency of agglomeration might be lower in case of manganese, since it is already better dispersed, so that the particles might be too small to be detected by XRD.

For MnSZ, the phase change, which is combined with the third weight loss, is observed earlier during the time scale of the experiment if the promoter content is higher; in 2.0FeSZ the phase change takes place at similar time and temperature as the phase change in 0.5MnSZ. Fe is not as well incorporated into the zirconia lattice as Mn, but located at the surface.³⁹ The number of incorporated iron ions in 2.0FeSZ might thus be similar to the number of incorporated

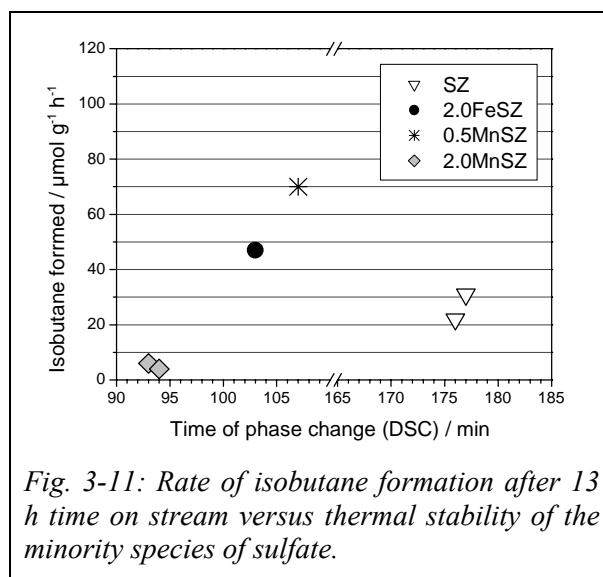


Fig. 3-11: Rate of isobutane formation after 13 h time on stream versus thermal stability of the minority species of sulfate.

manganese ions in 0.5MnSZ and correspond to about 0.5 wt%. The time of the phase change during the experiments seems to be correlated with the long-term activity of the catalysts. In Fig. 3-11 the rate after 13 h time on stream is plotted versus the time of the phase change that indicates the thermal stability of the minority species of sulfate. Two groups are distinguishable: promoted and unpromoted SZ. For the promoted catalysts, the rate increases linearly with the time of phase change; a similar trend might exist in case of the unpromoted samples. The long-term activity depends on the deactivation. Promoters increase the activity

ⁱⁱⁱ International Centre for Diffraction Data® (ICDD®), Powder Diffraction Files™ PDF 39-238(cubic) and PDF 33-664(trigonal).

by several orders of magnitude; more active catalysts deactivate faster. This is the reason for the indirect correlation between promoter content and the long-term rate. There is another correlation between promoter content and stability of sulfate. The incorporation of promoters results in a destabilization of the high-temperature stable sulfate species.

3.3.5 Summary

During the TG experiment all samples are first dehydrated, then the majority of sulfate is released as SO_3 (SO_2 and O_2) and, finally, the initially tetragonal samples change to the monoclinic phase under evolution of a minority species of sulfate as SO_2 . The total amount of sulfate is higher in catalysts calcined at lower temperature and reaches about 4 wt% SO_3 (about $560 \mu\text{mol}\cdot\text{g}^{-1}$). In 2.0FeSZ, separation of Fe_2O_3 from ZrO_2 is observed. Similar DSC curves for 0.5MnSZ and 2.0FeSZ hint similar numbers of incorporated ions. SZ based catalysts contain a thermally ($> 1200 \text{ K}$) very stable sulfate species (1–5 % of total sulfate), whose location is yet unknown. Promoters decrease the thermal stability of this fraction of sulfate, the tetragonal phase, and the long-term activity of the catalysts in *n*-butane isomerization. The high-temperature stable sulfate species could be trapped in bottleneck shaped pores that are destroyed or enlarged during the phase change. Another possibility would be a subsurface species that is destabilized by the incorporation of promoters in the lattice.

3.4 Interpretation of the IR Spectra of SZ and Promoted SZ

In chapters 5, 6, and 7 infrared (IR) spectroscopy is used to investigate sulfated zirconia-based catalysts. Thus the IR spectra of the respective catalysts must be known and understood. The spectra were recorded either in transmission or in diffuse reflectance mode. Before comparing and completely interpreting the infrared spectra of SZ, FeSZ, and MnSZ, the principles of transmission and diffuse reflectance IR spectroscopy are shortly presented.

3.4.1 Infrared Spectroscopy in Transmission and in Diffuse Reflectance

The electromagnetic radiation following the region of visible light towards increasing wavelengths is classified into near, mid, and far infrared radiation with respect to the energy of visible light (Tab. 3-2). The region of $0.8\text{--}1 \mu\text{m}$ is also called photographic IR.¹⁶³

Tab. 3-2: Wavelength and energy of electromagnetic radiation in the IR region

	Near IR (NIR)	Mid IR (MIR)	Far IR (FIR)
wavelength / μm	0.8 – 2.5	2.5 – 50	50 – 1000
frequency / s^{-1}	$3.75 \cdot 10^{14} - 1.2 \cdot 10^{13}$	$1.2 \cdot 10^{13} - 6 \cdot 10^{12}$	$6 \cdot 10^{12} - 3 \cdot 10^{11}$
wavenumber / cm^{-1}	12500 – 4000	4000 – 200	200 – 10

Classification according to Fadini and Schnepel¹⁶⁴

The product of wavelength (λ) and frequency (ν) of the radiation is constant and equivalent to the propagation speed of light (c). When interacting with matter, infrared radiation is absorbed, exciting molecules to vibrations in combination with rotations and stimulating solids to vibrations of the lattice and the functional groups on the surface. Absorption spectra are generated by plotting the intensity of the absorbed light versus its wavelength. In infrared spectroscopy band positions are usually not given in wavelengths but in wavenumbers ($\tilde{\nu}$) because these are directly proportional to the frequency and thus the energy of the radiation:

$$\tilde{\nu} = \frac{1}{\lambda} = \frac{\nu}{c} \quad \text{Eq. 3-7}$$

Light incident with intensity I_0 is scattered at the sample and reflected at phase boundaries so that the intensity I of the transmitted light is lower. Reflection of light at phase boundaries can be eliminated either through a reference measurement with same materials of cuvette and solvent or through variation of the sample thickness. Reflection by scattering is considerable for colloids and solids when the wavelength is in the order of magnitude of the particle size and can be reduced through embedding the particles in media with similar refractive index. This is achieved either by pressing tablets with KBr^{165,166} or by suspending the sample in Nujol^{167,168} (paraffin oil) or hexachlorobutadiene,¹⁶⁹ which complement each other since their absorption bands are at different positions. If luminescence and all types of reflection are negligible the absorption properties of the sample can be calculated from the transmitted light via the Lambert-Beer Law with absorptance (absorption factor, α), transmittance (transmission factor, τ), molar Napierian extinction coefficient (κ , in m^2/mol), molar concentration of absorbing species (c , in mol/m^3), and sample thickness (l):

$$1 - \alpha = \tau = \frac{I}{I_0} = e^{-\kappa \cdot c \cdot l} \quad \text{Eq. 3-8}$$

The absorbance is calculated either as Napierian absorbance (A_e) or as decadic absorbance (A_{10}), which is used by standard spectroscopy software, whereby ε is the decadic extinction coefficient:

$$A_e = \kappa \cdot c \cdot l = -\ln \tau \quad \text{and} \quad A_{10} = \varepsilon \cdot c \cdot l = -\lg \tau \quad \text{Eq. 3-9}$$

However, transmission in the IR regime can become very low and scattering very high for catalysts that are fine powders with high surface area. Embedding is not a possible solution for *in situ* studies, since the diluent can be effected by heating and results obtained during reaction may be falsified by interaction of the diluent with catalyst, reactant, and product. Here measuring the reflected instead of the transmitted light is a possible alternative.^{170,171} This reflection can be either specular as on mirror-type surfaces or diffuse as on mat surfaces. In the first case the reflecting power is called “reflectivity”, in the latter “reflectance” (reflection factor, ρ). According to the Kubelka–Munk Theory, which assumes the incident and reflected light to be diffuse (excluding specular reflection) and the particles to be randomly distributed and much smaller than the thickness of the layer, the reflectance is described by the quotient of absorption coefficient (k) and scattering coefficient (s) in the Kubelka–Munk function:

$$F(\rho_\infty) = \frac{(1 - \rho_\infty)^2}{2 \cdot \rho_\infty} = \frac{k}{s} \quad \text{Eq. 3-10}$$

Usually instead of the absolute reflectance ρ_∞ the reflectance ρ'_∞ is measured relative to a standard (here KBr or CaF₂). The Kubelka–Munk function is dependent on the wavelength and in case of a dilute species ($0.2 < \rho'_\infty < 0.6$) – similar to the Lambert-Beer Law – proportional to its concentration:

$$F(\rho'_\infty) \propto \frac{\varepsilon \cdot c}{s} \quad \text{Eq. 3-11}$$

3.4.2 Results

Prior to the IR measurements the catalysts were activated, i.e. they were heated at 723–773 K in gas flow (N₂ or O₂) or during evacuation (usually for 30 min; ramp: 25 K min⁻¹). DRIFT spectra were recorded in a commercial *in situ* cell (Environmental Chamber) with ZnSe window using Graseby Specac Selector Optics or a quartz cell using a home-made diffuse reflectance attachment; transmission spectra were obtained in a home-made high temperature *in situ* cell (Hochtemperaturzelle, HTZ). For further details see Chapter 9.8. DRIFT spectra are displayed in reflectance or Kubelka–Munk units (KM), transmission

spectra in transmittance or absorbance. In Fig. 3-12 the different methods of display are compared for both transmission and diffuse reflectance spectra using FeSZ as example. In Fig. 3-13 the spectra of SZ and MnSZ are shown. The spectra recorded in diffuse reflectance are of better quality than the transmission IR spectra, since the signal to noise ratio is higher, but the corresponding band positions are in good agreement; they are listed in Tab. 3-3.

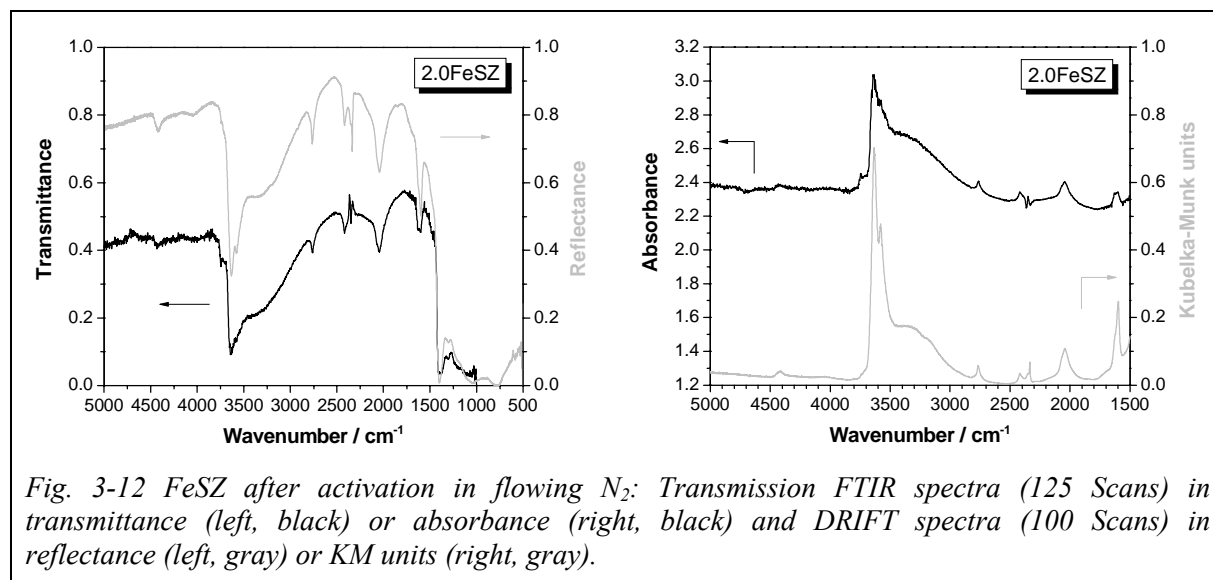


Fig. 3-12 FeSZ after activation in flowing N_2 : Transmission FTIR spectra (125 Scans) in transmittance (left, black) or absorbance (right, black) and DRIFT spectra (100 Scans) in reflectance (left, gray) or KM units (right, gray).

Tab. 3-3: Band positions of SZ, FeSZ, and MnSZ extracted from the DRIFT spectra

SZ	FeSZ	MnSZ	Assignment
3740 vw	3744 vw	3742 vw	$\nu(\text{OH})$
3714 vw	3719 vw	3718 vw	$\nu(\text{OH})$
3629 vs	3631 vs	3631 vs	triply bridged $\nu(\text{OH})$ next to $\text{S}_2\text{O}_7^{2-}$
3582 w *	3581 w *	3581 w *	$\nu(\text{H}_2\text{O}_{\text{ads}})$ next to SO_4^{2-}
3489 w	—	—	triply bridged $\nu(\text{OH})$ on dehydrated ZrO_2
2767 s	2765 s	2766 s	overtone of vibration around 1400 cm^{-1}
2417 w	2418 w	2417 w	combination of vibrations at 1400 and 1050 cm^{-1}
2340	2343 sh	2346 sh	overtone of vibration around 1213 cm^{-1}
2336 **	2336 **	2336 **	$\nu(\text{N}_{2,\text{ads}})$
2198 m	2218 sh	2220 vw	overtone or combination mode of $\nu(\text{S-O})$
2042 vs	2044 vs	2040 vs	overtone of vibration around 1050 cm^{-1}
1626 w	1629 w	1630 w	$\delta(\text{H}_2\text{O}_{\text{ads}})$
1603	1597	1597	$\delta(\text{H}_2\text{O}_{\text{ads}})$
1402	1400	1399	$\nu(\text{S=O})$ of $\text{S}_2\text{O}_7^{2-}$, $\text{S}_2\text{O}_7^{2-} \cdot \text{H}_2\text{O}$ or $\text{SO}_{3,\text{ads}}$
1378 sh	1375 sh	(sh)	$\nu(\text{S=O})$ of $\text{S}_2\text{O}_7^{2-}$ or SO_4^{2-}
1308	1300		$\nu(\text{S=O})$ of $\text{S}_2\text{O}_7^{2-} \cdot y\text{H}_2\text{O}$
(1211)	1211	1213	$\nu(\text{S-O})$ of $\text{S}_2\text{O}_7^{2-}$ or $\text{S}_2\text{O}_7^{2-} \cdot y\text{H}_2\text{O}$
		1145	$\nu(\text{S-O})$ of $\text{S}_2\text{O}_7^{2-} \cdot y\text{H}_2\text{O}$
1045	1045	1045	$\nu(\text{S-O})$ of $\text{S}_2\text{O}_7^{2-}$ or $\text{SO}_{3,\text{ads}}$

* only after activation in gas flow

** only after activation in flowing N_2

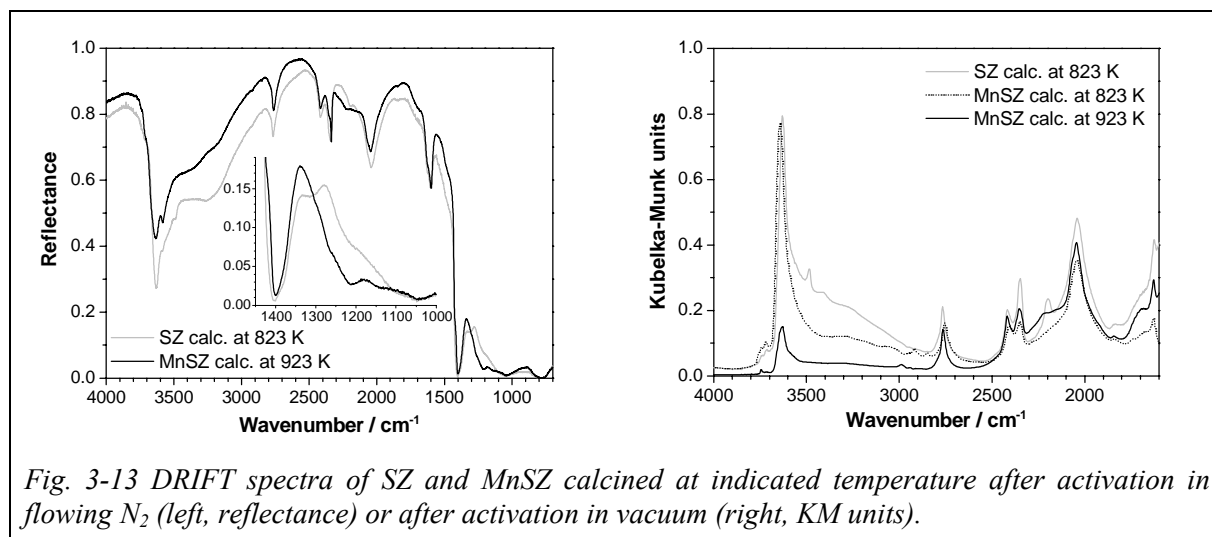


Fig. 3-13 DRIFT spectra of SZ and MnSZ calcined at indicated temperature after activation in flowing N₂ (left, reflectance) or after activation in vacuum (right, KM units).

3.4.3 Discussion

The IR spectra, measured in transmission or diffuse reflectance, are in good agreement (see Fig. 3-12). However, vibrations of surface species are more evident in diffuse reflectance spectra. Furthermore, the signal to noise ratio is higher in the spectra recorded in diffuse reflectance than in the transmission IR spectra, even if the number of collected scans is lower (100 vs. 125). This better quality may result partly from the different set-ups using different detectors. Another and more serious reason may be the low transmission through the wafer. Band positions do not change, when spectra are converted from transmittance to absorbance or reflectance to Kubelka–Munk units. Conversion of the measured spectra is thus only necessary when quantitative information is needed, since the absorbance (and similarly the KM function) is directly proportional to the concentration of the vibrating species.

Interpretation of the sulfate vibrations is difficult and conclusions about the structure of sulfate are not easily drawn. It is agreed, however, that vibrations around 1400 cm⁻¹ or lower are due to the stretching mode of the S=O double bond and vibrations around 1000 cm⁻¹ or higher are caused by the S-O single bond stretching mode.¹⁷² Bands at 1400 cm⁻¹ and above have been assigned previously to S₂O₇²⁻,^{47,48} bands at 1395 and 1402 on monoclinic SZ have been suggested to result from triply coordinated SO₄²⁻ in two different geometries.¹⁷³

Recently, DFT calculations of the vibrational spectra of sulfated zirconia have become available.^{62,iv} Hofmann and Sauer investigated the stability and spectral signature of various

^{iv} A. Hofmann, J. Sauer, personal communication.

sulfate structures in combination with different water contents on the (101) surface of the tetragonal phase. The (101) surface is the most stable one according to the calculations by Hofmann and Sauer. Benaissa et al. identified the (110) plane as most abundant using high resolution electron microscopy.¹⁷⁴ Morterra et al. reported “low Miller-index crystal planes”.⁴³ The investigated catalysts are tetragonal and although the facet planes are unknown, experimental and calculated frequencies can be compared to assist interpretation.

A number of bands arise from S=O and S–O vibrations. According to the calculations, some of them are characteristic: only S=O vibrations of $S_2O_7^{2-}$ species, which may be hydrated, or of adsorbed SO_3 , or of tridentate SO_4^{2-} yield band positions above 1395 cm^{-1} . The S=O band was shifted upwards during activation with progressing dehydration. Positions given in the literature will, thus, depend on the degree of hydration. Other interpretations can also be found; Riemer et al. interpreted a band at 1382 cm^{-1} as tridentate monosulfate.⁵⁹

According to DFT results the bands at $1308\text{--}1300\text{ cm}^{-1}$, detected for SZ and FeSZ, may arise from S=O vibrations of SO_4^{2-} on a strongly hydrated surface or of $S_2O_7^{2-}$ on a slightly hydrated surface. Another S=O vibration located at 1213 cm^{-1} (very intense for MnSZ) also originates from a, possibly hydrated, $S_2O_7^{2-}$ species. A hydrogen bridge to a neighboring OH group causes the, for a double bond, relatively low frequency. The bands at 1145 and 1045 cm^{-1} are clearly S–O bond vibrations, and again several interpretations are possible. The band 1145 cm^{-1} is in the range of S–O vibrations of SO_4^{2-} on a strongly hydrated surface or of $S_2O_7^{2-}$ on a weakly hydrated surface; the band at 1045 cm^{-1} could be assigned to $S_2O_7^{2-}$ on a dehydrated surface or adsorbed SO_3 . According to the spectra and the estimated water content of $60\text{--}125\text{ }\mu\text{mol g}^{-1}$ (see Chapter 7.3.1), the surface is still hydroxylated after activation but only moderately hydrated. It therefore seems appropriate to exclude the presence of SO_4^{2-} species on a richly hydrated surface. Definitely, $S_2O_7^{2-}$ species are present on all three catalysts, and the nearest surroundings of these species sometimes feature adsorbed water. In comparison to the two other samples MnSZ exhibits more of the $S_2O_7^{2-}$ species absorbing at 1213 cm^{-1} . Since all samples have about equal sulfate content (Chapter 3.3), MnSZ should then have lower concentrations of other sulfate species. Weaker in the spectrum of MnSZ than in those of SZ and FeSZ is the band at $1300\text{--}1308\text{ cm}^{-1}$, which belongs to the “pyrosulfate with adjacent water” configuration. Given the slightly better dehydration of MnSZ the band at 1213 cm^{-1} may be assigned to a dehydrated pyrosulfate state.

More bands due to S=O and S–O vibrations are observed. The bands at 2767 , 2345 and 2040 cm^{-1} are assigned to overtones of the vibrations at around 1400 , 1213 and 1050 cm^{-1} . The band at 2416 cm^{-1} is believed to be a combination mode of the bands at 1400 and

1045 cm^{-1} . The wavenumber of combination modes should exactly fit the sum of the wavenumbers of the vibrations it is composed of, which is not the case here; the difference is about 30 cm^{-1} . However, no other plausible explanation for this band exists.

Interpretation of bands resulting from OH groups on zirconia has been given before. Bands around 3760 cm^{-1} and 3640 cm^{-1} are due to stretching vibrations of OH at the surface,⁵⁴ which have been assigned to terminal (higher frequency band) and bi- or tri-bridged (lower frequency band) OH groups.^{52,175} The two very weak bands at 3740–3745 cm^{-1} and 3715–3720 cm^{-1} are thus indicative of OH groups on ZrO_2 . If Si was present as impurity, a vibration at 3740 cm^{-1} could also result from silanol groups, Si-OH;¹⁷⁶ Hertl, however, attributed a band at 3744 cm^{-1} to vibrations of OH on tetragonal zirconia.¹⁷⁷ Babou et al. reported a band at 3645 cm^{-1} for sulfated zirconia, and at 3665 cm^{-1} for non-sulfated zirconia.⁵³ Morterra et al. assigned a band at 3640 cm^{-1} to "free surface OH groups of the ZrO_2 system" because its position and behavior upon dehydration resemble that of a band of non-sulfated zirconia.⁵⁴ Riemer et al. observed a band at 3640 cm^{-1} only when sulfate was present and favored the idea of an OH group bridging sulfur and zirconium.⁵⁹ The spectrum of gas phase sulfuric acid exhibits vibrations of S–OH groups at 3609 cm^{-1} .¹⁷⁸ The bands in the spectra of SZ, FeSZ, and MnSZ are around 3630 cm^{-1} and thus located in the range between the OH bands of pure zirconia (3771 and 3672 cm^{-1})¹⁷⁹ and sulfuric acid. From the DFT calculations several possibilities emerge for the band at 3630 cm^{-1} , some of which can be excluded for lack in plausibility such as a richly hydrated zirconia surface. It is not possible to distinguish from the positions between scenarios involving either SO_4^{2-} (dehydrated or highly hydrated) or $\text{S}_2\text{O}_7^{2-}$ species (dehydrated or singly hydrated). In light of the sulfur-oxygen vibrations, which suggest $\text{S}_2\text{O}_7^{2-}$ (pyrosulfate) as the predominant species, a triply-bridged OH group next to $\text{S}_2\text{O}_7^{2-}$ is the best interpretation.

The vibration at 3580 cm^{-1} is characteristic for a surface with SO_4^{2-} species and only detected, if the catalysts were activated in gas flow. It originates from adsorbed water and could represent a hydroxonium ion, since Morterra et al. attributed a band at ca. 3590 cm^{-1} to the OH vibration in H_3O^+ .⁵⁴ The band at 3489 cm^{-1} , which does not appear in the spectra of the promoted samples, is similar to a band observed at 3510 cm^{-1} for a sulfate-free mixture of tetragonal and monoclinic zirconia (ca. 1:3) and can, with the help of the DFT calculations, be attributed to triply-bridged OH groups on a dehydrated zirconia surface. It is not understood why on the SZ sample more sulfate-free surface should be exposed, because the sulfate density is not lower than on the promoted samples (estimation on the basis of sulfate content and surface area).

The relative intensity of the OH stretching bands is lower in the spectra of promoted SZ than in the spectrum of SZ (comparison of SZ and MnSZ in Fig. 3-13, left). However, in order to achieve optimum isomerization performance, SZ has been calcined at 823 K while all promoted SZ have been calcined at 923 K. A decrease in the OH pattern with increasing calcination temperature has been reported for unpromoted SZ.¹⁷² The spectrum of a MnSZ sample calcined at the same temperature as SZ, namely 823 K, shows OH band intensities comparable to those in the spectrum of SZ (Fig. 3-13, right). Hence, the reduced number of OH groups on MnSZ or FeSZ after calcination at 923 K is due to the calcination temperature and not to the promoters.

Around 1600 cm^{-1} the OH deformation mode of water appears. Babou et al. assigned a band at 1628 cm^{-1} to adsorbed water.⁵³ The two bands at about 1625 and 1600 cm^{-1} are thus attributable to deformation vibrations of adsorbed water, indicating that the surface is not completely dehydrated during activation. A value of 1600 cm^{-1} results from DFT calculations only for water configurations on a sulfated but not on a pure zirconia surface. The band at 1625 cm^{-1} is unspecific according to the calculations; it is not observed for unsulfated zirconia and thus the corresponding water species should be associated with a sulfate species. The stretching vibrations of water vapor are located at 3651.7 cm^{-1} and 3755.8 cm^{-1} , the deformation at 1595.0 cm^{-1} ; a combination mode of stretching and deformation vibrations is found at 5332.0 cm^{-1} .¹⁸⁰ A band around 5300 cm^{-1} is thus always indicative of adsorbed water on the catalyst, if vibrations are visible in the OH stretching region and around 1600 cm^{-1} .

The band at 2336 cm^{-1} (overlapping with the band at 2040 cm^{-1}) is noticeably sharper than the sulfate overtones and combination modes, appears only when nitrogen is used for activation, and is located slightly above the gas phase frequency for nitrogen of 2330 cm^{-1} .¹⁸¹ It is therefore assigned to the stretching vibration of adsorbed nitrogen. This band is absent after activation in O_2 , instead a band at $\approx 1595\text{ cm}^{-1}$ (hidden underneath the OH deformation bands) indicates the presence of adsorbed O_2 ¹⁸² (gas phase frequency 1556 cm^{-1})¹⁸¹.

3.4.4 Summary

The results obtained by diffuse reflectance IR spectroscopy are consistent with the transmission IR data. On pure SZ, an extra OH vibration is found at 3489 cm^{-1} that is missing on the promoted catalysts. The presence of this OH band is independent of the calcination temperature, by which the amount of OH groups is determined. Otherwise, the influence of the promoters on the spectra is marginal. Comparison of the measured frequencies with DFT calculations clearly points towards $\text{S}_2\text{O}_7^{2-}$ as prevailing surface species on the activated

samples; single water molecules are often nearby. Evidence for other species such as SO_4^{2-} is only indirect through OH-stretching vibrations, and the data in the sulfur-oxygen region do not favor this interpretation. The spectra of SZ, FeSZ, and MnSZ differ slightly, but are all dominated by the pattern of $\text{S}_2\text{O}_7^{2-}$.

4. Design of a Three-Channel Fixed Bed Reactor

4.1 Motivation

High-throughput techniques are used as screening-tools in combinatorial chemistry and had a great influence on discovery and optimization of pharmaceuticals.¹⁸³ With the development of a multichannel microreactor for evaluation of six catalysts (≤ 1 g) that perform various types of gas-conversion this strategy entered the field of heterogeneous catalysis 20 years ago.¹⁸⁴ Since then, these techniques have been developed further and gained importance in parallel synthesis and testing of catalysts. For instance, a more active and selective sulfated zirconia-based catalyst for hydroisomerization of C₅–C₇ alkanes, which contains niobium besides platinum, was discovered using a system of 16 fixed bed reactors operating in parallel.¹⁸⁵ With the help of simultaneously conducted experiments the optimum preparation or reaction conditions can be determined in short time: results that take years and dozens of PhD students to be obtained by standard laboratory reactor tests will be received within months. Due to the performance of sometimes more than hundred reactions and the simultaneous analysis of their products such experiments are very demanding. Furthermore, the enhancement in through-put is accompanied by a loss of accuracy in analysis. Usually, the process of catalyst discovery and optimization consists of several steps, whereby the number of simultaneous tests decreases while the accuracy of the experiments increases.¹⁸⁶

For efficient investigation of catalytic performance it is generally desirable to conduct experiments in parallel. Sometimes an only slight acceleration conserving high accuracy is preferable. In order to investigate the influence of three different aging conditions on the catalytic activity of sulfated zirconia materials as described in Chapter 5.2, the performance of the differently stored catalysts has to be tested in certain time intervals. To exclude an influence of duration of storage on the results, all three samples should be analyzed simultaneously. Since it —especially for promoted SZ— takes 10 hours and longer times on stream to reach steady-state conditions, performing one conventional catalytic test lasts at least one day. A difference in age of two days between the samples is negligible after one year, but for comparison after one month or one week this time difference amounts to 7 or 25 %, and is thus too large. To solve this problem, a set-up on laboratory scale was designed and constructed, in which three catalysts (2 ml bed volume each) can be tested simultaneously under exactly the same temperature and feed-stream conditions without loss of product analysis information. This three-channel fixed bed reactor is also suitable for long-time experiments lasting several days.

4.2 System Requirements

The reaction of interest is the isomerization of *n*-butane at low temperatures (323–378 K) after activation of the catalyst at 723 K. The system should operate in an even larger temperature range from temperatures at or below room temperature for investigation of *n*-pentane isomerization up to 923 K to allow *in situ* calcination (see Chapter 3.1) of the catalysts. The heating should be isothermal and a fast cooling to reaction temperature after activation or calcination should be possible to reduce time loss. The analysis of products has to be fast, because three catalytic tests have to be monitored at the same time. A proper separation of reactant and product is necessary, which means that a small amount of isobutane (ca. 1 ppm as impurity in the feed) has to be detected in a surplus of *n*-butane (10 000–50 000 ppm). Therefore, the system must fulfill the following conditions:

- (1) Isothermal heating over a wide temperature range (273–923 K),
- (2) rapid heating and cooling to reaction temperature after activation (calcination),
- (3) fast and quantitative gas phase analysis.

4.3 Design and Experimental Details

The requirements lead to the construction of a reaction vessel in which three tubular reactors are positioned symmetrically (Fig. 4-1); the geometry is similar to the apparatus described by Purnama that contains three stainless steel reactors positioned in an aluminium heating block.¹⁸⁷

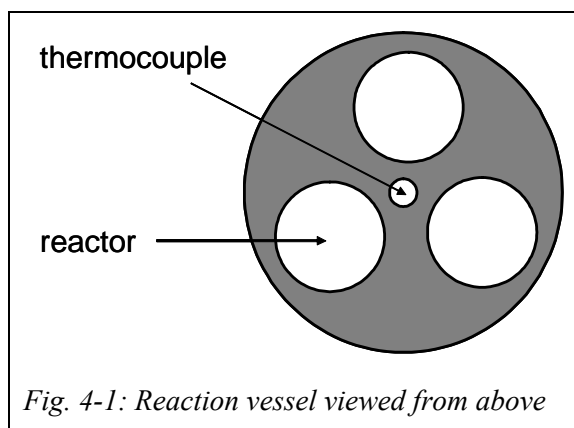


Fig. 4-1: Reaction vessel viewed from above

4.3.1 Reactors

The tubular reactors are U-shaped (inlet: $d_{\text{out}} = 12 \text{ mm}$ / $d_{\text{in}} = 10 \text{ mm}$, outlet: $d_{\text{out}} = 6 \text{ mm}$ / $d_{\text{in}} = 5 \text{ mm}$) to be connected to from above (Fig. 4-2). They are fixed at the top of the reaction vessel by seals made of polytetrafluorethylene to avoid discharge of the sand (see Chapter 4.3.2). A high surface in the holder of the seals due to ribs and cooling of the lid by an air flow avoids thermolysis of the PTFE, which occurs above 530 K.¹⁸⁸ The three reactors are made from quartz both to withstand high temperatures and to allow

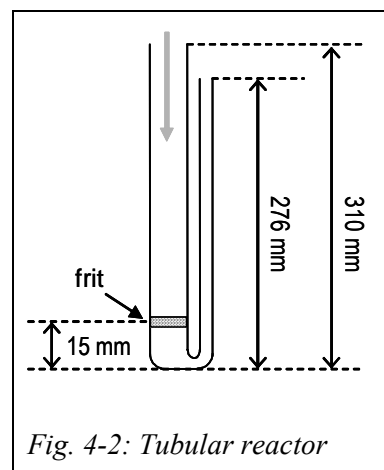


Fig. 4-2: Tubular reactor

observation of the catalyst bed during the loading so that a constant height is ensured. The catalyst powder is placed in the inlet tube of the reactors on a quartz frit (*Heraeus*, $d_{in} = 10 \text{ mm}$) with porosity 2 (40–100 μm) which has been lapped to uniform thickness to achieve a homogeneous resistance over the whole area cross-section.

4.3.2 Reactor Heating

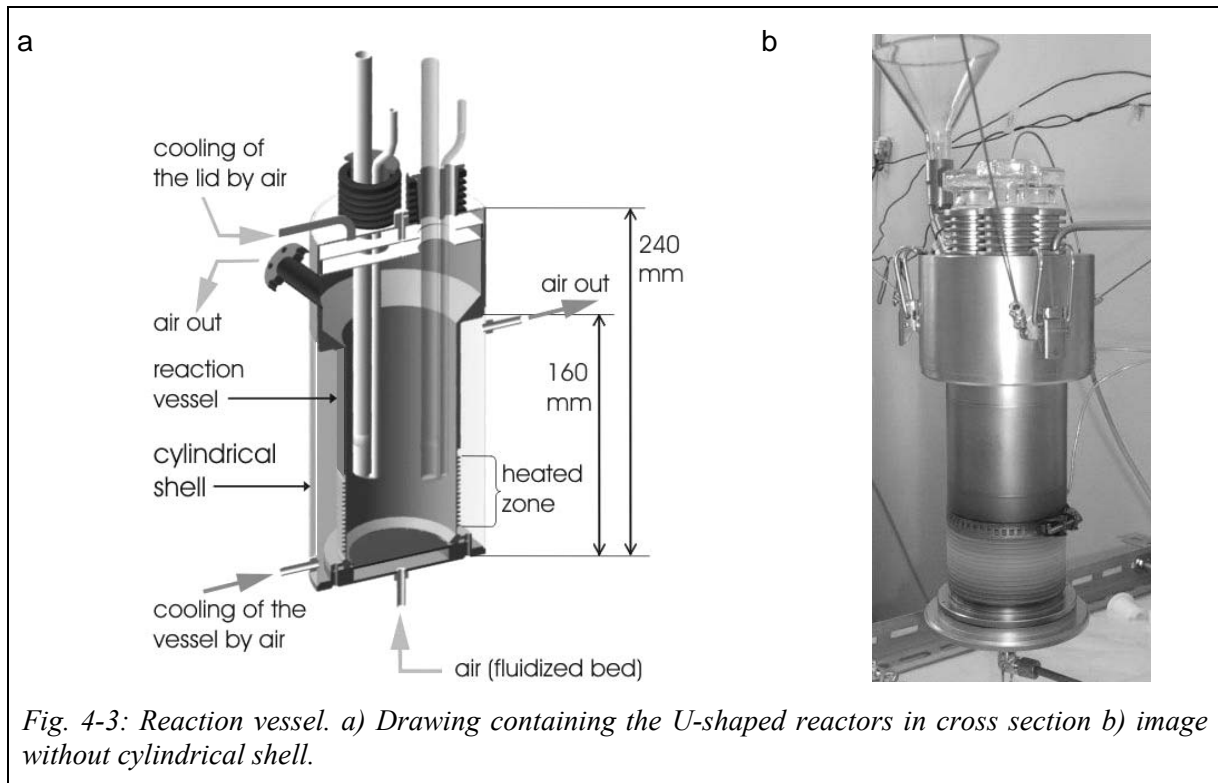


Fig. 4-3: Reaction vessel. a) Drawing containing the U-shaped reactors in cross section b) image without cylindrical shell.

Rapid heating and cooling together with an isothermal temperature profile of the three reactors is possible by heat transfer from a fluidized sand bed. A schematic cross-section through the reaction vessel containing the tubular reactors is given in Fig. 4-3a. The bottom of the vessel ($d_{out} = 82 \text{ mm}$) is heated electrically by a wire with cold ends (*Thermocoax*, $d = 2 \text{ mm}$, $l = 4 \text{ m}$, $R = 12.5 \Omega$, $T_{max} = 1273 \text{ K}$). It contains a wire mesh stack (*Haver & Boecker*, $d = 70 \text{ mm}$, $20 \mu\text{m}$) that supports the sand (50–70 mesh, ca. 500 ml). The sand is fluidized by air flowing through the frit (ca. 25 l/min) and collected at the outlet by a funnel (Fig. 4-3b). For experiments below room temperature the air can be cooled, e.g. by liquid nitrogen. The reaction vessel is enclosed by a cylindrical shell that can be purged with air for cooling. This together with the air passing directly through the sand bed guarantees a fast return to lower temperatures after activation or calcination. The temperature of the reactor is controlled by a thermocouple (*Thermocoax*, K-type) positioned in the center of the vessel (Fig. 4-1) via a linear temperature programmer (*Newtronic Micro 96*, $P_{max} = 2000 \text{ W}$). For

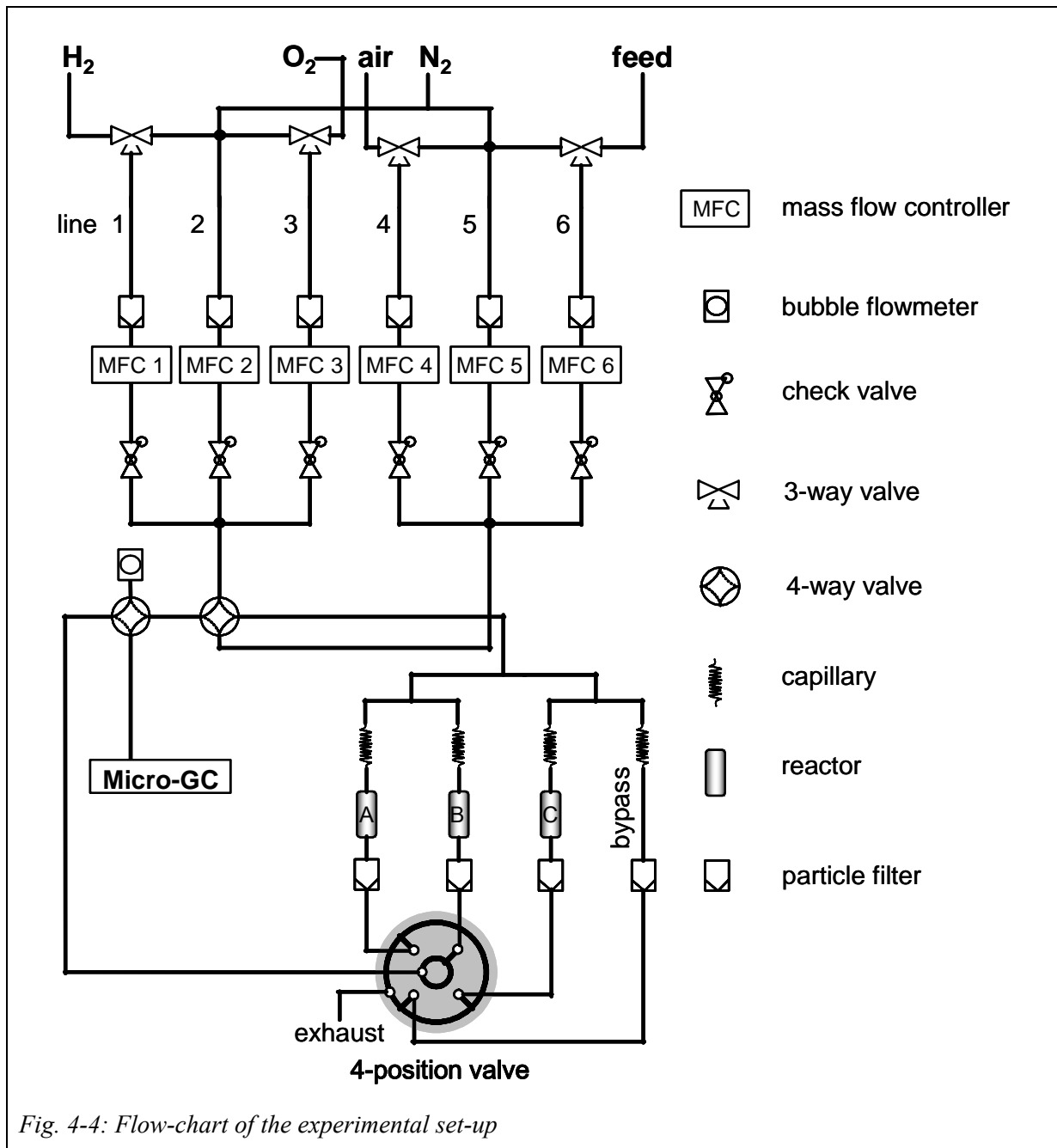
activation (fast temperature change) and reaction (constant temperature) two different parameter sets were used to achieve optimum temperature control (see Tab. 4-1). The temperature in each of the three reactors can be measured by further thermocouples (*Thermocoax*, K-type, stainless steel coated, insulated measuring point, $d = 1 \text{ mm}$, $l = 0.5 \text{ m}$).

Tab. 4-1: Parameter sets of the PID controller used for activation and reaction

Parameter	Set 1: Activation	Set 2: Reaction
maximum value of range / °C	700	700
minimum value of range / °C	0	0
X_P Proportional part	1.0	4.3
I Integral time / min	0.5	2.9
D Differential time / min	0.00	0.59
$\sqrt{\quad}$ PID configuration switching	0.90	0.90
\uparrow maximum set value (%)	100	100
\downarrow minimum set value (%)	0	0
CE communication enabled	0	0

4.3.3 Experimental Set-Up

Fig. 4-4 shows a flow-chart of the whole set-up which consists of gas dosing system, three-channel fixed bed reactor and product gas analysis as main components. All tubings are made from stainless steel (*Dockweiler*, $\frac{1}{8}$ " x 0.56 mm). For activation (line 1–3) and reaction (line 4–6) nitrogen or oxygen and 5 vol% *n*-butane in nitrogen were used, but further gases can be introduced into the system: Four three-way valves (*Parker*) allow the choice between nitrogen and a different gas for lines 1, 3, 4, and 6. To remove particulate matter, all gases flow through filters (*Swagelok*, 2 μm) before they reach the mass flow controllers (*Bronkhorst*, Flowbus, C_xH_y : D-type, rest: C-type, $\Delta p = 2 \text{ bar}$, test pressure: 8 bar), MFC 1–6, or the four-position valve. The check valves (*Parker*) prevent backflow of the gases. With help of two four-way valves (*VICI/Macherey-Nagel*) it is possible —like for the single tubular fixed bed reactor (see Chapter 9.9)— to activate the catalysts while the feed stream is conditioned and measured by the bubble flowmeter or analyzed by the GC. The gas flow is distributed to the reactors and a bypass in similar amounts using passive flow restrictors.¹⁸⁹ These restrictors, capillaries (*CS-chromatographie Service*, $d_{\text{out}} = 1/16$ "^c, $d_{\text{in}} = 0.13 \text{ mm}$) of 0.85 m length, cause a pressure drop that is higher than the ones induced by the frits and catalyst beds. Thus the resistance in all four channels is about the same and the feed splits evenly into four parts. The bypass is necessary to check if the composition of the feed gas is constant and to determine its initial amount of isobutane.



4.3.4 Product Analysis

The outlet of either one of the three reactors or the bypass is selected by a four-position valve (VICI/Macherey-Nagel, RS232 interface, $1/8''$ fittings) with micro electric actuation, the other three channels go to exhaust. Analysis of the gas phase is performed by a Micro-GC (Varian CP 4900) equipped with a module containing injector („Solid-State“, max. 10 μ l, 313 K), column (Siloxan 5, $l = 8$ m, 318 K) and detector (micro thermal conductivity detector, 200 nl, 1 ppm–100 %) using the Varian Star Chromatography Workstation software in combination

with Valve Control. The column oven is kept isothermal at 318 K during analysis; the gas pressure is static 1.19 bar (17.3 psi); helium is used as carrier gas. Tab. 4-2 shows the time events during analysis of one of the three reactors or the bypass.

Tab. 4-2: Time events during the gas phase analysis

Time / s	Event
0	start of sampling with membrane pump
20	injection onto column
21	start of analysis
35	switch of four-position valve to next position

During analysis of one channel, 15 s after injection, the line to the Micro-GC is already purged with the product gas of the next channel to equilibrate the gas stream. The time between two injections should not be less than 60 s; if pentanes and hexanes are expected, the analysis takes 180 s.

4.4 Test Results

4.4.1 Gas Distribution

Resistances at the walls and changes in the direction of the flow lead to frictional losses of reactant and product gas in tubes, bends, formed parts, mass flow controllers, valves, and fixed beds. The resulting pressure drops increase with flow velocity, length of the tubes, and height of the fixed bed. The purpose of the artificial high pressure drop induced by the capillaries is to balance differences between the three reactors and the bypass. Thus, the four streams reach similar flow velocities when gases enter the system at 4.2 bar overpressure (Tab. 4-3). The deviations in flow ($\pm 3\text{--}4\%$) could in principle be reduced by increasing the length of the capillary. However, the maximum pressure at the outlet of the butane gas bottle (30 bar max.) is limited to 4.8 bar by the currently used pressure regulator. Sufficiently high inlet pressure for longer capillaries cannot be achieved.

Tab. 4-3: Comparison of the flow (ml min^{-1}) through the three reactors and the bypass

desired flow	reactor A	reactor B	reactor C	bypass
25	25	24	26	25
40	40	39	41	39

4.4.2 Heating and Cooling

The isothermal properties of the fluidized sand bed are almost perfect. It is possible to keep the three reactors at the desired temperature with deviations of only ± 1 K during the course of the reaction (Fig. 4-5).

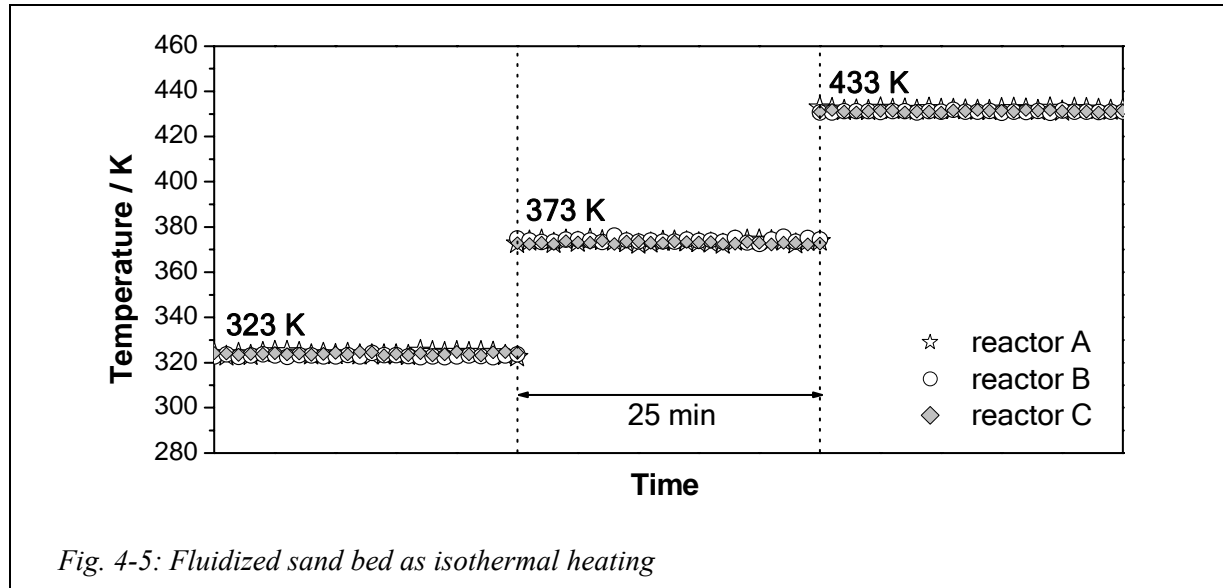


Fig. 4-5: Fluidized sand bed as isothermal heating

The temperatures for activation and reaction can be reached in the desired time interval as Fig. 4-6 shows, a 25 K/min heating ramp is possible. After activation it takes about 55 min to cool from 723 K to 323 K reaction temperature (35 min from 723 K to 373 K). This is as fast as for the standard tubular fixed bed reactor in our laboratory that is equipped with a furnace without isolation.

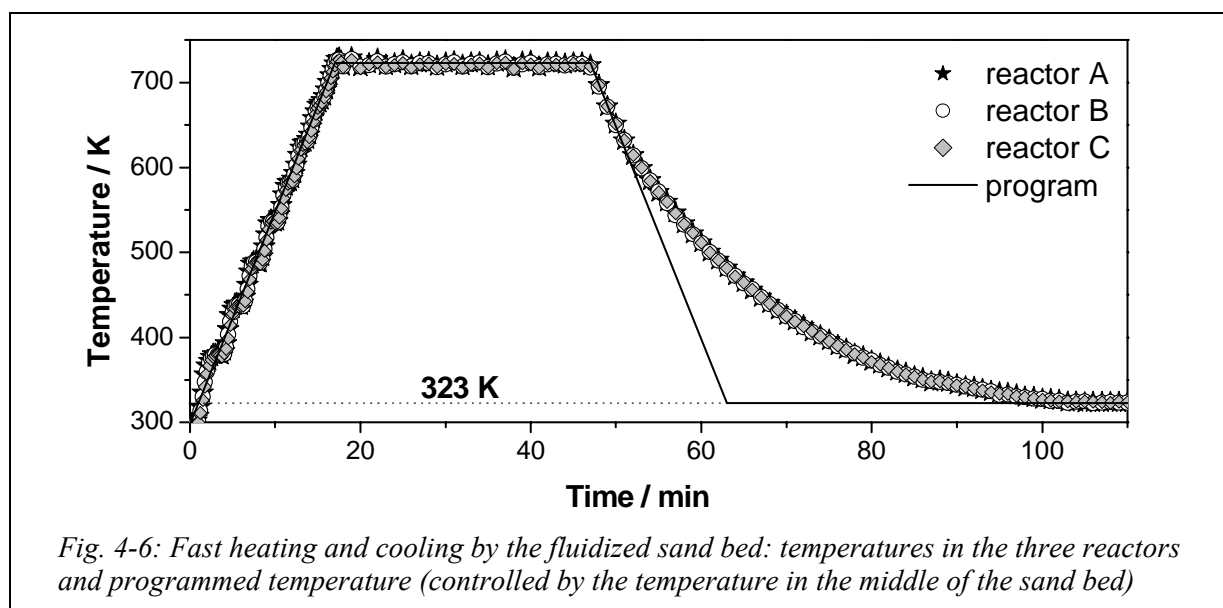


Fig. 4-6: Fast heating and cooling by the fluidized sand bed: temperatures in the three reactors and programmed temperature (controlled by the temperature in the middle of the sand bed)

4.4.3 Gas Phase Analysis

Analysis of the product stream by the Micro-GC allows separation of *n*-butane and isobutane within the required range of compositions; 1 ppm isobutane can be detected in 1–5 % *n*-butane (Fig. 4-7). Fast analysis is possible due to the short retention times (< 3 min) of *n*-butane and its isomerization and cracking products (Tab. 4-4). To separate the butane isomers the chromatogram is acquired in only 1 min; to detect the possible byproducts, pentane and hexane, the analysis takes 180 s.

Tab. 4-4: Retention times of possible products

gas	retention time / s
nitrogen/methane	23
ethane	26
propane	30
isobutane	39
<i>n</i> -butane	45
<i>n</i> -pentane	78
<i>n</i> -hexane	159

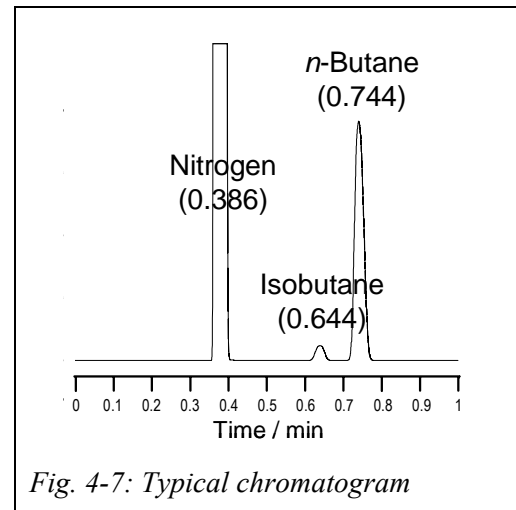


Fig. 4-7: Typical chromatogram

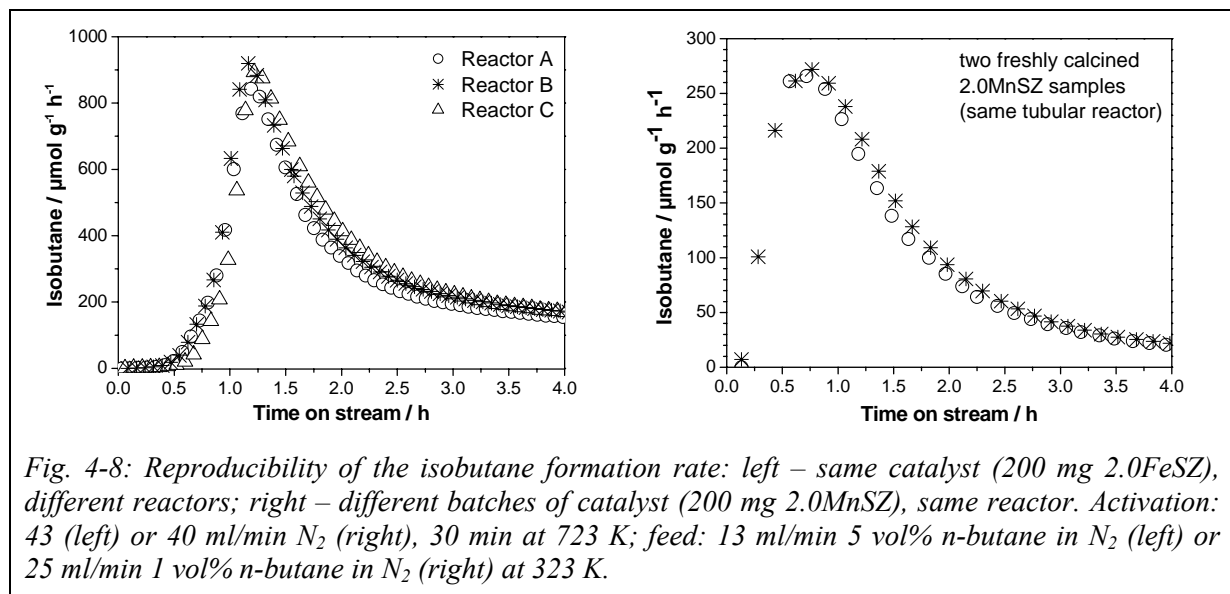


Fig. 4-8: Reproducibility of the isobutane formation rate: left – same catalyst (200 mg 2.0FeSZ), different reactors; right – different batches of catalyst (200 mg 2.0MnSZ), same reactor. Activation: 43 (left) or 40 ml/min N₂ (right), 30 min at 723 K; feed: 13 ml/min 5 vol% *n*-butane in N₂ (left) or 25 ml/min 1 vol% *n*-butane in N₂ (right) at 323 K.

The results of the gas phase analysis are plotted in Fig. 4-8. The isomerization of *n*-butane to isobutane conducted in the three reactors with equal amounts (200 mg) of the same catalysts (sulfated zirconia promoted with 2.0 weight percent iron) results in similar rates, which reach a maximum of ca. 900 μmol g⁻¹ h⁻¹ after the same time on stream (Fig. 4-8, left).

To check the reproducibility in catalyst preparation and to verify the agreement of repeated experiments, two freshly calcined batches of 2.0MnSZ were tested in performance of *n*-butane isomerization in the same reactor placed at the same position in an interval of four days. The resulting rates are well reproducible (Fig. 4-8, right).

4.5 Summary and Outlook

An apparatus was constructed, which allows a threefold enhancement in throughput for catalytic reactor tests on laboratory scale. The fluidized sand bed is well suited for heating since it provides good isothermicity and can be heated and cooled rapidly. Using a Micro-GC allows a fast gas phase analysis and enables separation and quantification of reactant and product. Slight deviations in the flow should be eliminated by a higher pressure drop in the moderating capillaries; this requires a different pressure reducer for an increased inlet pressure at the flow controllers. However, in the present state of the system the catalytic results received under the same conditions are consistent for the three reactors.

5. Handling of Sulfated Zirconia-Based Catalysts

5.1 Influence of Mechanical Stress on Sulfated Zirconia-Based Catalysts

5.1.1 Motivation

Despite intense research, a convincing structure-activity relationship for catalysts based on sulfated zirconia (SZ) has not evolved. One point of debate is the role of the bulk phase of zirconia. The room temperature stable phase of zirconia is the monoclinic phase ($m\text{-ZrO}_2$).²⁸ However, in the usual preparation of zirconia catalysts through calcination of an amorphous hydroxide precursor at 723–923 K, the tetragonal phase ($t\text{-ZrO}_2$) or mixtures of both phases are obtained. The presence of sulfate increases the fraction of $t\text{-ZrO}_2$.¹⁵ A stabilizing effect for the tetragonal phase has thus been ascribed to the sulfate. Cationic promoters such as Mn or Fe are incorporated into the zirconia lattice and stabilize the tetragonal or the cubic phase.^{38,190,191} For many years it has been believed that only the tetragonal phase in SZ is catalytically active in *n*-butane isomerization.⁴³ Recent work shows that mainly monoclinic SZ has a rate, which is only by a factor of two lower than that of partly monoclinic SZ after 2 h on stream, and exhibits “reasonably high activity”.⁴⁴ Transformations between the two phases can be triggered through mechanical stress. For pure zirconia, it has been reported that the phase transitions of crystalline ($t\text{-ZrO}_2 \rightarrow m\text{-ZrO}_2$ and $m\text{-ZrO}_2 \rightarrow t\text{-ZrO}_2$)¹⁹² or amorphous zirconia ($a\text{-ZrO}_2 \rightarrow t\text{-ZrO}_2$ or $m\text{-ZrO}_2$)¹⁹³ can be achieved by ball milling, and the transition $t\text{-ZrO}_2 \rightarrow m\text{-ZrO}_2$ can be achieved by pressing.¹⁹⁴

Obviously, the zirconia bulk is a rather dynamic system. Similarly, the large number of sulfate structures published¹⁵ may indicate a very dynamic surface. This dynamic behavior of sulfated zirconia may be the reason why it so far has been impossible to identify an active site. The system responds to many kinds of treatment like temperature and activation conditions, which prompts the question of whether sulfated zirconia is a material too sensitive to be investigated without difficulties. The aim of this research was to reveal if and how normal laboratory procedures, as they are used to prepare samples for a certain type of analysis, affect sulfated zirconia catalysts. The focus was on mechanical stress treatments such as milling and pressing, and on their effect on the bulk phase composition and the catalytic activity. To receive information on the stabilizing effect of the promoters on the bulk phase, sulfated samples containing 0.5 or 2.0 wt% Mn or Fe were investigated in addition to unpromoted SZ and pure zirconia (Z).

5.1.2 Results

5.1.2.1 Structure

Z consists of a mixture of m-ZrO₂ and t-ZrO₂ after calcination at 823 K; the fraction of m-ZrO₂ is 75–80 wt%. For SZ and promoted SZ (2.0 wt% Mn or Fe) calcined at 823 or 923 K, respectively, only t-ZrO₂ is detected (m-ZrO₂ < 5 wt%). A lower concentration of the promoter (0.5 wt% Mn or Fe) leads to a t-ZrO₂ phase containing ca. 6 wt% m-ZrO₂.

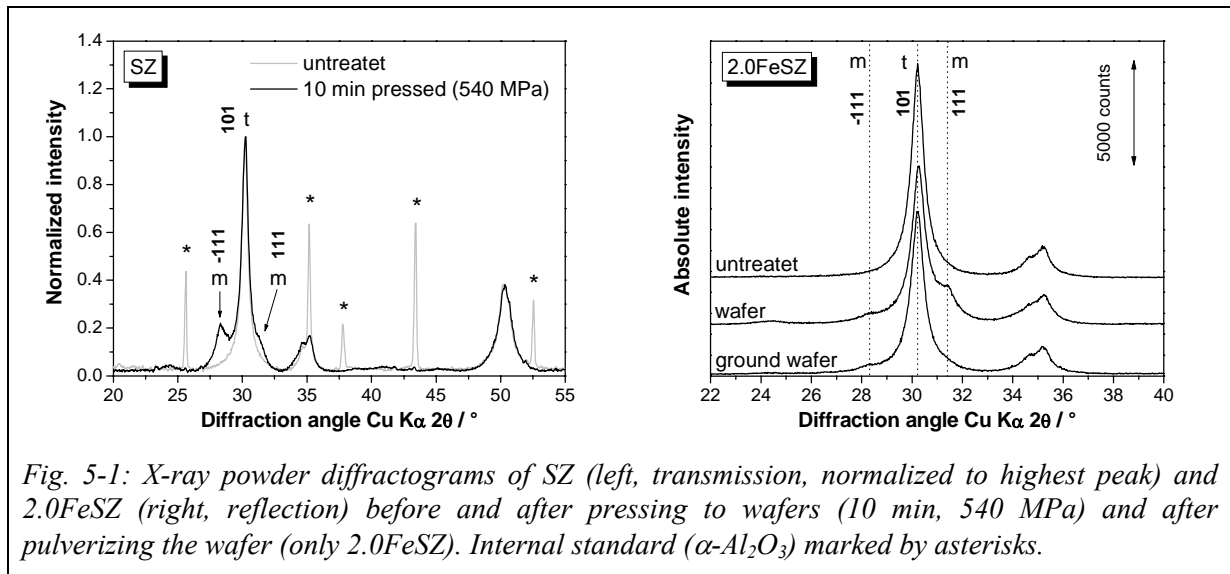


Fig. 5-1: X-ray powder diffractograms of SZ (left, transmission, normalized to highest peak) and 2.0FeSZ (right, reflection) before and after pressing to wafers (10 min, 540 MPa) and after pulverizing the wafer (only 2.0FeSZ). Internal standard (α -Al₂O₃) marked by asterisks.

In Fig. 5-1 the diffractograms of SZ and 2.0FeSZ are displayed before and after pressing to self-supporting wafers (10 min at 540 MPa). Since the wafers could not be mixed with the standard, the diffractograms of SZ measured in transmission geometry are normalized to the most intense peak (30.2°, 101 / t-ZrO₂). For samples measured in reflection mode (Bragg-Brentano geometry) normalization is unnecessary, since always the same amount was analyzed (FeSZ; Fig. 5-1, right). In 2.0FeSZ pressed to a wafer the reflection of the monoclinic phase at 31.5° (111 / m-ZrO₂) is more intense than the one at 28.2° (-111 / m-ZrO₂). If the wafer is gently ground to give a powder the intensity ratio changes; additionally the fraction of m-ZrO₂ decreases from 30±6 wt% to 20±5 wt%. Reflections of m-ZrO₂ are also present in the diffractogram of the SZ wafer, and indicate 33 wt% of m-ZrO₂. The phase composition of SZ changed even under more moderate pressing conditions. Fig. 5-2 shows diffractograms of pure and sulfated zirconia before and after pressing to pellets of 0.5–1.0 mm diameter; the pellets were ground gently prior to the XRD measurements. A pressure of 10 MPa during 2 s is sufficient to increase the fraction of m-ZrO₂ to ca. 90 wt% in Z. In SZ, which was tetragonal before the treatment, a fraction of ca. 26 wt% m-ZrO₂ is detected after pressing.

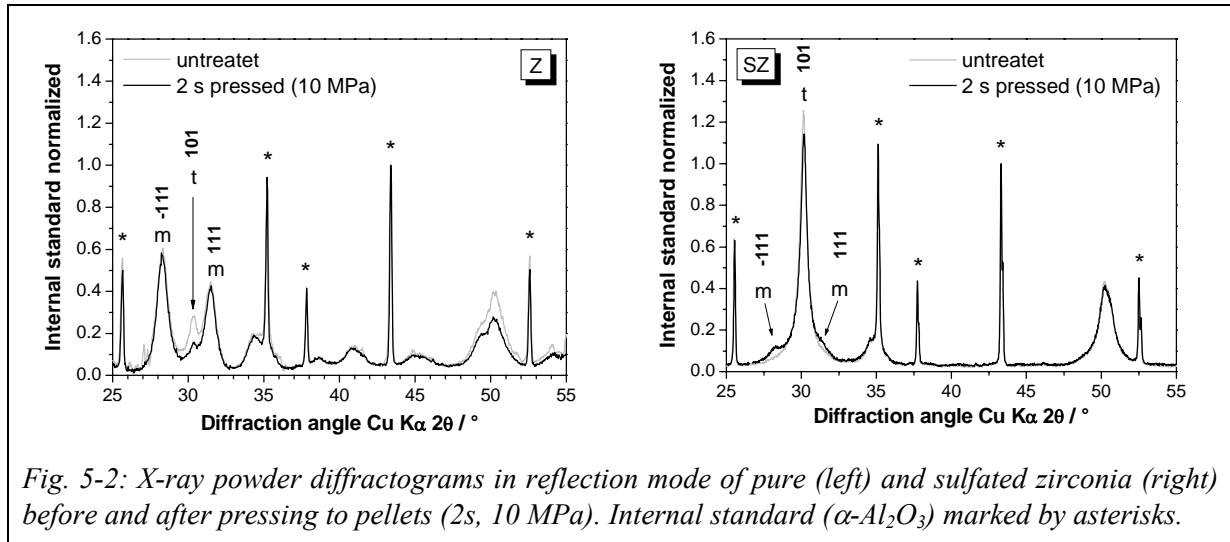


Fig. 5-2: X-ray powder diffractograms in reflection mode of pure (left) and sulfated zirconia (right) before and after pressing to pellets (2s, 10 MPa). Internal standard (α - Al_2O_3) marked by asterisks.

When Z is treated in a vibrating ball mill, the fraction of m- ZrO_2 increases from about 75 wt% in the original sample to 87 wt% after 10 min. The fraction of m- ZrO_2 in SZ (Fig. 5-3, left) is about 30 wt% after 10 min of milling. Promoting SZ with 2.0 wt% Mn or Fe does not prevent the phase transformation during milling; like for SZ ca. 30 wt% m- ZrO_2 are detected in the initially tetragonal samples after 10 min. After the same milling time 40–50 wt% of monoclinic phase is detected in the samples with lower promoter content (0.5 wt% Mn or Fe) that already contained about 5 wt% m- ZrO_2 after calcination. Fig. 5-3 (right) shows the diffractograms of unmilled and 5 or 10 min milled 0.5FeSZ; the fraction of m- ZrO_2 increases from ca. 4 wt% in the untreated sample over 38 ± 5 wt% (5 min) to 45 ± 5 wt% (10 min) with duration of milling. An increase of the relative amount of m- ZrO_2 to t- ZrO_2 with increasing milling time was observed for all samples.

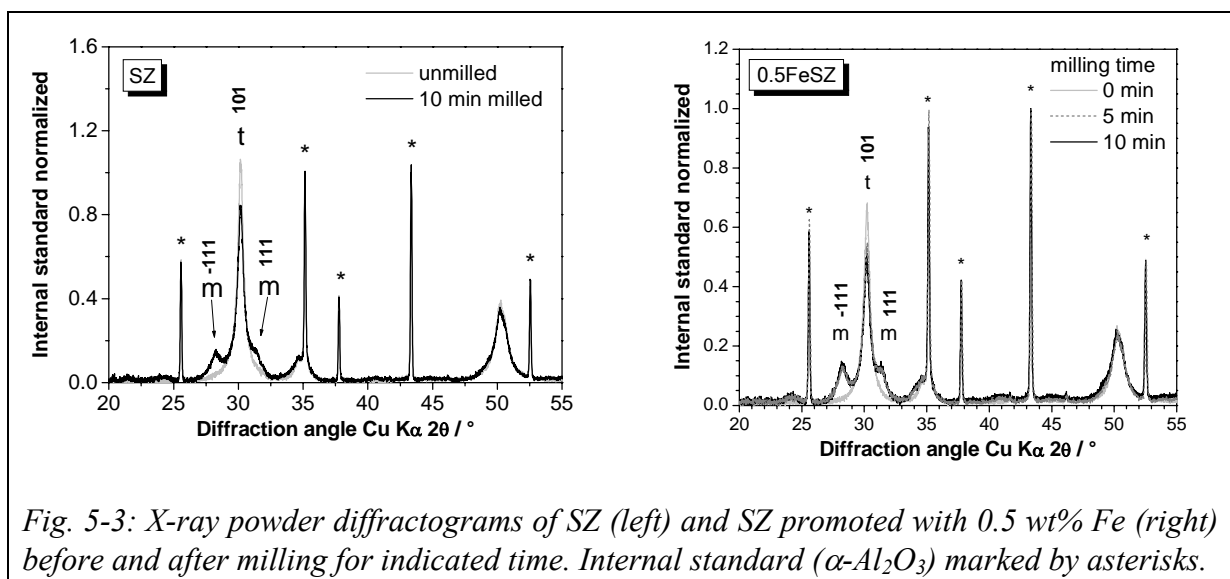


Fig. 5-3: X-ray powder diffractograms of SZ (left) and SZ promoted with 0.5 wt% Fe (right) before and after milling for indicated time. Internal standard (α - Al_2O_3) marked by asterisks.

Fig. 5-4 presents the X-ray absorption spectra (XAS) on the Mn or Fe K-edge. 2.0MnSZ shows almost no changes in the near edge structure due to milling; for 0.5MnSZ the intensity of the first two post-edge peaks in the XANES changes if the sample is milled for 10 min (Fig. 5-4, left). In FeSZ, the altered intensity ratio of the first two post-edge peaks, which is more pronounced for 0.5FeSZ than for 2.0FeSZ, indicates changes in the local structure of Fe (Fig. 5-4, right).

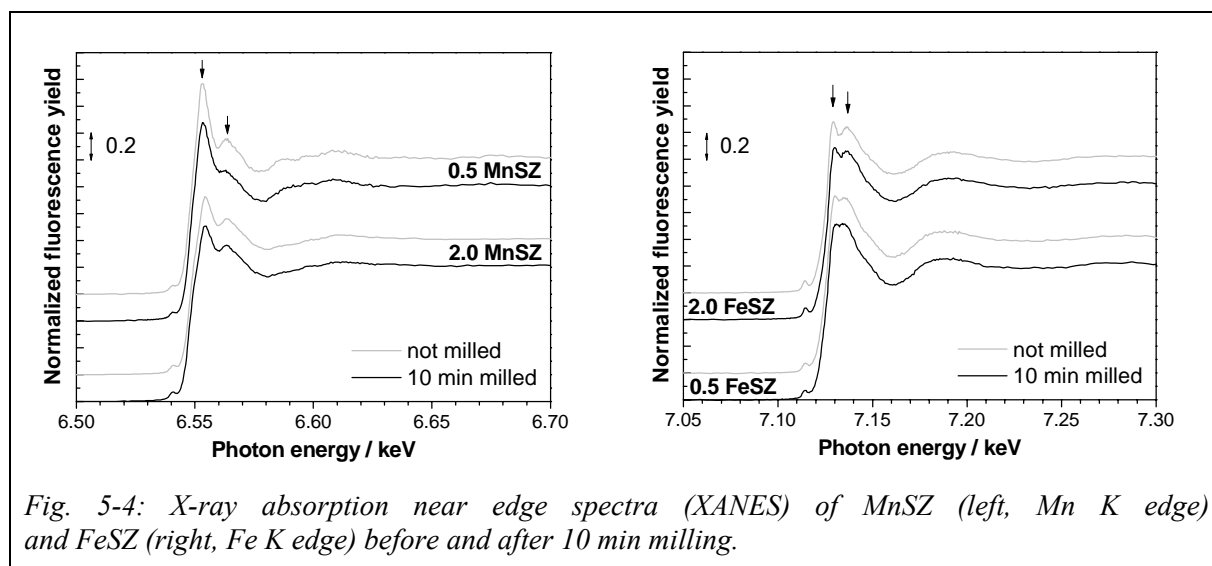


Fig. 5-4: X-ray absorption near edge spectra (XANES) of MnSZ (left, Mn K edge) and FeSZ (right, Fe K edge) before and after 10 min milling.

In Fig. 5-5 the radial distribution function (RDF) is presented for 0.5MnSZ, 2.0MnSZ, and 2.0FeSZ before and after milling. No data are available concerning 0.5FeSZ. 0.5MnSZ shows a first maximum at 1.6 Å; a second maximum is shifted from 3.5 to 3.7 Å when the sample is milled. The RDF of 2.0MnSZ has maxima at 1.3 and 2.0 Å; there is no influence of milling on the spectra. 2.0FeSZ shows only one maximum at 1.5 Å and no significant changes in the extended X-ray absorption fine structure upon 10 min milling.

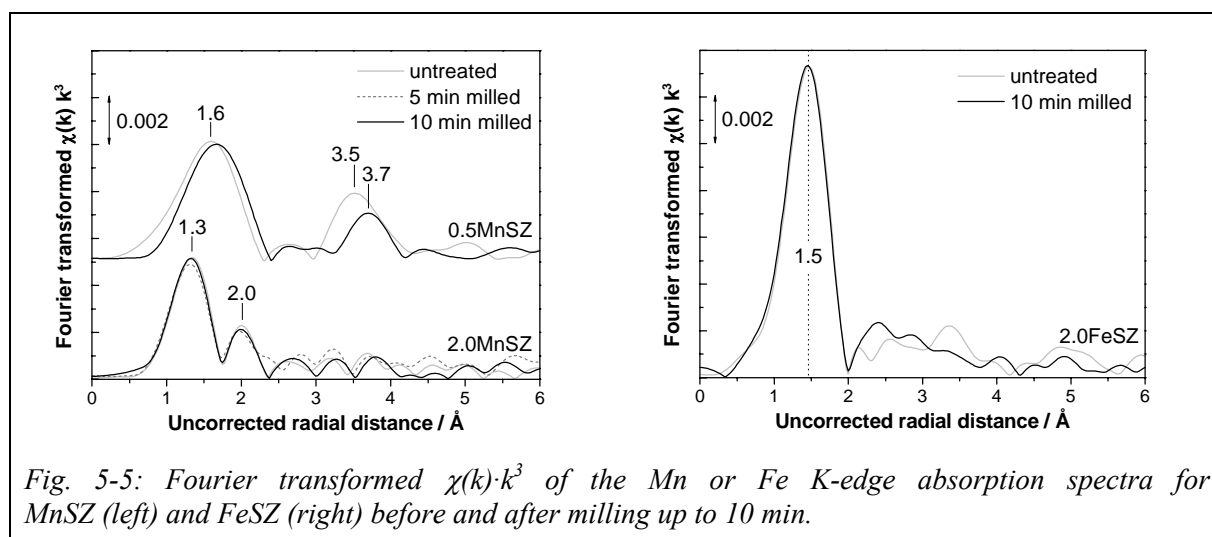


Fig. 5-5: Fourier transformed $\chi(k) \cdot k^3$ of the Mn or Fe K-edge absorption spectra for MnSZ (left) and FeSZ (right) before and after milling up to 10 min.

The average valence of Mn in the catalysts can be determined from the Mn K-edge shift of the sample relative to a Mn foil (6539 keV) after calibration with spectra of MnO and Mn₂O₃ references.^{148,195} The edge positions, edge shifts, and resulting values for the average Mn valence of 2.0MnSZ and 0.5MnSZ are listed in Tab. 5-1.

Tab. 5-1: Edge energy, edge shift relative to Mn⁰ (6539 keV), and average Mn valence of MnSZ containing 0.5 or 2.0 wt% promoter before and after milling for indicated time.

sample	milling time / min	edge energy / keV	edge shift / keV	average Mn valence
0.5MnSZ	0 min	6547.168	8.168	2.54
	10 min	6547.198	8.198	2.55
2.0MnSZ	0 min	6547.599	8.599	2.65
	5 min	6547.311	8.311	2.58
	10 min	6547.435	8.435	2.61

Only changes in the valence larger than 0.03 are significant. Milled 2.0MnSZ is slightly reduced, the average valence of Mn in 0.5MnSZ is lower than in 2.0MnSZ and unaffected by milling.

5.1.2.2 Surface Area

BET surface areas were measured after outgassing the samples in vacuo at 473 K for 16 h using a *Quantasorb Junior* or an *Autosorb-6* apparatus. The results are listed in Tab. 5-2.

Tab. 5-2: BET surface areas of the investigated catalysts after milling in 300 g batches for indicated time before and after *n*-butane isomerization at 323 K.

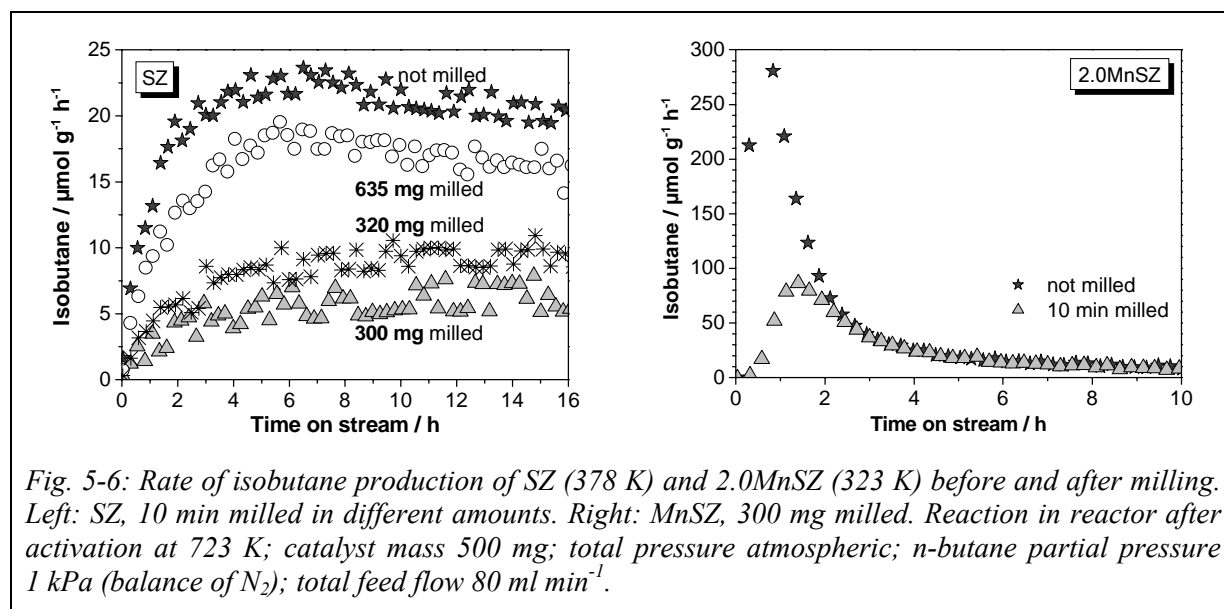
	0 min (= not milled)	5 min milled	10 min milled
	before reaction		
SZ*	129 m ² g ⁻¹		135 m ² g ⁻¹
0.5MnSZ*	114 m ² g ⁻¹		
2.0MnSZ	107 m ² g ⁻¹		
2.0MnSZ*	112 m ² g ⁻¹		119 m ² g ⁻¹
0.5FeSZ	106 m ² g ⁻¹		
2.0FeSZ	114 m ² g ⁻¹		
	after reaction		
0.5MnSZ	105 m ² g ⁻¹	105 m ² g ⁻¹	103 m ² g ⁻¹
2.0MnSZ	105 m ² g ⁻¹	105 m ² g ⁻¹	104 m ² g ⁻¹
0.5FeSZ	104 m ² g ⁻¹	106 m ² g ⁻¹	105 m ² g ⁻¹
2.0FeSZ	108 m ² g ⁻¹	109 m ² g ⁻¹	

* measured with Quantasorb Junior (all others with Autosorb-6)

SZ has with ca. 130 m² g⁻¹ the highest surface area, which increases slightly upon milling. Also for 2.0MnSZ a higher surface area is observed after milling. The surface areas of all

promoted samples are about $110 \text{ m}^2 \text{ g}^{-1}$. The areas seem to decrease during reaction, especially if the catalysts were milled. Milling does not seem to influence the pore size distribution. According to the BJH method, all samples possess pores in the 2–3 nm range.

5.1.2.3 Catalytic Performance



Tests of the catalytic activity in *n*-butane isomerization focus on untreated or milled samples because these materials can be tested as fixed powder beds without further sample manipulation. The tests were conducted in a tubular fixed bed reactor using 500 mg of catalyst or an *in situ* DRIFTS cell (about 160 mg). The results received in these different setups are similar and show the same trends.^{179,196} In Fig. 5-6 the isobutane production rate measured in the tubular reactor is plotted as a function of time on stream for untreated and milled sulfated zirconia catalysts. The amount of sample used for milling influences the rate: Milling of 635 mg SZ for 10 min results in a rate reduced to 80 % of its value for the unmilled sample; SZ milled for 10 min in 300 mg batches passes through an induction period similar to the one observed for its unmilled state, but there is no deactivation within 16 h and the maximum isobutane formation rate is reached later (10 vs. 6 h on stream) and is severely reduced after the treatment to only about 25 % of its value for untreated SZ (Fig. 5-6, left). The initial maximum conversion to isobutane of 2.0MnSZ is similarly reduced from 280 to $85 \text{ } \mu\text{mol g}^{-1} \text{ h}^{-1}$ by milling; the long term activity ($> 2 \text{ h}$) remains unaffected (Fig. 5-6, right). The results obtained for 2.0MnSZ in the DRIFTS cell confirm the decrease of the maximum rate with milling time (0 min: $197 \text{ } \mu\text{mol g}^{-1} \text{ h}^{-1}$; 5 min: $128 \text{ } \mu\text{mol g}^{-1} \text{ h}^{-1}$; 10 min: $95 \text{ } \mu\text{mol g}^{-1} \text{ h}^{-1}$).

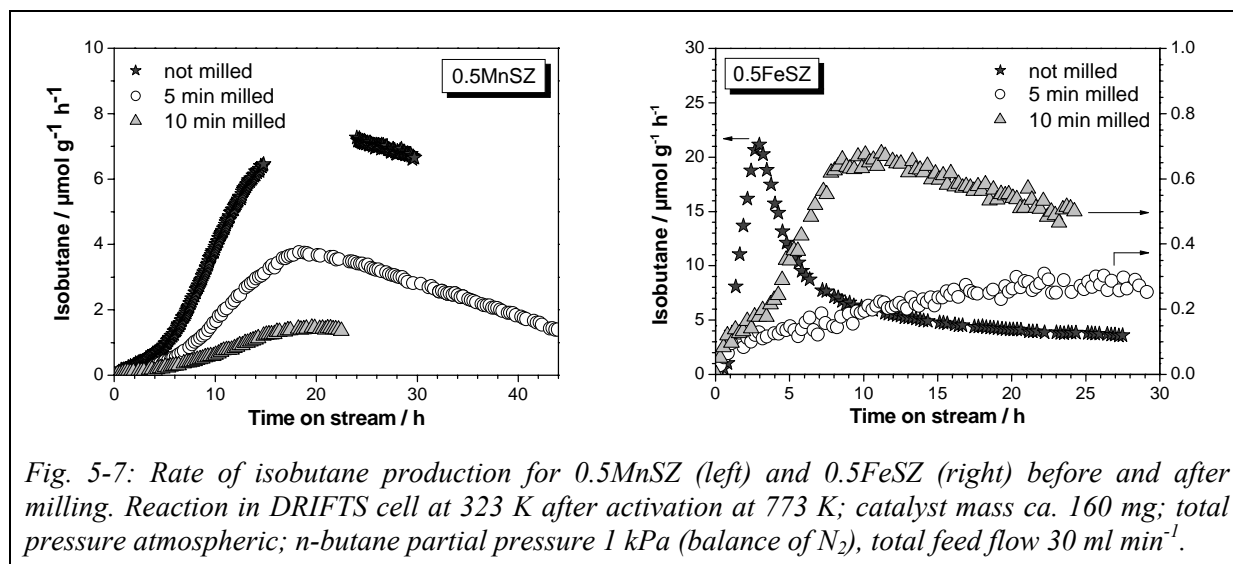


Fig. 5-7: Rate of isobutane production for 0.5MnSZ (left) and 0.5FeSZ (right) before and after milling. Reaction in DRIFTS cell at 323 K after activation at 773 K; catalyst mass ca. 160 mg; total pressure atmospheric; *n*-butane partial pressure 1 kPa (balance of N₂), total feed flow 30 ml min⁻¹.

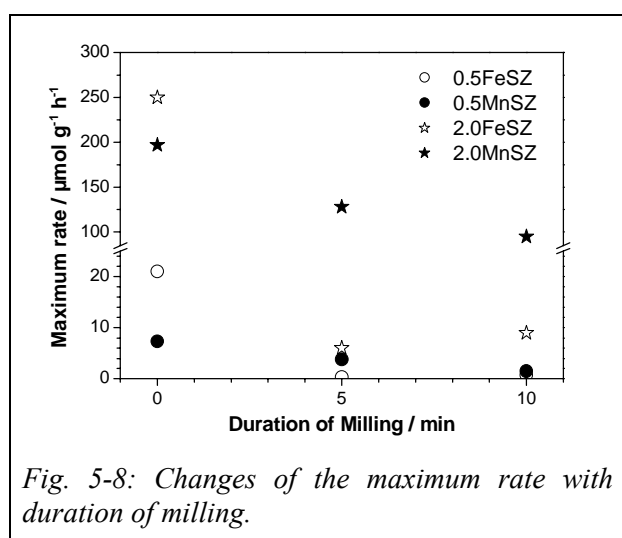


Fig. 5-8: Changes of the maximum rate with duration of milling.

0.5MnSZ with lower promoter content reaches the maximum rate extremely late, after 19 h time on stream (Fig. 5-7, left). The observed decrease in rate with increased milling time (0 min: $\geq 7.3 \mu\text{mol g}^{-1} \text{h}^{-1}$; 5 min: $3.8 \mu\text{mol g}^{-1} \text{h}^{-1}$; 10 min: $1.5 \mu\text{mol g}^{-1} \text{h}^{-1}$) is comparable to that of 2.0MnSZ. Both catalysts containing Fe show drastic changes in the rate profile after 5 min milling; the rate maximum of $250 \mu\text{mol g}^{-1} \text{h}^{-1}$ (2.0FeSZ) or $21 \mu\text{mol g}^{-1} \text{h}^{-1}$ (0.5FeSZ) disappears after 5 min milling and the resulting rate of $6 \mu\text{mol g}^{-1} \text{h}^{-1}$ (2.0FeSZ) or $0.3 \mu\text{mol g}^{-1} \text{h}^{-1}$ (0.5FeSZ) is lower than the long-term rate of the unmilled catalysts, which is $20 \mu\text{mol g}^{-1} \text{h}^{-1}$ (2.0FeSZ) or $4 \mu\text{mol g}^{-1} \text{h}^{-1}$ (0.5FeSZ) after 18 h time on stream. Longer milling times (10 min) resulted in a higher rate with a maximum of $9 \mu\text{mol g}^{-1} \text{h}^{-1}$ (2.0FeSZ) or $0.7 \mu\text{mol g}^{-1} \text{h}^{-1}$ (0.5FeSZ). In Fig. 5-7 (right) the influence of milling on the rate is displayed for 0.5FeSZ; Fig. 5-8 presents an overview over the influence of milling time on the maximum rate for all promoted catalysts.

5.1.2.4 DRIFT Spectroscopy and TG

From the spectra obtained after activation (30 min at 773 K) in the DRIFT cell it is obvious that the intensity of the sulfate vibrations is lower for milled than for untreated catalysts. The band intensity increases with the number of vibrating groups and is thus a measure for concentration. In Fig. 5-9 the overtones of the sulfate vibrations are depicted for 0.5MnSZ.

For MnSZ the band area of the sulfate vibrations decreases with milling time. However, in 2.0FeSZ the sulfate bands after 10 min milling are more intense than after 5 min, while the milling time had not much influence on the band area of 0.5FeSZ. The sulfate content can be estimated by means of thermogravimetry coupled with mass spectrometry (see Chapter 3.3); the weight loss at about 1000 K is attributed to the decomposition of sulfate (evolution of SO₂ and O₂). This weight loss is 4.6 wt% for the unmilled SZ and 4.2 wt% for the 10 min milled SZ. The respective weight loss for unmilled 0.5FeSZ amounts to 4.0 wt% and to 3.9 wt% for 5 and 10 min milled 0.5FeSZ. The high temperature stable sulfate species described in Chapter 3.3 is still present after milling. Since it is only a small fraction of the total sulfate (1–5 %), an influence of milling on its amount is not measurable. As there are results indicating that only a fraction of the sulfate actually contributes to the catalytic activity,^{143,v} the significance of this species remains to be clarified. The trends observed for the sulfate band intensity of MnSZ and FeSZ correlate with the changes in isomerization activity with milling time as shown in Fig. 5-10, where the maximum rate is plotted versus the area under the sulfate band at 2763 cm⁻¹.

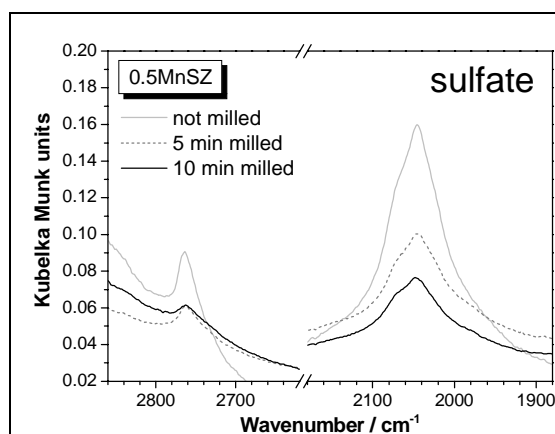


Fig. 5-9: DRIFT spectra of milled and untreated 0.5MnSZ after activation at 773 K showing sulfate overtone vibrations.

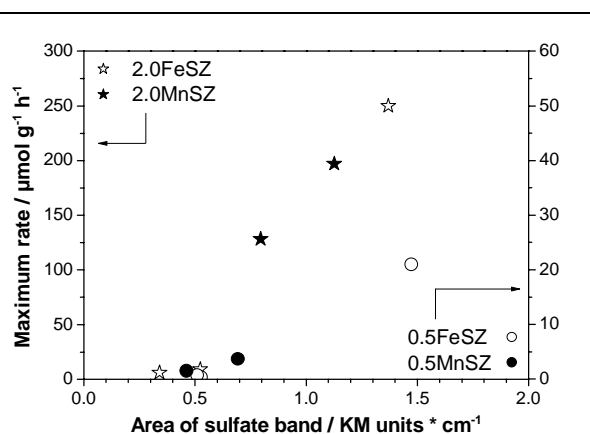


Fig. 5-10: Correlation of maximum rate with area of sulfate band at 2763 cm⁻¹ after activation for milled and untreated samples.

^v S. Wrabetz, F.C. Jentoft, unpublished results.

5.1.3 Discussion

5.1.3.1 Structural Changes Induced by Pressing

A pressure of 540 MPa equals about the pressure necessary in the making of self-supporting wafers for transmission IR spectroscopy; it has already been reported that wafers of pure zirconia may contain an increased fraction of m-ZrO₂.¹⁹⁴ Also a lower pressure of only 10 MPa causes a phase transformation to m-ZrO₂ (see Fig. 5-2). Despite the presence of sulfate which stabilizes the tetragonal phase, at least with respect to thermal treatments,¹⁹⁷ tetragonal SZ is partly transformed to m-ZrO₂ when pressed to a wafer. The t-ZrO₂ → m-ZrO₂ transformation is not prevented but decelerated by Fe promotion. Measurements at the 2.0FeSZ wafer show a preferential orientation of the m-ZrO₂ crystallites indicated by the unusual intensity ratio of the m-ZrO₂ peaks at 28.2° and 31.5°. The preferential orientation vanishes upon pulverization and the m-ZrO₂ fraction decreases. Because of the high absorption coefficient of Zr (ca. 890 cm⁻¹ at 8 keV Cu K α radiation) the X-rays penetrate only the upper layers of the wafer. The surface of the wafer is thus enriched with m-ZrO₂ and the t-ZrO₂ → m-ZrO₂ phase transformation does not affect the whole wafer. To reach random distribution of the m-ZrO₂ crystallites, the wafer is pulverized. This was done very gently, since it was known that grinding of promoted SZ (0.5 wt% Mn) results in a t-ZrO₂ → m-ZrO₂ phase transformation with simultaneous loss in catalytic activity.¹⁹⁸ For pure zirconia it is reported that also gentle grinding in a mortar at room temperature leads to an increase of m-ZrO₂.¹⁹⁹ Here, in 2.0FeSZ the m-ZrO₂ fraction is lower after pulverization. Further monoclinization during the grinding can, thus, be excluded. Moreover, the assumption is supported that the wafer is only monoclinic in the outer part.

5.1.3.2 Milling

Formation of m-ZrO₂ occurs also when the mechanical stress is induced by milling. There are hints that conditions less forceful than in a ball mill suffice for the t-ZrO₂ → m-ZrO₂ transition: Whitney observed that gentle grinding of pure zirconia in a mortar at room temperature is sufficient to rapidly transform t-ZrO₂ into m-ZrO₂; he attributed this to the formation of dislocations in the lattice, which act as nucleation sites for m-ZrO₂.¹⁹⁹ However, the extent of phase transformation during manual grinding is poorly reproducible: The partial transition from t-ZrO₂ to m-ZrO₂ in 0.5MnSZ upon 10 min grinding resulted in an increase of m-ZrO₂ from about 8 wt% to 19 or 57 wt%.¹⁹⁸ To exclude an operator influence, milling was performed in a vibrating ball mill.

Effects observed during milling of pure zirconia are consistent with reports in the literature.^{192,193} The phase stability of SZ-based catalysts and their activity in *n*-butane isomerization are influenced both by the duration of milling and the amount of the sample that is subjected to the treatment. The longer the milling time or the less powder is milled, the more intensive is the contact with the ball in the mill and, thus, the mechanical stress exerted on the sample. A comparison of the extent of phase transformation for sulfated zirconia materials with that for pure zirconia is difficult because of the different initial m-ZrO₂ content.

The initially tetragonal SZ contains 30 wt% m-ZrO₂ after 10 min milling and its rate of isobutane formation is reduced to 25 % compared to unmilled SZ; addition of 2 wt% Fe or Mn cannot prevent the phase transformation but results in a similar fraction of m-ZrO₂. Samples with lower promoter content of 0.5 wt% are more sensitive to the treatment. This might be, because they are already partly monoclinic before the milling. The fraction of m-ZrO₂ in SZ is larger in samples calcined at a higher temperature.⁴¹ Promoters lead to further stabilization of the tetragonal phase, so that catalysts containing 2 wt% manganese or iron are tetragonal after calcination at 100 K higher temperature compared to that of unpromoted SZ. However, in the presence of only 0.5 wt% promoter monoclinization cannot be prevented at this higher temperature. Because Mn ions can be incorporated into the t-ZrO₂ lattice^{38,190,191} and a number of different (incorporated) cations are known to stabilize the tetragonal phase,³⁸ Mn-promoted sulfated zirconia might be expected to remain unaffected by milling; but this is not the case. Also for promoted samples, milling resulted in a reduced rate. However, in 2.0MnSZ only the induction period during the first 2 h is concerned, whereas in Fe-promoted SZ additionally the long term activity after 30 h is reduced upon milling. Possibly, also for 0.5MnSZ only the maximum rate is reduced, but this is reached only after 19 h even for the untreated sample so that the steady state could not be reached within 30 h (see Fig. 5-7). Changes in local structure of the Mn or Fe (Fig. 5-4 and Fig. 5-5) are consistent with a phase change. Both are more pronounced for samples with lower promoter content. The average Mn valence is lower in the sample with less promoter, which is much less active than 2.0MnSZ. This is in line with the observed linear correlation between the average Mn valence after activation and the maximum rate in *n*-butane isomerization.¹⁴⁸

After 10 min milling the BET surface areas of SZ and 2.0MnSZ are about 5 % higher than before the treatment. This is expected when the particle size is decreased, and milling is a possibility to increase the surface area of catalysts. A larger surface area should lead to a higher activity. But this is not the case for SZ-based catalysts that always show a lower rate of isobutane formation when milled. After reaction, when the catalysts are partly deactivated, the

surface areas of milled and unmilled samples are lower than before reaction and show no significant differences. Thus, either the particles sintered, which does not seem likely because of the low reaction temperature, or the accessible surface area is reduced due to coke deposits produced from adsorbed hydrocarbons.

The sulfate vibrations in the DRIFT spectra decrease in intensity when samples are milled which indicates a loss of sulfate or a reduction to e.g. sulfite. From the thermal analysis of SZ it is obvious that sulfur is lost. The TG data of promoted samples point in the same direction, but the differences in sulfate content are very small and within the errors of the measurement. For Fe-promoted samples the catalytic activity after 10 min milling is exceeding the one after 5 min treatment, while the amount of m-ZrO₂ is increasing with duration of milling. Rather than with the phase change the catalytic activity is correlated to the sulfate content of the samples, which shows a similar trend. The correlation of the maximum rate with the band area of the sulfate overtone at 2763 cm⁻¹ (see Fig. 5-10) for samples with 2 wt% promoter does not pass through the origin, which means that the band is overlapping with another species that has no influence on the rate. The sulfate loss due to milling is low; it amounts to 2.5 wt% in case of 0.5FeSZ. Instead the band area is decreased by 65 %. This observations indicates that a minor sulfate species is responsible for activity, since the absence of this species leads to a loss in activity.

5.1.4 Summary

For many experiments it is necessary or common practice to press powders, e.g. in order to produce particles of a certain size for a catalytic test, to produce a wafer or pellet for transmission spectroscopy, or to avoid uncontrolled distribution in a vacuum environment. Equally, grinding is often used to homogenize samples or to mix them with standards or diluents. Particularly *in situ* experiments often require such sample preparation techniques.

The presented results demonstrate that all these “standard laboratory practice” treatments do not only convert the metastable tetragonal phase of ZrO₂ into the thermodynamically stable monoclinic phase, but concomitantly alter the catalytic properties of sulfated zirconia catalysts. The sensitivity towards mechanical stress renders investigation of sulfated zirconia catalysts difficult and explains why the system has so far escaped fundamental understanding. Data correlation is hindered because data obtained in experiments that involve different sample handling procedures can reflect the properties of partially different materials and, thus, do not represent pieces of the same puzzle.

5.2 Storage and Aging of Sulfated Zirconia-Based Catalysts

5.2.1 Motivation

As shown in the preceding chapter (5.1), zirconia is a sensitive material. Even after stabilization by sulfate and cationic transition metals, mechanical stress like grinding, milling, or pressing induces changes in its structure and catalytic activity.¹⁹⁸ Alterations in catalytic performance of SZ are also observed with time of storage. A freshly calcined SZ sample tested in an *in situ* UV-vis cell²⁰⁰ has a shorter induction period (43 instead of 90 min) and a higher yield (9.7 vs. 6.0 %) than a catalyst stored in the laboratory for 60 days.²⁰¹ Crystallization and phase transformations of amorphous zirconia are accelerated under hydrothermal conditions.²⁰² Bulk phase transformations of doped zirconia occur at 338–393 K within 120 h (Y-doped) or at 353–573 K within 160–360 h (Ce-doped) in the presence of water vapor.^{203,204} Even in the framework of zeolites, changes are detected when they are exposed to moisture over months.²⁰⁵ In order to understand the aging phenomenon observed for SZ and to elucidate the influence of water in the storage atmosphere, systematic investigations are needed. Thus SZ and MnSZ (2.0 wt% manganese) were stored in three different concentrations of water vapor directly after calcination: (i) in a laboratory cupboard, (ii) in air saturated with water vapor at 313 K (“tropical”), (iii) in dry Ar atmosphere (glovebox). After certain aging times, BET surface areas of the differently stored catalysts were measured, their bulk phase was analyzed by XRD, and their activity in *n*-butane isomerization was tested.

5.2.2 Results

5.2.2.1 Color, Moisture, and Structural Changes upon Aging

The aged MnSZ samples exhibit an increase in darkness from grey to dark grey in the order laboratory << glovebox < tropical. SZ remains white. BET surface areas measured with a *Quantachrome Autosorb-1* are constant during 7 months and amount to about 140 m²/g for SZ and to 115±8 m²/g for the promoted samples. Before the BET measurements, the catalysts were degassed for 16 h at 473 K to remove adsorbed water. An estimation of the water content is possible by comparing the weight of each sample before and after the outgassing. The loss in weight increases with the water content of the storage atmosphere: glovebox < laboratory < tropical (Tab. 5-3).

This observation is supported by IR spectroscopy, which permits information about the water content of the catalysts. DRIFT spectra of MnSZ after 7 months aging in dry (glovebox)

and wet (tropical) atmosphere are compared in Fig. 5-11. The range 3600–3000 cm^{-1} is typical for hydroxyl stretching vibrations, the OH bending mode of adsorbed water is located around 1600 cm^{-1} , the combination of stretching and bending vibrations of water gives rise to a band around 5200 cm^{-1} (see Chapter 3.4). Before thermal treatment (activation procedure) of the catalysts, MnSZ stored under tropical conditions contains much more water than MnSZ stored in the glovebox, the area under the water deformation peak centered at 1600 cm^{-1} is ca. 2.5 times larger. This correlates well with the weight loss observed during outgassing, which is 2.4 times larger for MnSZ stored under tropical conditions (see Tab. 5-3). After the heat treatment most of the water is removed and the combination mode centered at 5220 cm^{-1} (glovebox) or 5180 cm^{-1} (tropical) disappeared. Still the samples are slightly hydrated; the bands observed around 1600 cm^{-1} possess nearly the same integral intensity, indicating that the water content of both samples is similar. However, the amount of hydroxyl groups present after activation is larger for MnSZ aged under tropical conditions. Instead, the intensity of the band at 2336 cm^{-1} due to the stretching vibration of adsorbed N_2 is larger for MnSZ stored in the glovebox. The DRIFT spectra of MnSZ aged in the laboratory do not change significantly over years, band positions remain unchanged.

Tab. 5-3: Weight loss during outgassing (16 h, 473 K) prior to BET measurements

	SZ	MnSZ
glovebox	3.12 %	4.91 %
laboratory	5.91 %	7.07 %
tropical	11.55 %	11.63 %

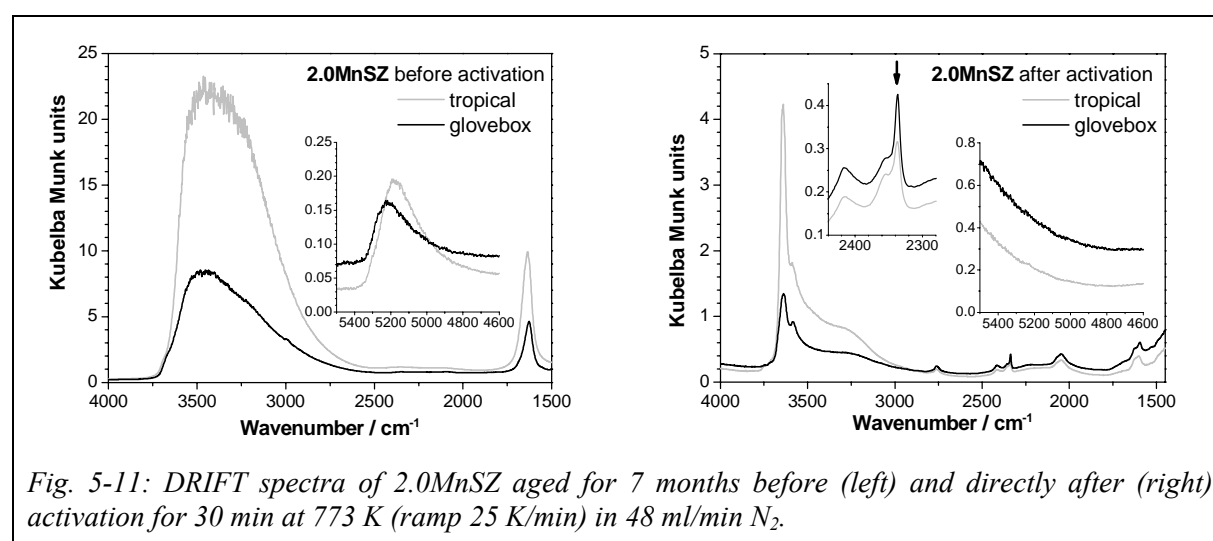


Fig. 5-11: DRIFT spectra of 2.0MnSZ aged for 7 months before (left) and directly after (right) activation for 30 min at 773 K (ramp 25 K/min) in 48 ml/min N_2 .

All samples are tetragonal after calcination for 3 hours at 823 K (SZ) or 923 K (MnSZ). For MnSZ, independent of the atmosphere no changes in phase composition are discernable in

the X-ray diffractograms upon aging up to six months, whereas for SZ when aged under tropical conditions already after two months monoclinic reflections appear that increase in intensity with longer aging times (Fig. 5-12). After six months in tropical atmosphere, the total amount of crystalline material seems to be increased. However, the results are not necessarily quantitative, since the moist samples and the Al_2O_3 standard do not mix very well, but tend to separate. When aged in the glovebox, SZ is still tetragonal after two months, but after six months monoclinic reflections become visible. SZ aged in the laboratory is most stable; after nine months only tetragonal reflections are measured.

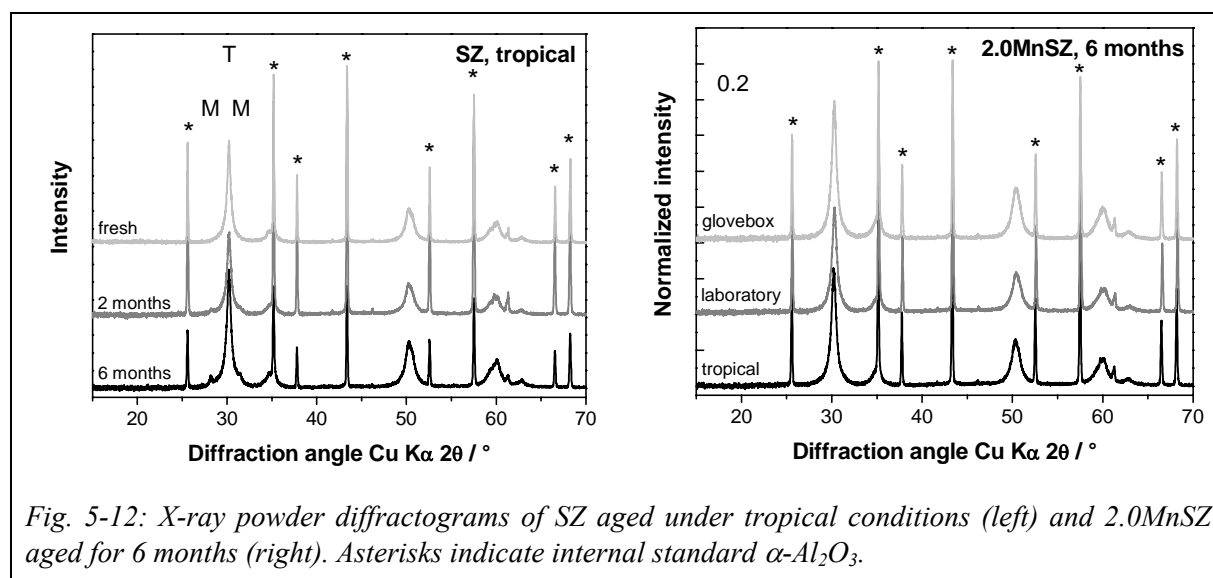


Fig. 5-12: X-ray powder diffractograms of SZ aged under tropical conditions (left) and 2.0MnSZ aged for 6 months (right). Asterisks indicate internal standard α - Al_2O_3 .

5.2.2.2 Changes in Catalytic Performance with Aging Time

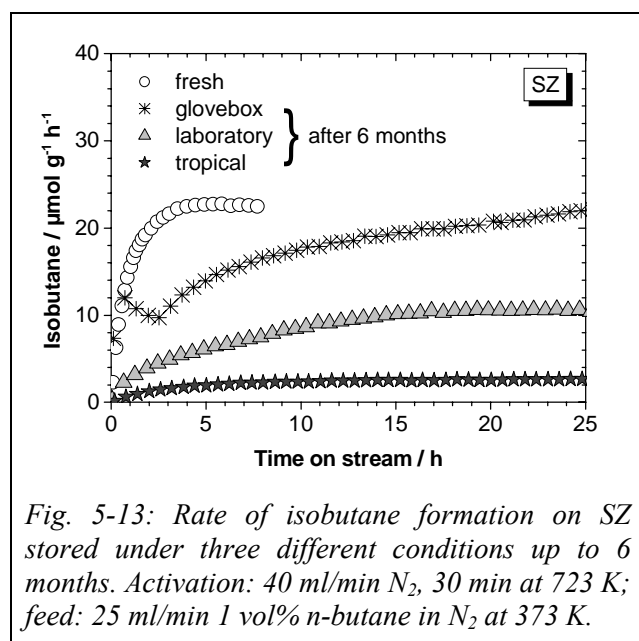


Fig. 5-13: Rate of isobutane formation on SZ stored under three different conditions up to 6 months. Activation: 40 ml/min N_2 , 30 min at 723 K; feed: 25 ml/min 1 vol% *n*-butane in N_2 at 373 K.

Isomerization was carried out after activation in 40 ml/min nitrogen at 723 K using 25 ml/min 1 vol% *n*-butane in nitrogen at 373 K (SZ) or 323 K (MnSZ). Unpromoted SZ catalysts hardly deactivate. Fig. 5-13 shows the isomerization rate of fresh and 6 months aged SZ. After calcination, the maximum rate after ca. 3 h amounts to about 20 $\mu\text{mol g}^{-1} \text{h}^{-1}$. Six months storage in the laboratory lead to a delay and a decrease: The maximum rate of about 10 $\mu\text{mol g}^{-1} \text{h}^{-1}$ is reached only

after ca. 17 h time on stream. Storage under tropical conditions results in a clearly visible decrease of the maximum rate to about $3 \mu\text{mol g}^{-1} \text{h}^{-1}$. SZ stored in the glovebox for six months has a local maximum in rate after 1 h, after 2.5 h the rate increases again and is after 25 h as high as in the fresh catalyst. This behavior was reproduced with a second sample.

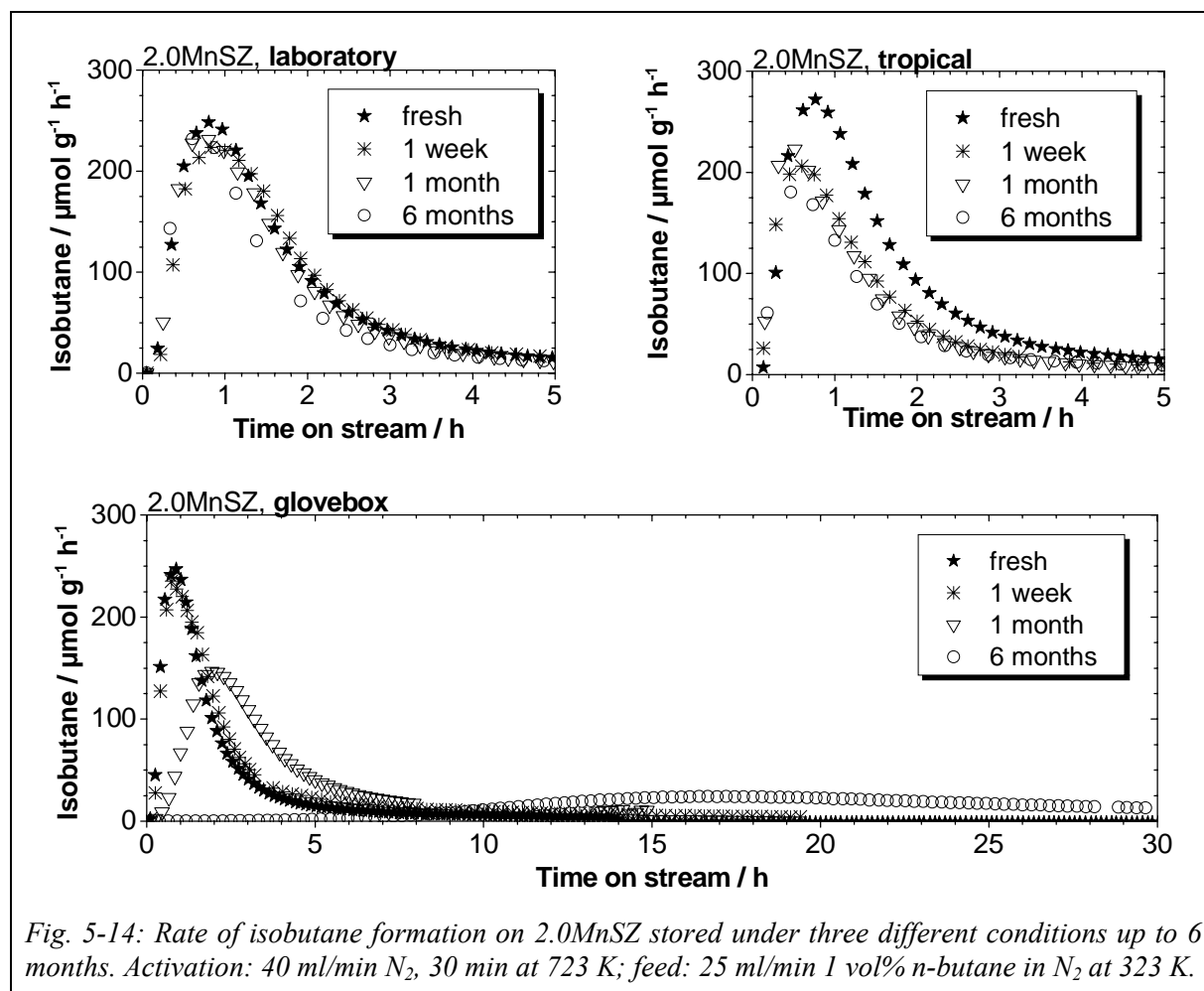


Fig. 5-14: Rate of isobutane formation on 2.0MnSZ stored under three different conditions up to 6 months. Activation: 40 ml/min N_2 , 30 min at 723 K; feed: 25 ml/min 1 vol% n-butane in N_2 at 323 K.

The catalytic performance of MnSZ is more strongly influenced by the storage conditions than that of SZ. Fig. 5-14 compares the rates of isobutane formation of fresh MnSZ and MnSZ stored for the time of one week up to half a year in the laboratory, exposed to water vapor, or in the H_2O ($< 1 \text{ ppm}$) and O_2 ($\leq 8 \text{ ppm}$) depleted environment of a glovebox. The activity profile of MnSZ kept in the laboratory does not change significantly during half a year. The sample stored under tropical conditions shows a decrease in maximum rate after one week, but no significant changes during further aging. Drastic changes are observed in the isomerization activity of MnSZ stored in the glovebox: The maximum rate decreases from ca. 250 to 150 $\mu\text{mol g}^{-1} \text{h}^{-1}$ after one month and to only 24 $\mu\text{mol g}^{-1} \text{h}^{-1}$ after half a year; concomitantly the maximum shifts from about 1 to 16 h time on stream. The integral conversion to isobutane during the observation span up to 30 h (Fig. 5-14, below) decreases

from 589 $\mu\text{mol g}^{-1}$ after one week storage to 409 $\mu\text{mol g}^{-1}$ after six months in the glovebox. The amount of isobutane produced is, thus, in the same order of magnitude as the promoter content in the MnSZ samples, which amounts to 364 $\mu\text{mol g}^{-1}$.

5.2.3 Discussion

The catalytic performance of all samples is deteriorated upon aging. The degree of activity loss is determined by the storage atmosphere. A possible explanation for the difference in activity could be changes to the bulk structure of the catalyst.¹⁹⁸ For SZ, appearance of a monoclinic phase is observed for samples aged in water rich (tropical) and less pronounced in water and oxygen poor atmosphere (glovebox). A phase change from tetragonal to monoclinic zirconia has been suggested to cause deactivation,^{136,146} since monoclinic SZ is less active than tetragonal SZ.^{43,45} However, after six months aging in the laboratory, SZ is still tetragonal, but less active than SZ stored in the glovebox. A decrease in activity due to an increase of the monoclinic fraction alone seems, thus, unlikely. This is supported by the fact that the diffractograms of fresh and aged MnSZ indicate only tetragonal zirconia without visible effect of the different conditions, whose influence on the performance is even greater than for SZ. The aged samples differ explicitly in the H₂O content, as evidenced by weight loss during heating and in the DRIFT spectra. Activated in flowing nitrogen, 2.0MnSZ possesses more OH groups (Brønsted sites) and a smaller amount of adsorbed N₂ (Lewis sites) after aging under tropical conditions than after storage in the glovebox. The 'right' amount of H₂O on the catalyst has been inferred to be important and concentrations of 75 $\mu\text{mol g}^{-1}$ or 200 $\mu\text{mol g}^{-1}$ have been proposed to result in best performance.^{206,207} From the relative intensities of sulfate and OH stretching bands in the DRIFT spectra after aging in the laboratory (not shown), the glovebox, and under tropical conditions (see Fig. 5-11, right), it can be concluded that MnSZ is further hydroxylated under tropical conditions rather than dehydroxylated in the glovebox. Excess water from humid storage conditions can be removed in the activation procedure before the isomerization reaction,¹⁹⁶ but lacking water due to dry storage conditions would not be replenished. However, traces of water from the feed system may adsorb on the catalyst while on stream. This scenario could explain why the MnSZ catalyst that had been stored in the glovebox for six months started producing isobutane after ca. 10 h on stream. The maximum rate, though, was only $1/10$ of that of the fresh sample (see Fig. 5-14). The differences in color of differently stored MnSZ might also be explained by different moisture content. However, a change in the Mn oxidation state could also be responsible for the color change in the MnSZ samples. Aging in the glovebox has an effect on

the catalytic activity of SZ, but not as dramatic as in case of MnSZ. This means that the changes upon storage in the glovebox are concerning manganese, which e.g. could be reduced. This would be consistent with the observed decrease in the maximum rate of isobutane formation with the average Mn valence after activation.¹⁴⁸

5.2.4 Conclusions and Outlook

The storage conditions (temperature, O₂ and H₂O partial pressure) can influence the performance of sulfated zirconia catalysts. Storage in the laboratory proved to be the best way to prevent a loss in catalytic activity of MnSZ and structural changes in case of SZ. A phase transformation of tetragonal to monoclinic zirconia is favored by water, consistent with the literature,^{202–205} and by the oxygen depleted atmosphere in a glovebox. The tetragonal phase might be just a prerequisite to generate sites connected to defects. A reduction of Zr⁴⁺ to Zr³⁺ and formation of oxygen vacancies could result in a sevenfold coordination of the metal ions, as in the monoclinic phase of zirconia, and facilitate the phase transformation. For MnSZ, the decrease in isomerization rate upon aging in the glovebox could be caused by a reduction of manganese ions to Mn²⁺.

The decrease in catalytic activity of SZ by ca. 90 % after 6 months aging under tropical conditions is not proportional to the phase transformation into monoclinic zirconia of less than 25 wt%. Possibly, the fraction of the tetragonal phase that is most active and probably connected to the defects is converted most easily. This could explain the unproportional loss in activity and should be investigated further.

The sensitivity of sulfated zirconia catalysts towards the aging conditions holds the possibility to generate different materials from the same parent compound through variation of these conditions. Such samples provide a unique opportunity to identify properties that are relevant for activity.

6. Sites of Sulfated Zirconia-Based Catalysts

A useful tool to investigate the sites of metal oxide catalysts is adsorption of probe molecules and observation of the corresponding IR spectra. The most commonly used probes to detect acid sites on sulfated zirconia are CO and pyridine (see Chapter 2.3). However, characterization of the activated (dehydrated) catalysts does not necessarily provide any information about the catalytic performance in *n*-butane isomerization, since the sulfated zirconias are only pre-catalysts that need to be in contact with the feed during the so called induction period to become active. Nevertheless, there are two possibilities to get information on activity: (i) experiments can be carried out “quasi *in situ*” which means that reaction is carried out for certain times on stream prior to adsorption, or (ii) the reactant can be used as probe. Both approaches were used and the results are described in chapter 6.1 and 6.2.

6.1 Quasi *in situ* *n*-butane isomerization and CO adsorption on FeSZ

6.1.1 Motivation

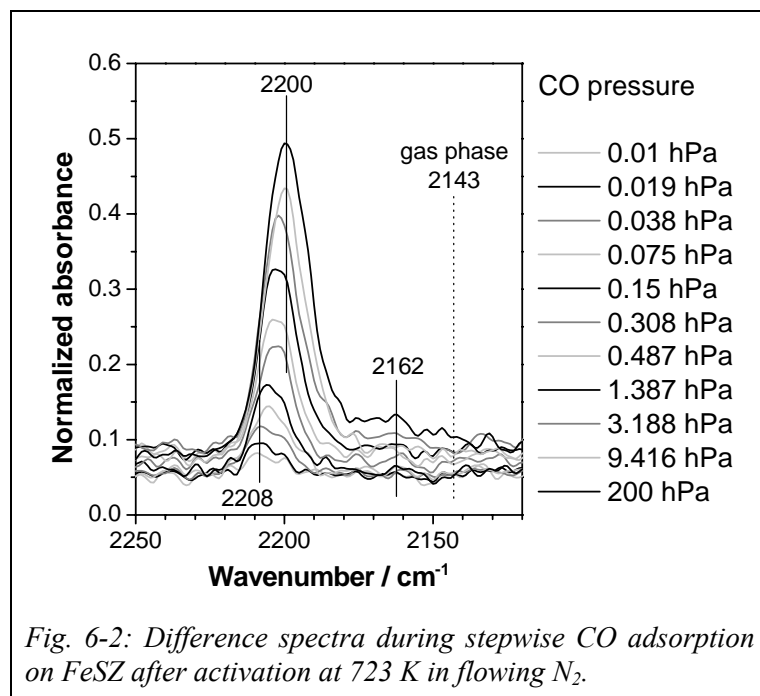
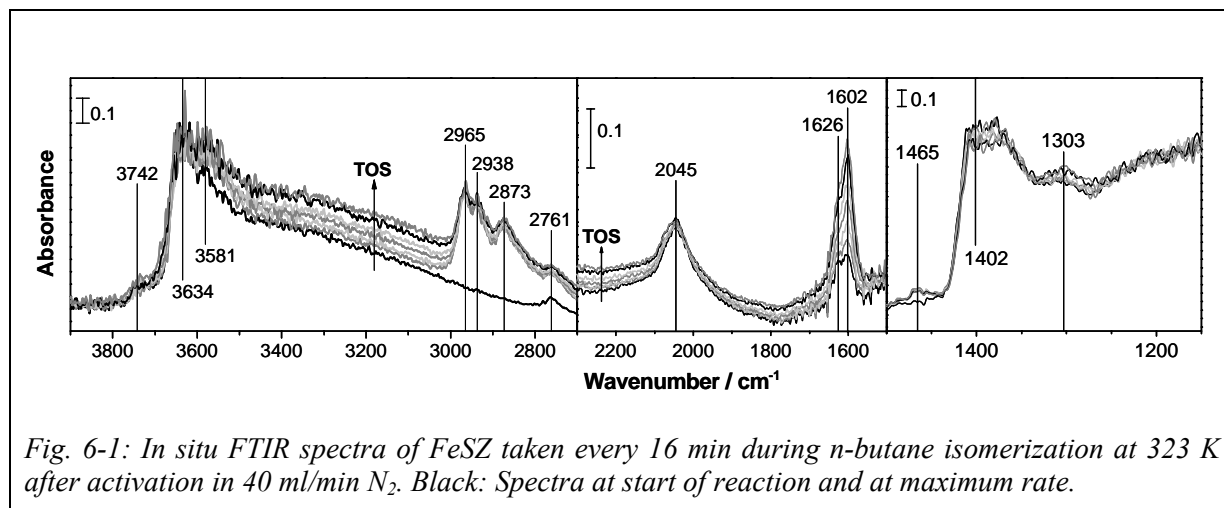
Sulfated zirconia is known to be an acid material; it was even claimed to be superacidic.⁷ Acidic oxides like SZ possess different types of acid sites, Brønsted and Lewis acid sites. Skeletal isomerization of *n*-butane is a typical example for an acid catalyzed reaction in liquid phase.⁶³ Thus the active site on SZ is considered to be acidic. Many attempts have been made to probe the active sites on SZ, but the results are not clear. Brønsted acid sites⁷⁴ as well as Lewis acid sites⁷⁵ or a combination of both⁴¹ have been proposed to be responsible for activity.

CO is a weak base and thus well suited to probe acid sites of different strength. At low temperature (77 K) CO interacts also with weakly acidic sites, strongly acidic Lewis sites can be probed even at room temperature. In order to test catalysts that are active a combination of *in situ* and adsorption experiments was used. *n*-Butane was isomerized at 323 K on FeSZ (containing 2 wt% Fe) in a high temperature cell (HTZ) for FTIR spectroscopy in transmission. The reaction was stopped at different stages of performance and CO was adsorbed after evacuation. This quasi *in situ* CO adsorption allows determination of the amount of CO adsorbed on FeSZ at a certain catalytic activity.

6.1.2 Results

n-Butane isomerization was carried out *in situ* after activation of the FeSZ wafer in flowing N₂. The wafer is active in *n*-butane isomerization and shows a catalytic profile with a maximum in conversion after 1.5–2 h time on stream.

The FTIR spectra taken every 16 min during *n*-butane isomerization are displayed in Fig. 6-1; the spectrum at the start of the reaction and the spectrum corresponding to the maximum rate are shown in black. The band around 3580 cm^{-1} increases and bands at 2966, 2938, 2873, and 1465 cm^{-1} become visible as soon as the feed gas is admitted to the cell. Bands at 1602 and 1626 cm^{-1} increase with time on stream. For the band at 1402 cm^{-1} a shift towards lower wavenumbers and an intensity decrease are observed, while the band at 1303 cm^{-1} increases with time on stream.



Difference spectra for CO adsorption on fresh FeSZ activated in flowing N_2 were created by subtraction of the spectrum of FeSZ before CO adsorption from the spectrum of FeSZ after CO adsorption (Fig. 6-2). At low CO partial pressure only one band is visible at 2208 cm^{-1} . With increasing partial pressure the band increases in intensity and is red-shifted towards 2200 cm^{-1} . At very high partial pressure of ca. 200 hPa CO a second band appears at 2162 cm^{-1} . On FeSZ activated in vacuum a partial pressure of 5 hPa is sufficient to create the band around 2160 cm^{-1} , which is increased and shifted to ca. 2155 cm^{-1} with increasing CO pressure (not shown).

CO adsorption on FeSZ was carried out *quasi in situ*, i.e. *n*-butane isomerization was performed and stopped at different stages of catalytic activity by purging with N₂ until all bands of butane were removed before CO was admitted after evacuation for 1 h; the total pressure was always below 10⁻⁶ hPa. This allows determination of the adsorbed amount of CO at a certain catalytic activity. In Fig. 6-3 (left) the rates are displayed for three FeSZ wafers. Circles indicate the last data point before CO adsorption that was taken either directly after activation of FeSZ in flowing N₂ (black) or after activation and *n*-butane isomerization at maximum rate (grey) or after deactivation (light grey). The resulting spectra at a partial pressure of 9 mbar are compared in Fig. 6-3 (right) and show that the intensity of the CO band at 2200 cm⁻¹ decreases with time on stream.

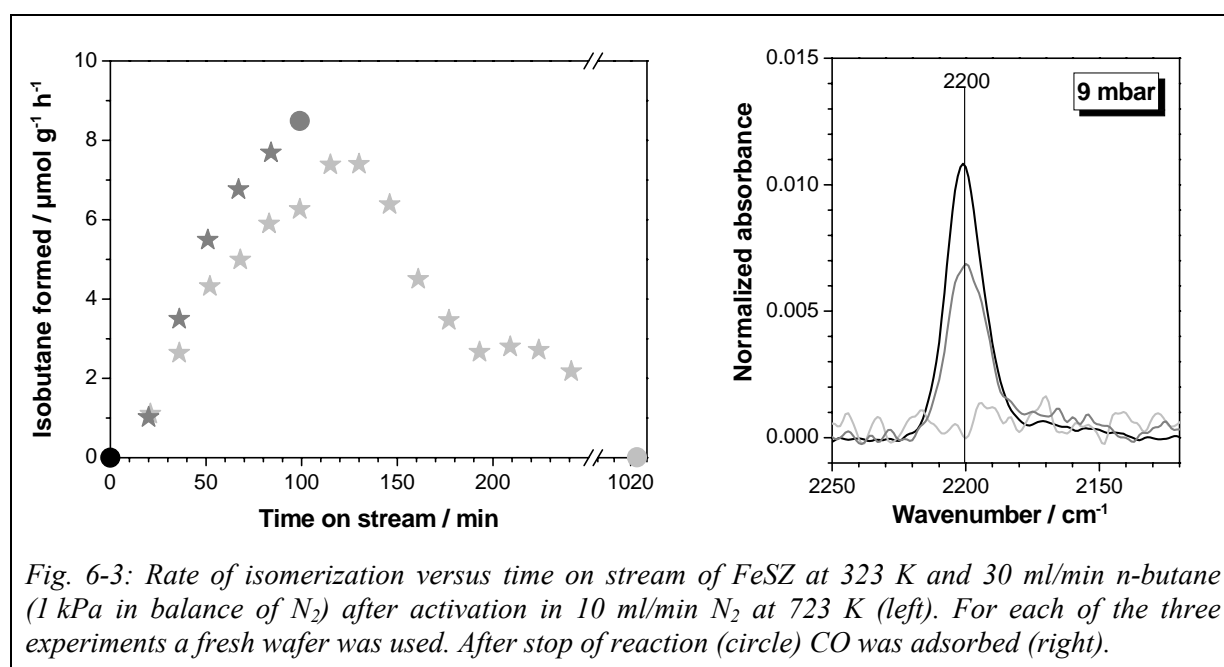


Fig. 6-3: Rate of isomerization versus time on stream of FeSZ at 323 K and 30 ml/min *n*-butane (1 kPa in balance of N₂) after activation in 10 ml/min N₂ at 723 K (left). For each of the three experiments a fresh wafer was used. After stop of reaction (circle) CO was adsorbed (right).

6.1.3 Discussion

Before the IR experiments FeSZ had to be pressed to a self-supporting wafer. As discussed in Chapter 5.1, the metastable tetragonal FeSZ transforms its phase partly when pressed for 10 min with 540 MPa to reach 20–30 wt% of the stable monoclinic form. Here the wafer was pressed under less harsh conditions (20 s at 270 MPa) to minimize the phase transformation.

The spectra obtained in the HTZ have a lower signal-to-noise ratio than the spectra recorded in the DRIFTS cell, which makes determination of small shifts difficult. The lower quality of the transmission spectra is due to the available detector and the poor transmittance of the self-supporting wafers that need a certain thickness to be stable. The signal-to-noise ratio of the spectra could be enhanced by embedding the sample in a diluent like KBr, but

interaction of the diluent with reactant or the probe molecule would falsify the results. However, bands at 2966, 2938, 2873 cm^{-1} and 1465 cm^{-1} are typical for CH stretching or CH deformation vibrations that originate from *n*-butane in the gas phase. Interaction of butane with the hydroxyl groups of FeSZ leads to the increase of the OH stretching band at ca. 3580 cm^{-1} . Water adsorption on the catalyst with time on stream is indicated by the increase of the OH deformation bands at 1602 and 1626 cm^{-1} . The structure of sulfate is influenced both by water and butane, which results in changes of the intensity and position of bands characteristic for sulfate vibrations. A detailed discussion of *in situ* spectra measured during *n*-butane isomerization will follow in Chapter 7, when data measured in diffuse reflectance are presented.

Lewis sites are probed by CO adsorption at room temperature. The band appearing at 2208 cm^{-1} after CO adsorption on FeSZ can be assigned to a CO stretching vibration of CO interacting with *cus* Zr^{4+} sites, since a band at the same position has been reported for monoclinic or partly tetragonal SZ.^{208,209} Pinna et al. found the band of *cus* Zr^{4+} on SZ to be shifted from 2200 to 2210 cm^{-1} with the CO partial pressure decreasing from 133 hPa–1.6 Pa.²¹⁰ Since iron is not very well incorporated into the zirconia lattice but accumulates on the surface,³⁹ CO should also interact with *cus* Fe species. CO at *cus* Fe^{3+} has been reported to show bands at 2150, 2138, and 2124 cm^{-1} on Fe-containing zirconia,²¹¹ while Fe^{x+} ($x < 3$) was found to show a band at 2170 cm^{-1} on Fe-promoted SZ.¹⁰² The CO band appearing around 2160 cm^{-1} at high partial pressure can thus be attributed to CO on Lewis acidic iron species. The capacity of FeSZ to adsorb CO on Zr^{4+} Lewis sites decreases with time on stream; at the same CO partial pressure of 9 hPa the band indicative of CO at Lewis sites is less intense after reaching the maximum rate than at the start of the reaction and has vanished after running the reaction for 17 h (Fig. 6-3). The amount of adsorbed CO can thus not be taken as a measure for the catalytic activity of FeSZ in the present state. Though CO is known to be a poison that inhibits isobutane formation as long as it is added to the feed,^{123,210} instead of blocking active Lewis sites that are necessary for isomerization,²¹⁰ it is reacting with the adsorbed carbenium ions,^{18,123} so that their transformation to isobutane is hindered. Quasi *in situ* CO adsorption shows that Zr^{4+} sites, which are able to interact with CO, are blocked during *n*-butane isomerization. Either the reactant or its product or byproducts could be responsible for the consumption of Lewis sites. From the spectra recorded *in situ* during *n*-butane isomerization, it is visible that water is formed. This water formation can occur via oxidative dehydrogenation of *n*-butane according to the following equation: oxidized catalyst + C_4H_{10} → C_4H_8 + H_2O + reduced catalyst (see Chapter 7). Because of its high electron density (free

electron pairs) water is a much stronger Lewis base than alkanes. Thus, it is the water that adsorbs on FeSZ and blocks the Lewis sites.

6.1.4 Summary

The transmission high temperature IR cell was used as reactor. The information obtained from *in situ* transmission IR spectra is consistent with the one from *in situ* DRIFT spectra as described in chapter 7. Lewis sites of FeSZ were characterized by room temperature CO adsorption after *n*-butane isomerization, which was stopped at different states of activity. With time on stream a decrease in the number of Lewis acid Zr^{4+} was detected. This decrease is probably due to water, which can be formed as a side product during activation of butane via oxidative dehydrogenation and is adsorbed more strongly than CO.

6.2 Adsorption of hydrogen and *n*-butane on SZ and Fe- or Mn-promoted SZ

Characterization of the surface of SZ catalysts has focused on acidic sites using probe molecules with free electron pairs such as ammonia, pyridine or carbon monoxide. These investigations did not deliver an unambiguous picture. A more weakly interacting probe is H_2 , which can serve as a model for the reactant butane since both molecules exhibit only sigma-bond basicity. H_2 has been used to probe Brønsted as well as Lewis acid centers of zeolites or metal oxides at low temperatures, using IR spectroscopy for analysis.^{212,213} Lewis acid sites can be probed with high sensitivity because shifts of the H–H stretching frequency tend to be large due to polarization of the corresponding bond.^{214,215} At higher temperature, hydrogen can be employed to test the reducibility (i.e. oxidation potential) of the catalyst, so that the plausibility of an initiation of skeletal isomerization by oxidative dehydrogenation (ODH) can be evaluated. Furthermore, useful reference spectra for hydrides may be generated, because frequencies given in the literature for zirconium hydrides span a wide range and overlap with species such as water. Essential for the catalysis is the interaction with the reactant, *n*-butane, which can also be followed by IR spectroscopy. According to the mechanisms proposed for carbenium ion formation as initial step in skeletal isomerization —(i) protonation of the alkane by very strong Brønsted sites, (ii) hydride abstraction by strong Lewis sites, or (iii) oxidative or non-oxidative dehydrogenation of the alkane (see Chapter 2.5)— reaction with butane should result in (i) a shift or decrease of bands of OH groups, (ii) formation of a hydride, or (iii) oxidation to e.g. an alkene with water or hydrogen as a side product.

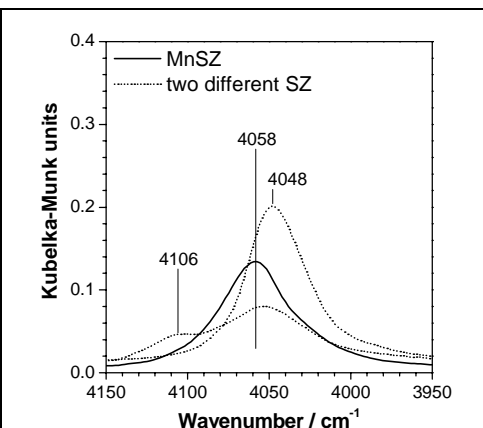
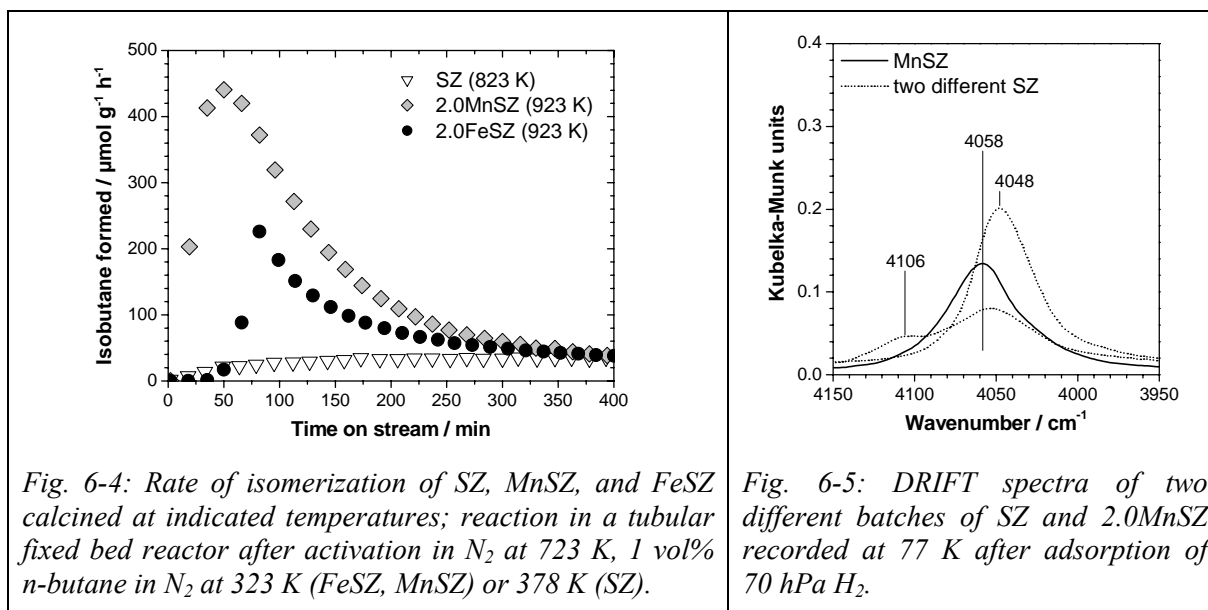
To identify the relevant sites and analyze the role of the promoters in SZ catalysts, elucidate the mechanism(s) for *n*-butane activation, and investigate the function of sulfate and hydroxyl groups therein, the Brønsted and Lewis acid sites on the surface of SZ and iron- or manganese-promoted SZ (2.0MnSZ, 2.0FeSZ) were probed with hydrogen at 77 K or butane at room temperature using DRIFTS as analytical technique. Probes were dosed into vacuum and reactions were performed in batch mode. The products of reaction with hydrogen or butane at increasing temperatures delivered information on the reaction initiation and the oxidation potential of promoted in comparison to unpromoted catalysts.

6.2.1 Results

For the DRIFT spectroscopic experiments the powders were pressed at 10 MPa for 2 s and sieved into fractions of 0.2–0.5 or 0.5–1.0 mm. Pressing can cause partial transition of tetragonal to monoclinic zirconia (see Chapter 5.1); analysis of selected samples after pressing revealed a minor fraction of monoclinic phase (10–20 %). Samples were placed into a quartz vacuum cell equipped with a CaF₂ window and pretreated in vacuum. A typical activation procedure was: heating under vacuum (10^{-3} – 10^{-4} hPa, diffusion pump with liquid N₂ trap) from ambient temperature to 383 K in 15 min, keeping at this temperature for 1 h to remove water, heating further up to 723 K for 1 h, evacuation at this temperature for 1 h, heating in 67 hPa of oxygen for 1 h to remove grease contaminations, and finally evacuation for 20 min at 723 K.

6.2.1.1 Catalyst characterization

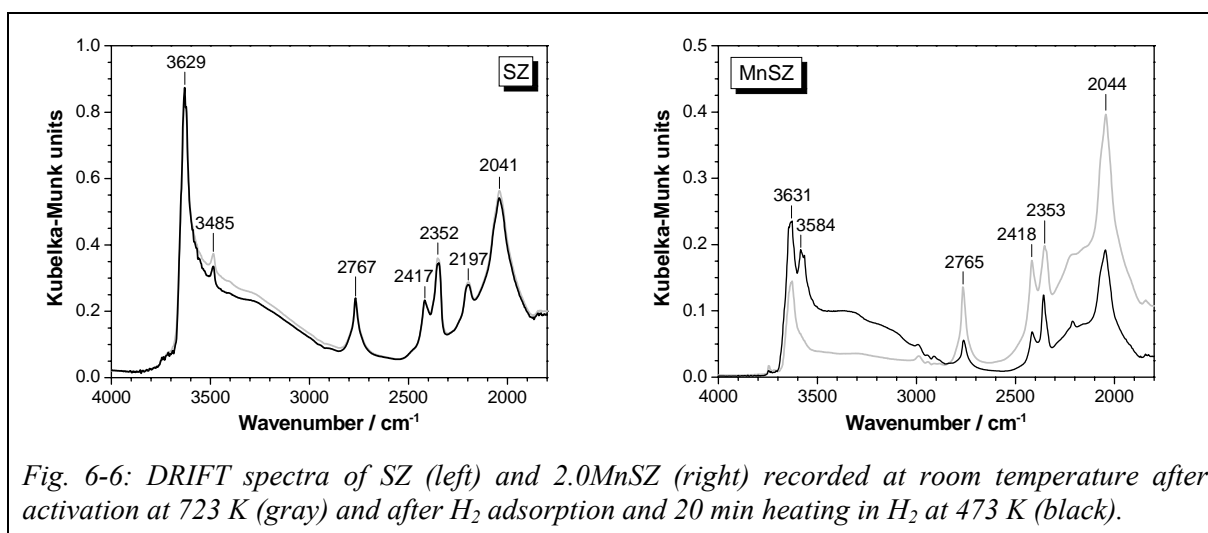
For all investigated samples, X-ray diffractograms before pressing showed reflections typical of the tetragonal phase of ZrO₂, no monoclinic phase could be detected. The following BET surface areas were obtained: 119 m²/g (SZ), 108 m²/g (2.0MnSZ), and 134 m²/g (2.0FeSZ). The rate of *n*-butane isomerization in a flow reactor is shown in Fig. 6-4. The promoted catalyst samples deactivate partially under the applied conditions. The measured maximum rate for FeSZ is 225 μmol·g⁻¹·h⁻¹ and that of MnSZ is 440 μmol·g⁻¹·h⁻¹. The long term activity (800 min) of FeSZ amounts to ca. 20 μmol·g⁻¹·h⁻¹ and exceeds that of MnSZ (ca. 5 μmol·g⁻¹·h⁻¹). SZ has a lower maximum rate (35 μmol·g⁻¹·h⁻¹) than the promoted catalysts, even though isomerization was carried out at a temperature that was 55 K higher. In contrast to the promoted samples it shows nearly no deactivation: the rate after 1000 min is still 30 μmol·g⁻¹·h⁻¹.



6.2.1.2 Low temperature adsorption of hydrogen

After adsorption of H_2 (70 hPa) on SZ or 2.0MnSZ at 77 K, bands of the perturbed H–H stretching frequency appear in the DRIFT spectra (Fig. 6-5). One band, located between 4058 and 4048 cm^{-1} , is always observed. Sometimes, an additional band at 4106 cm^{-1} is detected. Formation of the band at 4048 cm^{-1} is not connected with a shift of the OH groups; for the band at 4106 cm^{-1} such a correlation could not be excluded.

6.2.1.3 Reaction with hydrogen at elevated temperatures



The spectrum of SZ did not change significantly after heating in hydrogen to 473 K (Fig. 6-6, left and Fig. 6-7). This is different for MnSZ. After heating in hydrogen at 473 K the band at 3631 cm^{-1} shows a shoulder at 3645 cm^{-1} , an additional band appears with a maximum

at ca. 3584 cm^{-1} , and the intensity increases in the region between 3500 and 3000 cm^{-1} typical for stretching vibrations of H-bonded OH (Fig. 6-6, right). Furthermore, the intensity of the overtone and combination modes of sulfate vibrations decreases. Shifts of sulfate bands were less than 5 cm^{-1} . A band at 5243 cm^{-1} appears (Fig. 6-7, left). Several new bands are also observed between 1700 and 1558 cm^{-1} (Fig. 6-7, right), including a well-defined band at 1594 cm^{-1} and a broad feature between 1700 and 1660 cm^{-1} .

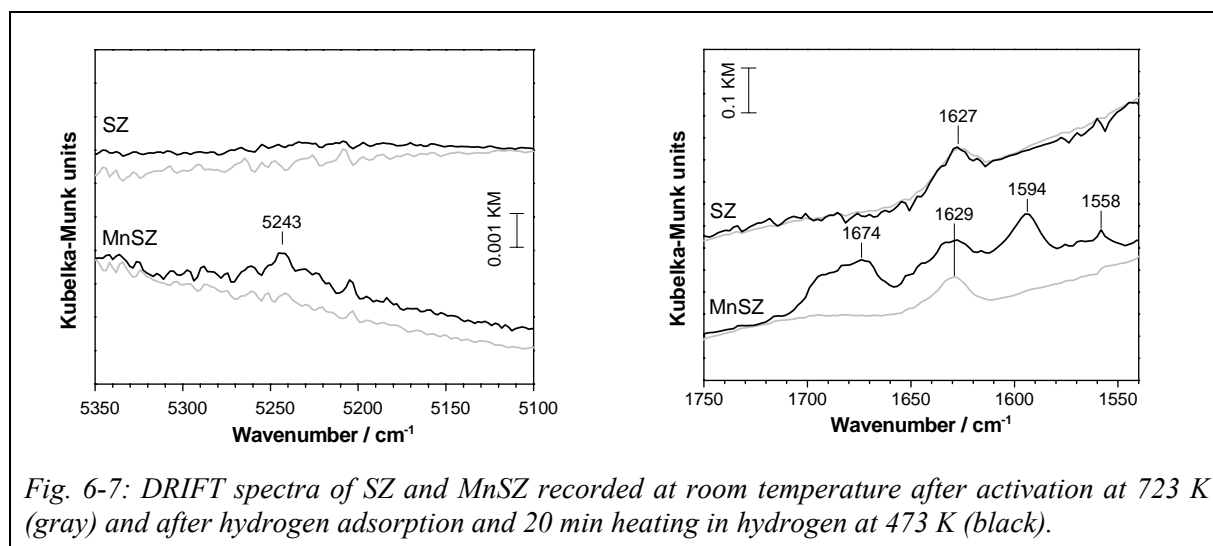


Fig. 6-7: DRIFT spectra of SZ and MnSZ recorded at room temperature after activation at 723 K (gray) and after hydrogen adsorption and 20 min heating in hydrogen at 473 K (black).

6.2.1.4 Adsorption of *n*-butane at room temperature

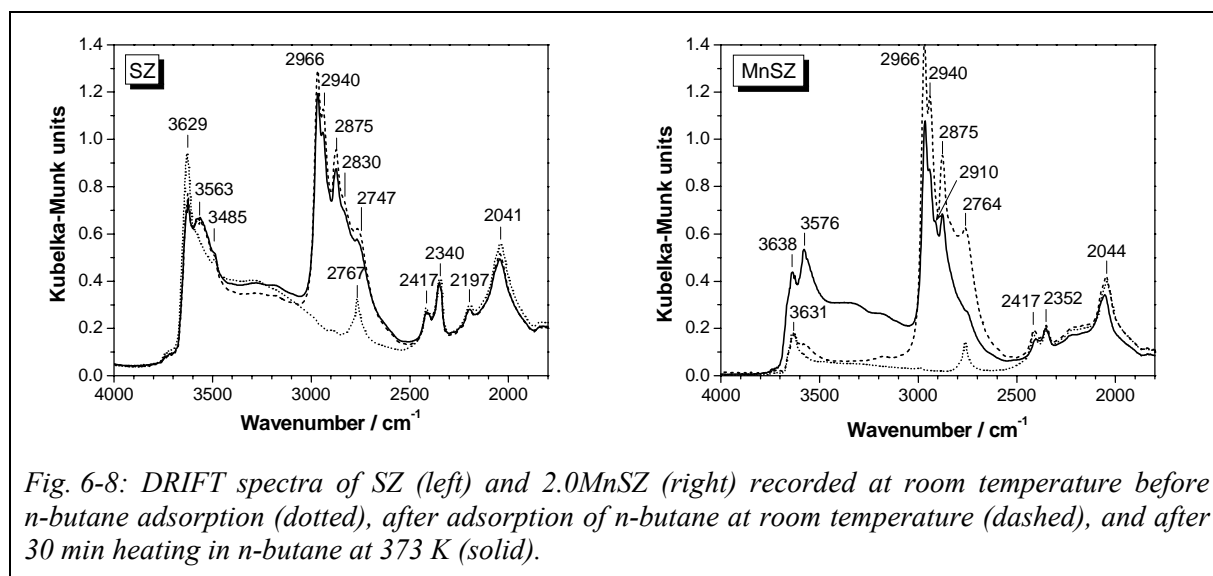


Fig. 6-8: DRIFT spectra of SZ (left) and 2.0MnSZ (right) recorded at room temperature before *n*-butane adsorption (dotted), after adsorption of *n*-butane at room temperature (dashed), and after 30 min heating in *n*-butane at 373 K (solid).

After addition of 10 hPa *n*-butane at room temperature to SZ, MnSZ or FeSZ, bands of CH vibrations are visible in the spectra. For all catalysts, there are five bands in the CH stretching region, three with distinct maxima at 2966 , 2940 , and 2875 cm^{-1} and two shoulders at 2830

and 2747 cm^{-1} (Fig. 6-8). Two bands in the CH deformation region are centered at 1465 cm^{-1} (shoulder at 1455 cm^{-1}) and at 1387 cm^{-1} (not shown).

After adsorption of 10 hPa *n*-butane on SZ at room temperature a band appears in the OH stretching region at ca. 3563 cm^{-1} , while the band at 3629 cm^{-1} decreases in intensity (Fig. 6-9). Addition of *n*-butane to the promoted catalysts at room temperature leads to appearance of a small broad band in the OH stretching region with a maximum near 3573 cm^{-1} ; concomitantly, the band at 3631 cm^{-1} shrinks. Two very weak bands at about 3742 and 3720 cm^{-1} are also diminished in intensity by adsorption of *n*-butane for all three catalysts; this effect is more pronounced at higher pressure (100 hPa). All shifts of OH bands are reversed upon evacuation.

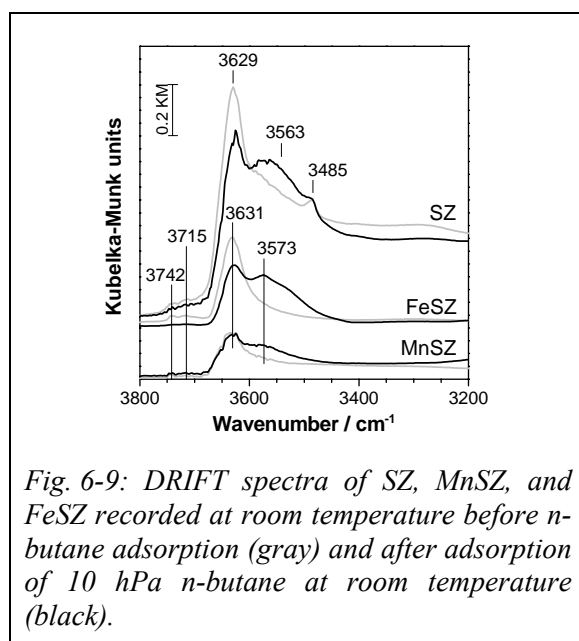


Fig. 6-9: DRIFT spectra of SZ, MnSZ, and FeSZ recorded at room temperature before *n*-butane adsorption (gray) and after adsorption of 10 hPa *n*-butane at room temperature (black).

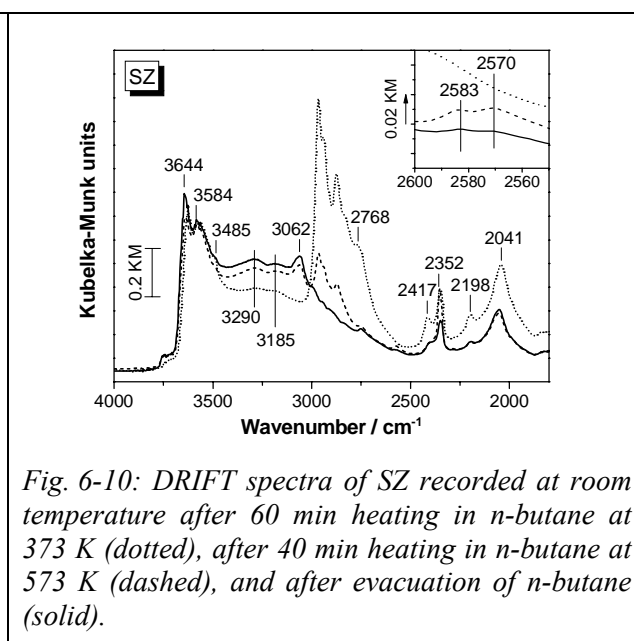


Fig. 6-10: DRIFT spectra of SZ recorded at room temperature after 60 min heating in *n*-butane at 373 K (dotted), after 40 min heating in *n*-butane at 573 K (dashed), and after evacuation of *n*-butane (solid).

6.2.1.5 Interaction with *n*-butane at elevated temperatures

After heating SZ for 30 minutes at 373 K in 10 hPa *n*-butane (pressure at room temperature), no changes are visible except a small decrease in the intensity of the CH vibration bands and a small increase in the region of H-bridging (Fig. 6-8, left). Longer heating at 373 K (one hour) and an increase of the temperature up to 473 K cause no further changes. The spectra change significantly only after heating the sample to 573 K (Fig. 6-10). At this temperature, the intensity of the CH bands decreases dramatically. A pronounced band in the region of CH stretching vibrations is recognized at 3062 cm^{-1} . The band at 3629 cm^{-1} is shifted to 3644 cm^{-1} . The overall intensity in the range $3500\text{--}3000\text{ cm}^{-1}$ increases. The broad features around 3290 and 3185 cm^{-1} indicate H-bridging. The sulfate bands at 2417 , 2198 , and

2041 cm^{-1} decrease in intensity and in part experience shifts (2041 \rightarrow 2053 cm^{-1} ; 2417 \rightarrow 2406 cm^{-1}). Two weak bands appear at 2583 and 2570 cm^{-1} . The band at 2352 cm^{-1} loses its shoulder at 2340 cm^{-1} without decreasing in intensity at all, i.e. most likely this band is actually increasing (Fig. 6-11). A band at 2285 cm^{-1} becomes discernable. The band at about 1627 cm^{-1} gains in intensity and shoulders form towards higher and lower wavenumbers with a distinct maximum at 1593 cm^{-1} (Fig. 6-12). A new band appears at 5228 cm^{-1} (Fig. 6-13). After evacuation, all bands of CH vibrations have almost but not entirely disappeared (Fig. 6-14) except for the bands at 3062 and at 1455 cm^{-1} . The band at 2352 cm^{-1} is reduced (Fig. 6-11). The other features remain unchanged.

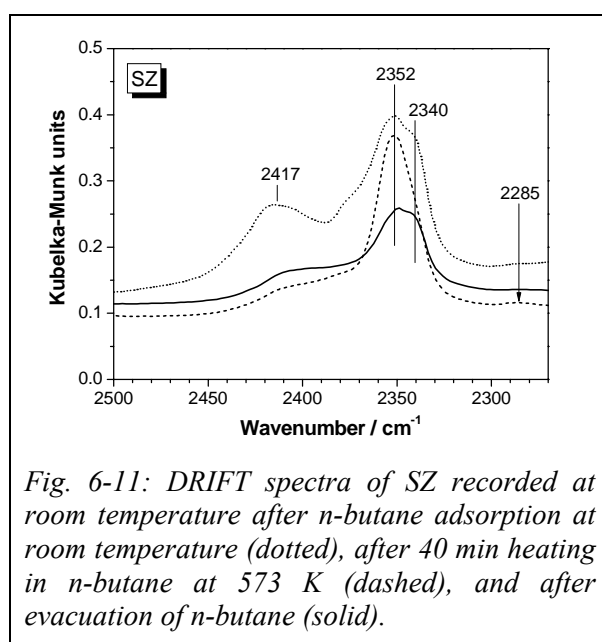


Fig. 6-11: DRIFT spectra of SZ recorded at room temperature after *n*-butane adsorption at room temperature (dotted), after 40 min heating in *n*-butane at 573 K (dashed), and after evacuation of *n*-butane (solid).

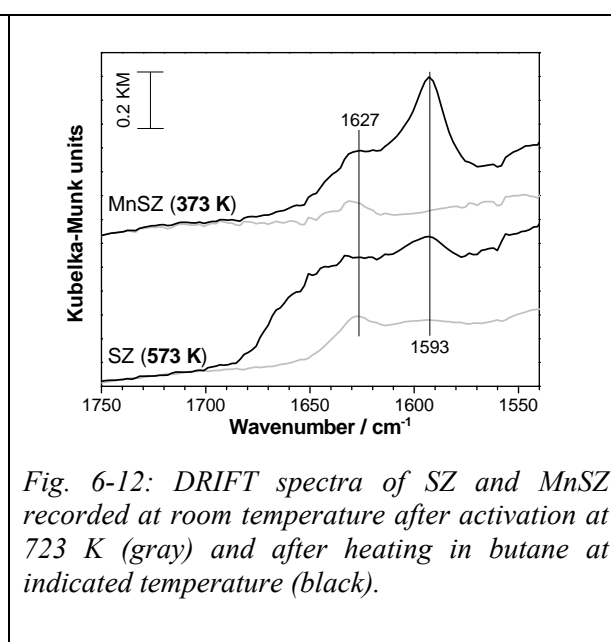


Fig. 6-12: DRIFT spectra of SZ and MnSZ recorded at room temperature after activation at 723 K (gray) and after heating in butane at indicated temperature (black).

In contrast to SZ, MnSZ and FeSZ react with *n*-butane already at 373 K. The intensity of the CH bands is decreased after 30 min of treatment (example MnSZ: Fig. 6-8, right). The OH stretching band at 3631 cm^{-1} increases and is shifted to 3638 cm^{-1} while the OH stretching band centered at about 3580 cm^{-1} that is present after adsorption of *n*-butane also grows and becomes more distinct. At the same time a general increase in intensity in the region 3500–3000 cm^{-1} is observed. The bands at 2764, 2417 and 2046 cm^{-1} lose in intensity. A shift can be recognized for the two lower frequency bands, after the treatment they are located at 2406 cm^{-1} and 2052 cm^{-1} . The band at 2352 cm^{-1} and its shoulder at 2340 cm^{-1} decrease slightly in intensity, but the area ratio remains unchanged. The band at 1632 cm^{-1} grows and an even larger, well-defined band develops at 1593 cm^{-1} (Fig. 6-12). Furthermore, a band is detected at 5238 cm^{-1} (Fig. 6-13). After evacuation of the sample, the intensity in the CH region is strongly diminished and four bands with maxima at 2982, 2941, 2906, and

2884 cm^{-1} become visible (Fig. 6-14). Otherwise, the spectra are unaffected. The results for FeSZ are largely comparable to those obtained for MnSZ, except that there is no distinct band at 5238 cm^{-1} and a less intense band at 1593 cm^{-1} . The CH stretching bands that are discernable after evacuation are located at about the same positions as for MnSZ (Fig. 6-14).

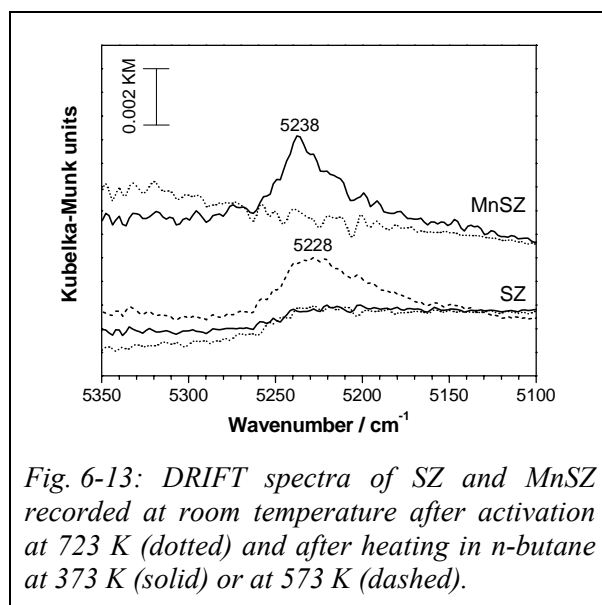


Fig. 6-13: DRIFT spectra of SZ and MnSZ recorded at room temperature after activation at 723 K (dotted) and after heating in *n*-butane at 373 K (solid) or at 573 K (dashed).

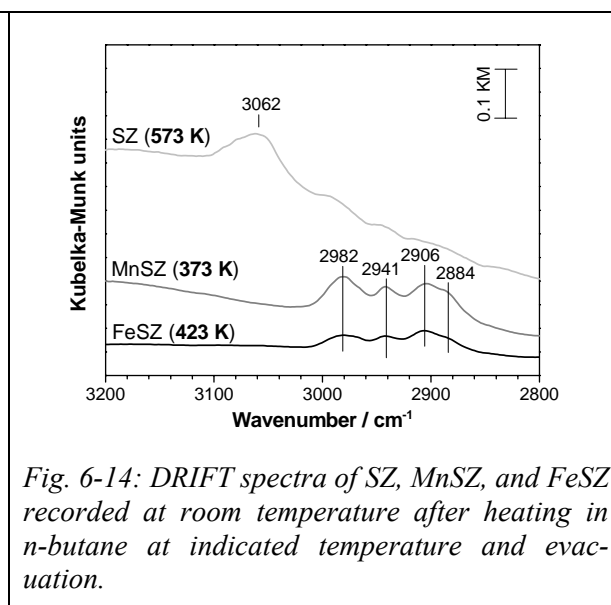


Fig. 6-14: DRIFT spectra of SZ, MnSZ, and FeSZ recorded at room temperature after heating in *n*-butane at indicated temperature and evacuation.

6.2.2 Discussion

Hydrogen and *n*-butane, which exhibit solely the very weak sigma-bond basicity, were used to investigate acid sites on SZ materials. At the chosen adsorption temperatures, 77 K for H_2 and room temperature for *n*-butane, both molecules can be desorbed through evacuation. The facile desorption of *n*-butane is consistent with calorimetric results, which, on SZ, yield differential heats of adsorption of 45–60 $\text{kJ}\cdot\text{mol}^{-1}$.²¹⁶ The surface is reverted to its pre-adsorption state, i.e. the molecules fulfill the requirements for probes.

6.2.2.1 Lewis and Brønsted acid strength

The bands resulting after low-temperature adsorption of 70 hPa hydrogen on SZ or MnSZ are red-shifted in comparison with the gas phase frequency (IR inactive, from Raman spectroscopy: 4160.2 cm^{-1}),²¹⁷ indicating a weakening of the H–H bond through electron donation towards acid sites.

The band at 4048 cm^{-1} observed for SZ can be assigned to H_2 adsorbed on Lewis acid sites because it is not associated with a shift of OH bands. The position is also very close to that of a band at 4054 cm^{-1} , which was previously reported by Kondo et al. for H_2 adsorbed on pure and thus not Brønsted-acidic ZrO_2 .²¹⁸ A slightly higher frequency of 4059 cm^{-1} is observed for

MnSZ. This band originates from H₂ adsorbed on Lewis sites as well, because of its position and because its intensity decreases with increasing degree of hydration (after heating the sample in hydrogen). The largest shift compared to the gas phase vibration of hydrogen is observed for adsorption on SZ (band at 4048 cm⁻¹), i.e. the presence of Mn does not enhance the Lewis acid strength. The shifts are ca. 110 cm⁻¹ (SZ) and ca. 100 cm⁻¹ (MnSZ) and are slightly smaller than that observed for H₂ adsorption on Si electron-acceptor centers in dehydroxylated ZSM-5, which is 130 cm⁻¹.²¹² Larger shifts are observed for adsorption on group 11 and 12 cations, e.g. 1035 cm⁻¹ (Cu⁺)²¹⁴ or 222 cm⁻¹ (Zn²⁺).²¹⁹

The band at 4106 cm⁻¹ (observed for SZ and MnSZ) cannot be unambiguously assigned to H₂ adsorbed on Brønsted or Lewis sites, but its position corresponds to that of H₂ coordinated to the bridging OH groups of [Al]-HZSM-5.²¹³ If this band arose from adsorption on OH groups, then the Brønsted acidity of SZ materials would approximately correspond to that of H-ZSM-5. Earlier, it was reported that the Brønsted acid sites of SZ catalysts are “weaker, at any rate not stronger than those of H-ZSM-5 and HY”.⁷⁷ For zeolites, the bands for H₂ adsorbed on Lewis acid sites are much less intense than those for H₂ on the Brønsted acid sites; here, the bands arising from H₂ adsorbed on Lewis acid sites were always stronger than the band at 4106 cm⁻¹. This intensity distribution reflects the different nature of the zirconia surfaces in comparison to the zeolites, whose acidic properties are dominated by the Brønsted functionality of the OH groups.

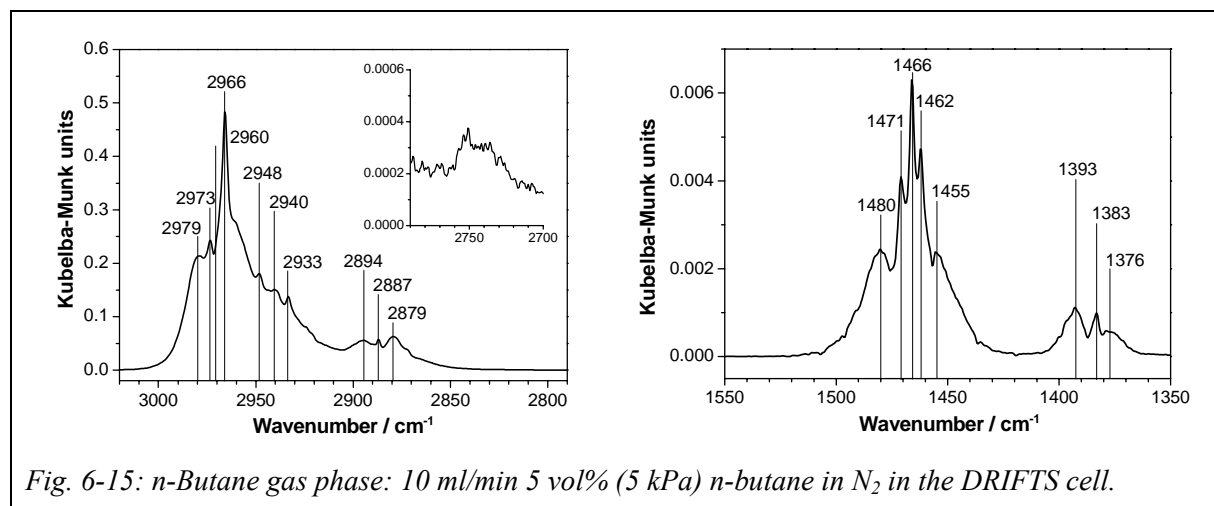


Fig. 6-15: *n*-Butane gas phase: 10 ml/min 5 vol% (5 kPa) *n*-butane in N₂ in the DRIFTS cell.

Admission of *n*-butane results in a pattern of CH stretching vibrations that differs from the gas phase spectrum (see Fig. 6-15). The intense narrow bands of the rotation-vibration spectrum of gas phase *n*-butane are not detectable in the spectra (see Fig. 6-8), which thus represent adsorbed species. The band at 2966 cm⁻¹ is less sharp and less pronounced; accordingly, the band at 2940 cm⁻¹, which is only a shoulder in the gas phase spectrum,

becomes distinct. The band at 2875 cm^{-1} is more intense and shifted by about -12 cm^{-1} with respect to the gas phase feature. Babou et al. reported a shift of the CH stretching vibrations of butane to lower frequencies upon adsorption on SZ at room temperature.⁵³ The largest intensity increase is observed for the bands at 2830 and 2747 cm^{-1} , which are barely discernable in the gas phase spectrum. Butane adsorption results in a measurable shift of the OH bands towards lower wavenumbers, indicating interaction between *n*-butane and Brønsted acid sites. An H-bridge from butane to the oxygen of an OH group could be responsible for the observed low frequency CH vibrations.

For the intense OH band at ca. 3630 cm^{-1} , the red-shift can be determined. At 10 hPa butane, the shift is ca. 66 cm^{-1} for SZ and ca. 58 cm^{-1} for MnSZ and FeSZ. Again, the values are similar and there is certainly no increased interaction due to addition of the promoters. Paukshtis et al. obtained a shift of ca. 92 cm^{-1} after adsorption of *n*-pentane on unpromoted SZ; however, the initial position of the OH band was higher. For comparison, the shift of the OH groups in H-mordenite after *n*-butane adsorption is ca. 110 cm^{-1} .^{vi} The interaction of the zirconia catalysts with *n*-butane, i.e. with the reactant, via OH groups is obviously weaker than in case of a typical acidic zeolite. From the OH-band shifts it seems unlikely that the activation of the alkane is achieved through interaction with OH groups on the zirconia catalysts. In any case, the OH groups serve as anchoring points for the reactant molecules at the surface.

Adsorption experiments with hydrogen and *n*-butane show that the promoters do not increase the acid strength of the catalyst. The same result is obtained when contacting a wet pH paper with powder of SZ or promoted SZ: The color change into red is more intense for unpromoted SZ indicating lower pH.

6.2.2.2 Interaction of SZ and MnSZ with hydrogen

As far as detectable by IR spectroscopy, pure SZ shows no interaction with hydrogen at room temperature or at 473 K. In contrast to these observations Paukshtis et al. found oxidation of hydrogen on promoter-free SZ at 473 K;¹¹⁷ the different behavior may be due to deviations in sample preparation or experimental procedure. At a hydrogen partial pressure of 100 hPa, a positive effect on the stability of the *n*-butane isomerization rate on SZ at 523 K has been observed by Garin et al., while a lower partial pressure of 80 hPa had no obvious

^{vi} J. Kröhnert, F.C. Jentoft, unpublished results.

influence.⁸⁵ These reaction kinetic results confirm that for interaction between SZ and molecular hydrogen a minimum partial pressure and a minimum temperature are required.

At room temperature, the spectra of MnSZ also remain unchanged, but during heating at 473 K for 20 min the sample reacts with hydrogen (Fig. 6-6, right and Fig. 6-7). The band at 1594 cm⁻¹ is attributed to the deformation mode of water because it matches nearly exactly the gas phase vibration at 1595.0 cm⁻¹.²¹⁷ The corresponding stretching vibration is seen as a shoulder of the band at 3631 cm⁻¹ appearing around 3645 cm⁻¹. The band at 5243 cm⁻¹ is a combination mode of these two, the deformation and stretching vibration of the water molecule (3645 + 1594 = 5239). The formation of OH groups (new band at 3584 cm⁻¹) and water together with the increasing intensity in the hydrogen bonding region (3500–3000 cm⁻¹) are evidence for the oxidation of hydrogen.

Several species could give rise to the absorption bands at 1700–1670 cm⁻¹. Reported frequencies for Zr–H are lower; they range from 1555 cm⁻¹ in ZrO₂ to 1660 cm⁻¹ in Zr(BH₄)/SiO₂.^{117,218} Molecular MnH or MnH₂ are also observed at lower wavenumbers (1493.3 cm⁻¹ or 1600.8 cm⁻¹ in solid neon).²²⁰ Vibrations of Mn–H in complexes occur at higher frequencies, which range from 1782 cm⁻¹ in HMn(CO)₅ to 1900 cm⁻¹ in HMn(CO)₂(π -Cp)SiPh₃.^{221,222} Thus, zirconium or manganese hydrides are unlikely to cause the vibrations. SH groups can be excluded as well, since they vibrate at a different position, ca. 2600 cm⁻¹.¹⁸¹ A possible explanation for the bands at 1700–1670 are water clusters. The bending vibration of water is known to shift to higher frequencies as the degree of association increases, e.g. bands at 1600 and 1618 cm⁻¹ are reported for the (H₂O)₂ clusters and 1640 for liquid water.^{181,223} In addition to the blue-shift, DFT calculations for small water clusters show an increase in the range of deformation vibrations from the dimer (1615–1636 cm⁻¹) to different octamer structures (1614–1701 cm⁻¹).²²⁴ Further support for this hypothesis comes from spectra of unactivated SZ catalysts (see Chapter 7), which show a broad band centered at 1630 cm⁻¹ that extends up to 1700 cm⁻¹. As the sample is heated and partially dehydrated, the high frequency species disappear, suggesting that they are aggregated water species. The fact that defined bands are observed here indicates the formation of water clusters of a distinct size.

On MnSZ, H₂ is—at least in part—oxidized and converted to OH groups and water. The position of the OH vibration is ambiguous; the band at 3584 cm⁻¹ can be assigned to S–OH of e.g. sulfuric acid,¹⁷⁸ to Zr–OH, or to water.^{vii} For proton formation, electrons must be accepted

^{vii} A. Hofmann, J. Sauer, personal communication.

by another species. There are three possible scenarios: (i) disproportionation of H_2 into H^+ and H^- , (ii) reduction of zirconium or manganese, and (iii) reduction of sulfur. According to Paukshtis et al.¹¹⁷ and Kondo et al.,²²⁵ species absorbing at 1555 or 1562 cm^{-1} could be Zr–H. However, the band detected at 1558 cm^{-1} is extremely weak, so H_2 disproportionation is not the main reaction path. Changes to the valence of manganese or zirconium cannot be directly detected by IR spectroscopy; there is only the possibility that functional groups attached to these ions change their vibrational frequency. There are not observed any dramatic band shifts. Furthermore, these components should be reduced only at higher temperatures, i.e. ZrO_2 above 473 K²²⁶ and Mn in MnSZ above 500 K.¹⁴⁸ SO vibrations of sulfate are strongly reduced in intensity and no new types of SO vibrations appear. Hence, oxygen from sulfate is at least in part being transferred to new OH groups and water. Reduced species such as e.g. adsorbed SO_2 would most likely absorb below 1200 cm^{-1} and would not be detectable with our setup. Strong reduction of the intensity of sulfate vibrations and formation of water indicate that reduction of sulfate is the most likely scenario.

6.2.2.3 Interaction of SZ and promoted SZ with *n*-butane

Upon heating in *n*-butane, the samples show different behavior. SZ does not react with *n*-butane up to 473 K, whereas for MnSZ and FeSZ already after heating to 373 K changes are seen in the spectra (Fig. 6-8, right). The intensity distribution in the CH stretching region is altered; specifically a band at 2906 cm^{-1} becomes visible. The position is typical for methyne groups, indicating that *n*-butane has been isomerized and a fraction of isobutane is present. For MnSZ, OH vibrations grow significantly as CH stretching vibrations decrease in intensity, indicating a transfer of H from hydrocarbon to catalyst. Specifically, the intensity in the hydrogen bonding region 3500–3000 cm^{-1} increases and two bands at 1593 and 5238 cm^{-1} appear (Fig. 6-12 and Fig. 6-13), which are stable during evacuation at room temperature. These two bands have been previously assigned to vibrations of water (see above). The simultaneous disappearance of *n*-butane and appearance of water can be explained by oxidative dehydrogenation (ODH) of *n*-butane. ODH is considered as one of the possible initiation reactions to form an alkene, which can be easily protonated to give a carbenium ion as active intermediate for the isomerization of *n*-butane.^{99,124,196} In analogy to the oxidation of hydrogen by MnSZ, the intensity of the SO bands of sulfate decreases after heating in *n*-butane as well, indicating that these groups are involved in the reaction with *n*-butane and possibly serve as oxidizing agent.

For FeSZ a decrease in CH vibrations is discernable and the methyne species are unambiguously present, but there are no obvious bands around 1600 cm^{-1} and 5200 cm^{-1} (water) and only a slight increase in the hydrogen bonding region $3500\text{--}3000\text{ cm}^{-1}$ is observed. This behavior does not fit the picture of *n*-butane activation by ODH. An alternative activation could be simple dehydrogenation, which has been postulated for unpromoted sulfated zirconia.¹¹⁹ However, non-oxidative dehydrogenation does not explain a decrease of the sulfate vibrations.

After evacuation the CH intensity is decreased, indicating that a large fraction of hydrocarbons is removed. Four individual bands become discernable in the region of CH stretching vibrations (Fig. 6-14). The positions and the intensity distribution are almost the same for MnSZ and FeSZ. The bands at 2982 and 2941 cm^{-1} are typical of asymmetric CH stretching vibrations of methyl and methylene groups, respectively, while the band at 2884 cm^{-1} arises from symmetric CH vibrations. The additional band at 2906 cm^{-1} can be assigned to methyne groups. Hence, alkyl species must be attached to the surface. The methylene groups indicate non-isomerized (*n*-butyl) species or longer chains containing a secondary carbon atom; the methyne groups indicate isobutyl species or longer chains containing a tertiary carbon atom.

For unpromoted SZ, differences in the spectra become apparent only after heating to 573 K (Fig. 6-10, Fig. 6-12, and Fig. 6-13). The CH bands are weakened in intensity. The formation of water is evidenced by the OH deformation band at 1594 cm^{-1} , the OH stretching band at 3644 cm^{-1} and their combination band at 5228 cm^{-1} . At the same time, the amount of hydrogen bonding increases. All SO bands of sulfate decrease. These results are similar to those obtained with MnSZ at 373 K and can be explained by an ODH reaction involving sulfate as oxidant. A fraction of the sulfate is completely reduced to H_2S , as evidenced by the according antisymmetric and symmetric stretching vibrations at 2583 and 2570 cm^{-1} (gas phase:¹⁸¹ 2628 and 2614 cm^{-1}) and the smell of the sample after the experiment. Similarly, Ng and Horvát reported the formation of H_2S during *n*-butane isomerization at 523 K in a flow experiment.¹³³

No bands of methyne groups appear in the spectra of SZ after reaction at 573 K , i.e. there is no significant fraction of isobutane. *n*-Butane is activated and converted, but not to its isomerization product. A new band in the CH stretching region at 3062 cm^{-1} indicates a species with an sp^2 -hybridized carbon atom as product. The band is not affected by evacuation; hence it must represent stable surface species. Corresponding C=C stretching vibrations are expected between 1600 and 1700 cm^{-1} , which is also a possible range for water

deformation vibrations. The bands at about 5230 cm^{-1} in the spectra in Fig. 6-13 suggest that about equal amounts of water are present on SZ and MnSZ. Hence, the pronounced high frequency shoulder in the spectrum of SZ in comparison to that of MnSZ (Fig. 6-12) is more likely due to C=C vibrations than to water clusters. The position at roughly $1650\text{--}1660\text{ cm}^{-1}$ is too high for the vibrations of aromatics, and bands of aryl CH stretching vibrations are also expected at somewhat lower frequency ($3040\text{--}3010\text{ cm}^{-1}$) than the observed band and should be weak. The spectrum shows no intense aliphatic CH stretching vibrations and only a sharp but weak band at 1455 cm^{-1} in the CH deformation region. A temperature of 573 K is sufficient for SZ to crack *n*-butane, e.g. into ethane and ethene,^{viii} and a strongly attached surface species could be formed from ethene upon cooling to room temperature. It follows that the adsorbate characterized by the band at 3062 cm^{-1} could be a short-chain alkene-type species.

An additional feature in the spectra of SZ is the band at 2352 cm^{-1} (Fig. 6-11). The position is very close to the gas phase vibration of CO_2 at 2349 cm^{-1} .¹⁸¹ A weak band at 2285 cm^{-1} for $^{13}\text{CO}_2$ confirms the presence of CO_2 , which desorbs upon evacuation.

6.2.2.4 Effect of Promoters

Through Mn or Fe promotion, sulfate becomes more reactive towards hydrogen and *n*-butane. It is not clear, whether sulfate is directly associated with the promoters. Yamamoto et al. proposed that Mn is present as MnSO_4 on the surface;¹⁰⁸ Tábora and Davis⁹² as well as Scheithauer et al.¹⁰⁶ reported small Fe_2O_3 rafts on the surface. However, the catalysts used here were prepared in a way that produces materials with a significant fraction of Fe and the majority of Mn incorporated into the zirconia lattice and a high fraction of Mn^{3+} .^{39,148} As a consequence, the unit cell size shrinks and oxygen defects are generated in the bulk due to the lower valence of Mn and Fe ions in comparison with Zr^{4+} . The sulfate may become more reactive because of the change in support structure, near-surface vacancies or the more easily reducible promoter ions may act as catalyst in the reduction process because they can accept negative charges. Definitely, the promoters enhance the oxidation potential of sulfate.

^{viii} F.C. Jentoft, B.C. Gates, unpublished results.

6.2.3 Conclusions

The Brønsted acidity of the OH groups of SZ, as probed with *n*-butane, is lower than those of strongly acidic zeolites. Manganese or iron do not enhance the Brønsted acidity of SZ. These promoters, thus, do not improve the ability of the catalyst to activate *n*-butane via protonation and subsequent cleavage of H₂. The Lewis acid sites of SZ, as probed with H₂, are comparable to those of other oxidic compounds. Manganese effects a slight decrease in Lewis acid strength rather than an increase. From these observations, it appears as if the promoters do not augment the hydride abstraction ability of the catalyst. The promoters do not increase the acid strength of the catalyst and their effect on the reaction rate must be related to a different functionality of the catalyst.

The results of interaction between H₂ or *n*-butane and SZ or promoted SZ at elevated temperatures are summarized in Table 2. Hydrogen gives information on the reducibility of the catalyst, which indicates its oxidation potential. At a temperature where SZ is inert, MnSZ oxidizes H₂ to water. In the experiments at 473 K, sulfate groups are consumed concomitantly with the formation of water. Sulfate could thus be the oxidizing agent, and the presence of manganese enhances its reactivity in comparison to unpromoted SZ.

Tab. 6-1: Reactivity of unpromoted and promoted SZ catalysts towards molecular hydrogen and *n*-butane at different temperatures observed by DRIFT spectroscopy

catalyst	temperature	reactant	observations made by DRIFT spectroscopy
SZ	473 K	H ₂	no change
MnSZ	473 K	H ₂	formation of H ₂ O, Zr-hydride; decrease of sulfate
SZ	573 K	<i>n</i> -C ₄ H ₁₀	formation of H ₂ O, H ₂ S, CO ₂ , alkene; decrease of sulfate
MnSZ	373 K	<i>n</i> -C ₄ H ₁₀	formation of H ₂ O, isoalkane; decrease of sulfate
FeSZ	373 K	<i>n</i> -C ₄ H ₁₀	formation of isoalkane; decrease of sulfate

n-Butane can be converted to isobutane by SZ at 358 K in a flow reactor (Fig. 6-4); the rate is very low and there is almost no deactivation. Significant spectral changes in the batch experiment became apparent only at 573 K. Under these relatively harsh reaction conditions, butane is being oxidized, as well partially to olefinic compounds as totally to CO₂, with simultaneous formation of water. Sulfate in turn is totally reduced to H₂S and clearly functions as an oxidizing agent in this case. Water is formed also during low temperature isomerization,^{124,196} indicating redox reactions as at high temperature and consistent with activation of a small fraction of *n*-butane molecules via ODH.

Manganese and iron lower the temperature for reaction of SZ with *n*-butane dramatically. Skeletal isomerization is detected at 323 K in the flow reactor and at 373 K in the batch system (Fig. 6-4 and Fig. 6-8, right). CO₂ and H₂S are not detected at 373 K, i.e. the redox reactions do not proceed as far as with SZ at 573 K. Alkenes are not detected, but according to the ODH initiation scenario they would be protonated immediately. Further indication of the ODH reaction is the formation of water in case of MnSZ. Again, sulfate may serve as an oxidizing agent, as its bands are diminished at 373 K. If sulfate species are the oxidizing agent also at low temperatures, the corresponding reduced sulfur species remains on the surface and can be reoxidized as the catalysts can usually be reactivated several times (see Chapter 7).

Rather than modifying the acidity or acting as oxidizing agents themselves, as suspected initially, the promoters enhance the reactivity of the sulfate. Taking into account the fact that promoters such as manganese are incorporated into the zirconia lattice,³⁹ the effect of the promoters may be indirect in that they alter the structural and electronic properties of the zirconia, which in turn affect the reducibility of the sulfate. Specifically, the promoters increase the oxidation potential of the sulfate and, thus, facilitate butane activation by ODH and accordingly isomerization at lower temperature.

7. *n*-Butane Isomerization on Sulfated Zirconia-Based Catalysts

7.1 Introduction

n-Butane isomerization is believed to proceed via carbenium ions as reaction chain carriers (see Chapter 2.5). It has been suggested that butane is activated by promoted SZ containing Fe and Mn through oxidative dehydrogenation (ODH) to give water and butenes, which are easily protonated to carbenium ions.⁹⁹ A more active material after activation in oxidizing atmosphere than in inert gas has been presented as evidence.^{99,105} Besides the optimal activation atmosphere, the activation temperature has been discussed, mainly in the context of the water content. Vera et al. reported increasing activity of SZ with higher activation temperatures for the range <898 K.¹¹⁸ Song and Kydd inferred that the Brønsted to Lewis ratio should be adjusted to 2:1 by hydration in SZ;²⁰⁷ the best pretreatment temperatures were 423 K for SZ and 723 K for promoted SZ.¹⁰⁵ Closely linked to the hydration degree is the state of a key component of these catalysts, the sulfate, as evidenced by a shift of the S=O vibration with variation of the activation temperature.¹⁴⁹

Initiation of the reaction by ODH,⁹⁹ with concomitant reduction of the promoter⁹⁹ or the sulfate and zirconium,¹¹⁸ and water formation^{99,118} is so far a hypothesis. Evidence for the formation of water or carbenium ions is lacking, but deactivation has been explained by reduction of the promoter for Fe-promoted SZ by Millet et al.¹²⁵ However, Yamamoto et al.¹⁰⁸ reported that the valence of Fe was unaffected by *n*-butane. The reaction of Mn upon exposure to butane¹⁰⁸ is not correlatable to the catalytic performance.^{147,148} Deactivation of promoted SZ catalysts may also be caused by effects that have been proposed to account for deactivation of SZ itself like coke formation, reduction of Zr⁴⁺ or sulfate, and poisoning by water (see Chapter 2.6). Attempts to regenerate SZ catalysts have been made using conditions resembling those of activation. Reactivation of SZ is possible in air or oxygen at 723–753 K and the DRIFT, Raman, or UV–vis spectra are identical to those of the fresh catalyst.^{135,141,142} Risch and Wolf obtained better results when they not only regenerated the catalyst in O₂ but also exposed it to water.²²⁷ Coke can be removed from the surface as CO₂ in inert gas but the sulfate decomposes concomitantly.^{118,138} Coke removal in oxidative conditions may disguise that the catalyst is also oxidized. Many of the investigations on catalyst activation and regeneration just report the influence of different treatments on the activity without characterization of the catalyst in the activated state. Equally, studies of interaction of SZ catalysts with alkanes using IR,^{53,55,117} EPR,²²⁸ or calorimetry²²⁹ lack information on the gas phase composition and potential reactions. Furthermore, most ideas on deactivation are based

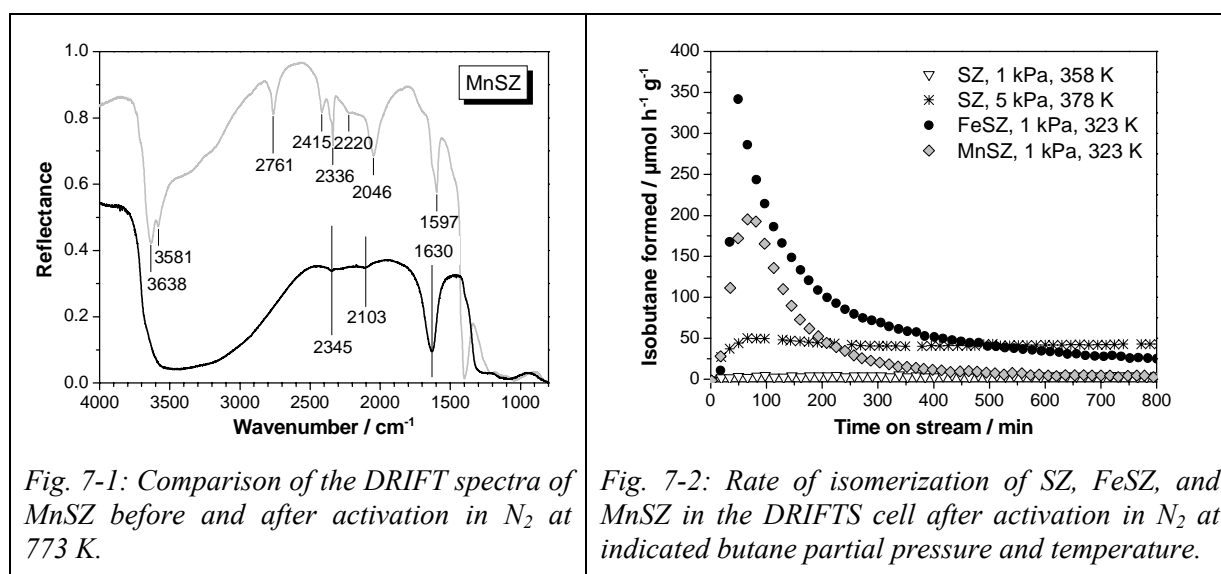
on the study of the catalysts after removal from the reactor. Few true *in situ* data with simultaneous analysis of SZ catalysts and their butane isomerization performance with time on stream exist,^{147,148,230} and the potential formation of water and the state of sulfate during the reaction have not yet been addressed.

Here, *in situ* IR spectroscopy in the diffuse reflectance is used in order to avoid pressing a wafer, which may cause partial transformation of tetragonal to monoclinic zirconia and also reduces activity (see Chapter 5.1). SZ, FeSZ, and MnSZ are compared after activation and during *n*-butane isomerization; MnSZ was selected to investigate activation and regeneration treatments in oxidizing or inert atmosphere.

7.2 Results

In all catalyst samples, only the tetragonal phase could be detected using X-ray diffraction. BET surface areas were: SZ 155 m²·g⁻¹, FeSZ 139 m²·g⁻¹, and MnSZ 112 m²·g⁻¹.

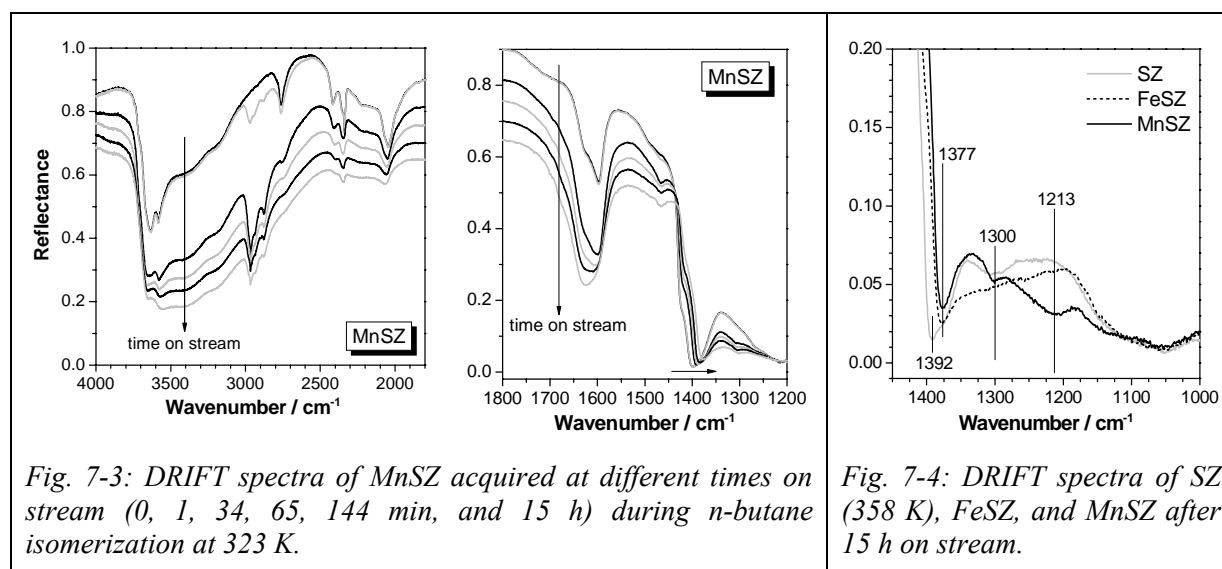
7.2.1 Activation in N₂ and *n*-butane isomerization



IR spectra of the calcined, not yet activated catalysts are typical of a hydrated surface with strong hydrogen bonding vibrations. As an example, the initial spectrum of MnSZ is shown in Fig. 7-1. The figure also contains the spectrum of MnSZ after activation in nitrogen flow at 773 K taken after cooling to reaction temperature, i.e. at 323 K. The activation procedure results in strong reduction of the broad band between 3700–3000 cm⁻¹, consistent with dehydration. The spectra are characterized by bands originating from hydroxyl groups and adsorbed water (3700–3500 and 1630–1600 cm⁻¹ ranges), from different sulfate structures (2800–1950 cm⁻¹ and 1400–1000 cm⁻¹ ranges), and from adsorbed nitrogen (2336 cm⁻¹). SZ

and FeSZ show the same trend during and similar but not identical spectra after activation (see Chapter 3.4).

Data from catalytic experiments in the *in situ* DRIFTS cell (Fig. 7-2) are compared to those generated using a tubular fixed bed plug-flow reactor (see Fig. 6-4). *n*-Butane isomerization in the two systems was performed at 358 K (SZ) or 323 K (promoted SZ) and the same weight hourly space velocity of 0.3 h⁻¹. Qualitatively, the same reaction profile is observed, consisting of induction period, a maximum in activity, and a deactivation period. The maximum rate is somewhat lower in the DRIFTS cell and is achieved about 15 min later (MnSZ) than in the tubular reactor. The considerable dead volume of the DRIFTS cell (ca. 100 ml) may account for this delay, because some time is needed to generate the desired *n*-butane partial pressure of 1 kPa (1 vol% *n*-butane in nitrogen). Certainly, the reaction data from the DRIFTS cell reflect the essential performance features of the catalyst and are of sufficient quality. SZ exhibited no measurable activity at 323 K (not shown), and even at 358 and 378 K, the maximum rates (0.1 or 0.2 % conversion to isobutane) are lower than those of FeSZ or MnSZ at 323 K. FeSZ produces a higher maximum isomerization rate (>350 μmol·g⁻¹·h⁻¹, 7.1 % conversion) than MnSZ (200 μmol·g⁻¹·h⁻¹, 4.2 % conversion). The promoted catalysts deactivate partially within hours, the MnSZ more rapidly than the FeSZ catalyst. At the low conversions achieved with SZ, hardly any deactivation is observed. The long-term activity (> 10 h) is seemingly highest for SZ; but the reaction temperature is 55 K above that used for the promoted systems.



IR spectra recorded of MnSZ during *n*-butane isomerization are shown in Fig. 7-3. Within the first minute on stream, bands at 2966, 2939, 2877 (CH stretching) and 1466 cm⁻¹ (CH bending) become visible. The following spectra represent the situation during the induction

period at ca. 2 % conversion, at maximum conversion (4.2 %), during deactivation at about 2 % conversion, and after 15 h time on stream. During the course of the reaction the overall reflectance between 4500 and 1200 cm^{-1} decreases. Further changes include growth of a band at around 5200 cm^{-1} (not shown), which is indicative of adsorbed water. Additional bands develop in the region 1630–1600 cm^{-1} . The OH stretching band at 3580 cm^{-1} gains in intensity and broadens. The band of adsorbed N_2 at 2336 cm^{-1} disappears during the induction period. While the isomerization reaction is progressing, the S=O band at 1399 cm^{-1} is slowly shifted to 1377 cm^{-1} (Fig. 7-3, right).

Changes in the spectra of SZ and FeSZ observed during *n*-butane isomerization are in principle the same as for MnSZ. Differences can only be discovered in the region between 1450 cm^{-1} and 1000 cm^{-1} , as spectra taken after 15 h of reaction show (Fig. 7-4). While the spectra of SZ and FeSZ remain unaffected in this region, a band at around 1300 cm^{-1} is formed in the case of MnSZ.

7.2.2 Activation and regeneration of MnSZ in N_2 and O_2

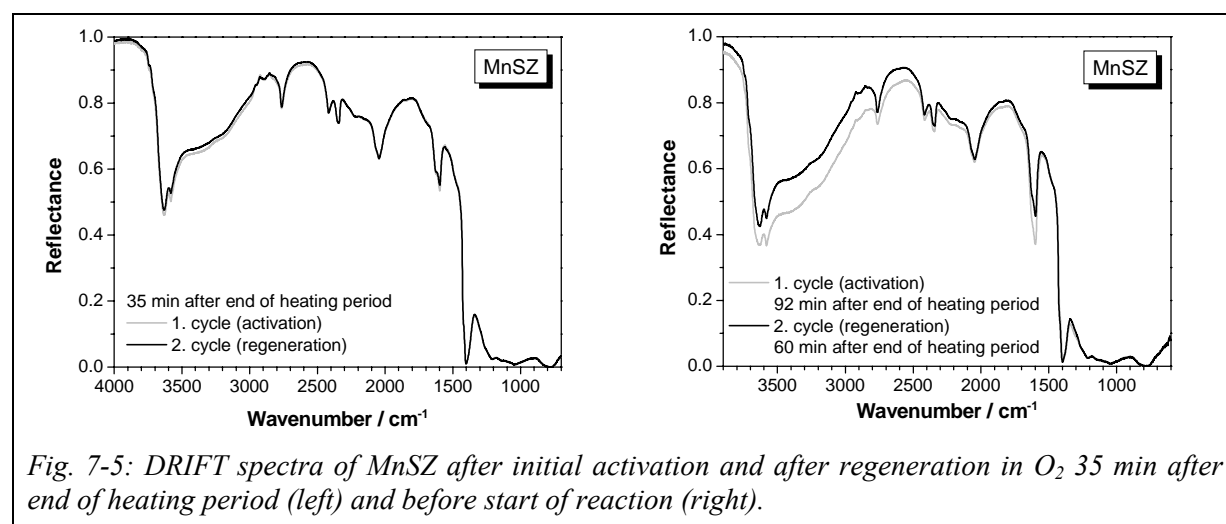
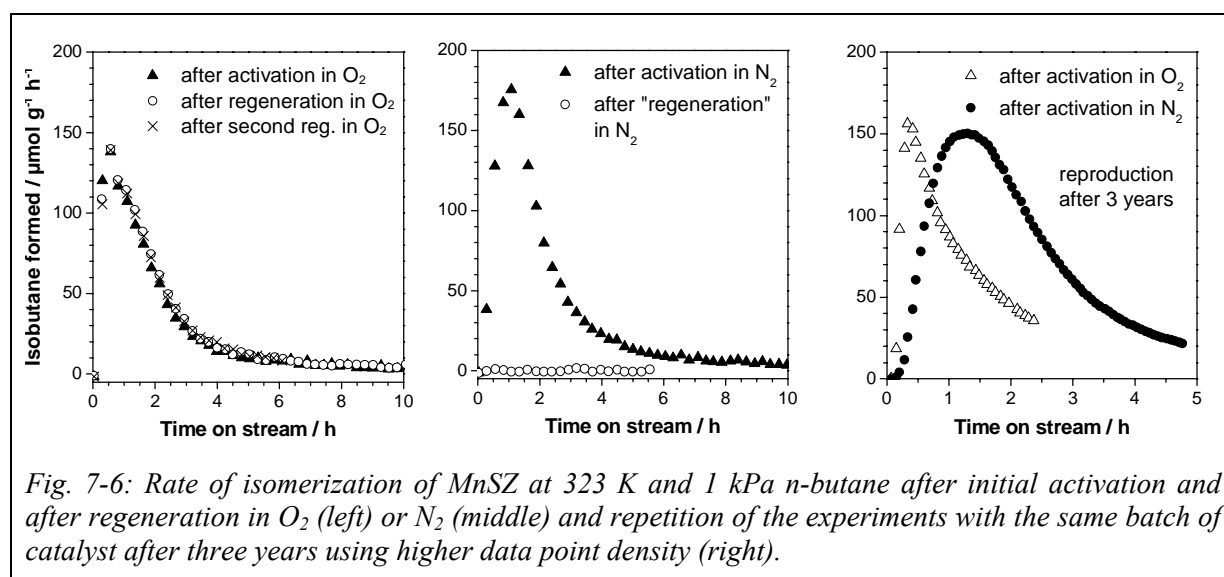


Fig. 7-5: DRIFT spectra of MnSZ after initial activation and after regeneration in O_2 35 min after end of heating period (left) and before start of reaction (right).

MnSZ, which exhibits distinct induction and deactivation periods at 323 K, was chosen for regeneration experiments. Fig. 7-5 (left) shows the DRIFT spectra of a MnSZ catalyst at 323 K after activation and after its regeneration in flowing 100 vol% O_2 following 16 h of isomerization reaction at 323 K. These spectra were recorded 35 min after the end of the holding time at 773 K, i.e. during the cooling phase. The band positions in the two spectra are identical, and the intensities differ only slightly in the region of OH stretching and deformation vibrations and between 3500 and 3000 cm^{-1} . The waiting time after cool-down determined the catalyst state immediately before the start of the reaction. Fig. 7-5 (right) shows spectra acquired 92 min and 60 min after the end of the heating period at 773 K. The

longer waiting time in O₂ flow after the regeneration in comparison to the initial activation leads to higher intensities of the water deformation bands (around 1600 cm⁻¹) and the bands caused by hydrogen bridges (3500–3000 cm⁻¹). This difference in the water content has no discernable influence on the rate of isomerization as can be seen in Fig. 7-6 (left), which shows the corresponding rate data. The MnSZ catalyst can be fully regenerated with the same reaction profile along time on stream. Using 100 % O₂ atmosphere, it is possible to regenerate the catalyst at least twice. Also after initial activation in N₂, regeneration in 100 % O₂ produces the same catalyst state as in the experiment with both activation and regeneration in O₂. Activation in N₂ seems to produce a slightly more active MnSZ catalyst than activation in 100 % O₂ (compare Fig. 7-6, left and middle); the maximum rate reaches 180 μmol·g⁻¹·h⁻¹ vs. only 140 μmol·g⁻¹·h⁻¹ after activation in O₂. However, the activity changes so rapidly that the time resolution of the GC analysis may be insufficient to detect the real maximum. Repeating the experiments three years later with better time resolution using a Micro-GC (see Chapter 4.4.3) shows, indeed, that MnSZ is rather more active after activation in O₂ than in N₂.



In 100 % N₂ atmosphere, a deactivated MnSZ catalyst cannot be regenerated; it is completely inactive (Fig. 7-6, middle). Fig. 7-7 shows the spectra of MnSZ after activation, after reaction and purging of the cell with nitrogen for 1 h, and after a regeneration attempt at 773 K in N₂. The spectrum after reaction exhibits bands indicative of adsorbed water including hydrogen bridges. A group of weak absorption bands between 2980 and 2850 cm⁻¹ could arise from surface hydrocarbon deposits. The post-reaction heating in N₂ does not lead to a complete recovery of the spectrum of the activated sample. Instead, two new bands appear in the CH deformation region of aliphatic and aromatic compounds at 1532 and

1465 cm^{-1} (Fig. 7-7, right). However, all bands arising from OH groups or sulfate species approach their original position and intensity.

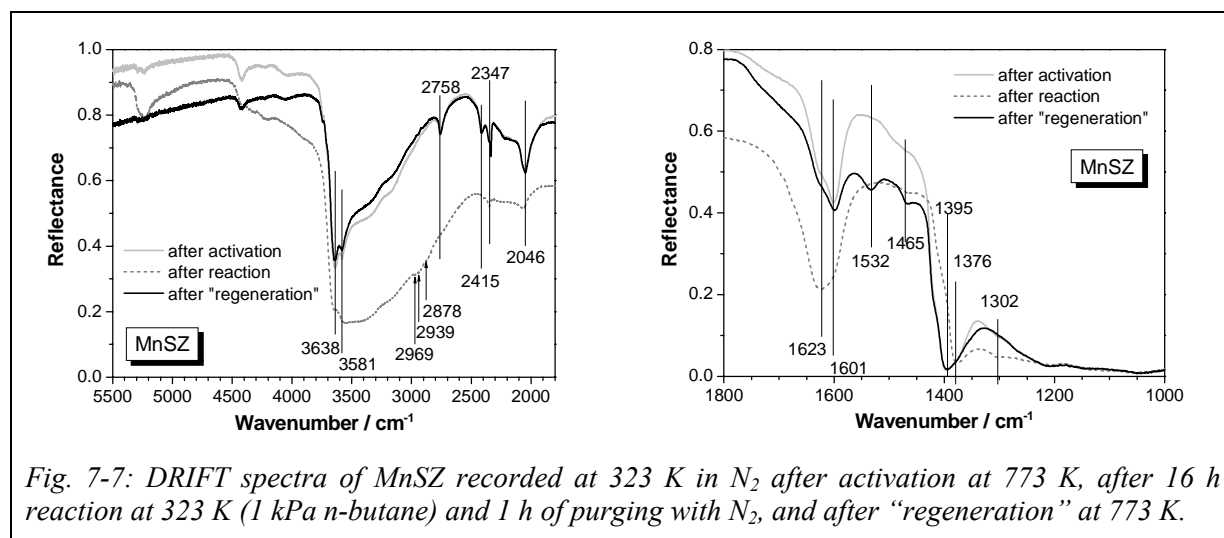


Fig. 7-7: DRIFT spectra of MnSZ recorded at 323 K in N_2 after activation at 773 K, after 16 h reaction at 323 K (1 kPa *n*-butane) and 1 h of purging with N_2 , and after "regeneration" at 773 K.

7.3 Discussion

7.3.1 Estimation of water content after activation

The main effect of activation that is visible in the IR spectra is dehydration. The bands indicative of hydrogen bridges in the range 3500–3000 cm^{-1} are reduced in intensity, as are the water deformation modes in the range 1630–1600 cm^{-1} . Thermogravimetry (TG) experiments of a number of promoted and unpromoted samples (stored in vials in the laboratory) show varying water contents, typically in the range 2.2–4.6 wt%, corresponding to 1.2–2.5 $\text{mmol}\cdot\text{g}^{-1}$ (see Chapter 3.3). A rough estimate of the amount of water removed during activation is given by the intensity of the bands in the region 1630–1600 cm^{-1} . The reflectance spectra were converted into Kubelka-Munk units and integration was performed over the width of the entire feature. For SZ, MnSZ, and FeSZ, the intensity was reduced by >95 % after activation at 773 K. The remaining water content is then estimated to be 60–125 $\mu\text{mol}\cdot\text{g}^{-1}$. The typical sulfur content (also from TG experiments, see Chapter 3.3) is about 560 $\mu\text{mol}\cdot\text{g}^{-1}$, meaning that in the activated catalysts, enough water is present to hydrate a considerable fraction of the sulfate species. For example, about 10–22 % of SO_4^{2-} or 20–44 % of $\text{S}_2\text{O}_7^{2-}$ groups could be singly hydrated.

7.3.2 Activation and catalytic performance

By choice of the activation conditions, the degree of hydration of the surface and the oxidation states of individual catalyst components are determined. As discussed above, the surface of the investigated catalysts was more than 95 % dehydrated. In this activated state, the surface is highly hydrophilic and adsorbs traces of water from the environment. Different waiting times in O₂ after cool-down to reaction temperature led to variations in the band intensity in the range 1630–1600 cm⁻¹; the areas and thus the water content of MnSZ corresponded to either 2.5 or 5 % of the initial area (Fig. 7-5, right). The influence of the activation conditions, which determine the surface hydration, has been stressed in several papers^{142,149,227,229,231,232} and González et al.²⁰⁶ inferred that a water concentration of 75 μmol·g⁻¹ is optimal, while Song and Kydd²⁰⁷ reported best performance at 200 μmol·g⁻¹. Here, a variation by a factor of two in the degree of hydration had no visible effect on the catalytic performance (Fig. 7-5, right and Fig. 7-6, left).

The atmosphere during activation does not seem to have an influence on the performance of SZ.¹⁰⁵ More investigations are available for catalysts promoted with Fe and Mn, because of the potential redox function ascribed to the promoters. Wan et al. found an effect of the atmosphere on the activity of Fe- and Mn-promoted SZ only for activation temperatures above 723 K; a treatment in air resulted in a conversion twice as high than a treatment in He at 923 K.⁹⁹ Morterra et al. observed a promoting effect of Fe and Mn only after activation in air and not after activation in He.¹⁰² Song and Kydd¹⁰⁵ found a higher conversion after activation in air than after activation in He, regardless of the activation temperature (range ca. 523–873 K). After activation in N₂, the investigated Fe- or Mn-promoted catalysts both exhibited, even at lower temperature, much higher maximum rates than sulfated zirconia. Activation of promoted catalysts in inert environment is thus possible, consistent with the observations of Wan et al.⁹⁹ and Song and Kydd.¹⁰⁵ SZ-based catalysts usually have been calcined in air at about 823–923 K, so there is no reason to expect further oxidation during an air treatment at lower temperature, rather the presence of oxygen may prevent some reduction in comparison to heating in inert.

Mn-promoted SZ activated in 100 % O₂ produced a maximum rate of 140 μmol·g⁻¹ h⁻¹ isobutane vs. 180 μmol·g⁻¹ h⁻¹ after activation in N₂. This difference was reproducible, however, errors could arise from lack of time resolution in the GC analysis (Fig. 7-6, left); specifically a rapid increase of conversion for the O₂-activated sample may have been missed as suggested by repeated experiments after three years (Fig. 7-6, right). Despite the use of the same batch of catalyst, the catalytic profile is not reproduced: The maximum rate after

activation in N₂ is lower and reached about 20 min later than in earlier experiments. However, the catalyst was not fresh at the time of the reproduction but three years old. A negative influence of the time of storage on the catalytic performance of MnSZ was shown in Chapter 5.2.

A positive effect of an oxidizing activation will be expected if a high oxidation state of the catalyst components is advantageous, i.e. in a reaction initiation through oxidative dehydrogenation with e.g. the promoters as oxidizing agents, or if more sites become available through removal of ubiquitous surface carbon contaminations. Data on the changes of the promoter valence as a consequence of potential ODH are controversy. Millet et al.¹²⁵ applied X-ray photoelectron spectroscopy and found Fe reduced after *n*-butane isomerization at 323 K, while Jentoft et al. could not find a performance-related change of the Mn valence with in situ X-ray absorption experiments at 333 K.^{147,148} However, activation of MnSZ in 50 % O₂ in He produced a catalyst with a better performance than activation in He,¹⁴⁸ similar to the trend reported in the literature for mixed, Fe- and Mn-promoted systems. All studies in the literature were conducted in air while 100 % O₂ was used here. Despite these extremes, namely 0 and 100 % O₂, in the activation of MnSZ, the short term isomerization rates were within close range and the long term (6–14 h on stream) rates were almost the same for both atmospheres. Hence, for the steady-state performance, the choice of activation atmosphere might be irrelevant.

7.3.3 IR spectra during *n*-butane isomerization

The bands in the IR spectra arise from four different classes of species, namely adsorbed hydrocarbon species, adsorbed N₂ (present after activation in N₂), OH groups and adsorbed water, and sulfate groups. During reaction, the spectral signature changes, and it was analyzed whether changes of one species are connected to changes of another species or to the catalytic performance.

The dominant contributions in the regions of hydrocarbon vibrations arise from gas phase species, as experiments with a non-reactive reference material (KBr) revealed. It was so far not possible, e.g. via the calculation of difference spectra, to identify bands attributable to adsorbed hydrocarbon species in the spectra recorded during butane isomerization.

The sharp band at 2336 cm⁻¹ that is only observed after activation in N₂ is slightly blue-shifted vs. the N₂ gas phase absorption (2330 cm⁻¹) as is typical of N₂ interacting with acid sites.²³³ At room temperature, N₂ is expected to interact with strong Lewis acid sites and not with OH groups. The band disappears already during the induction period. The feed contains

95–99 % N₂, so desorption due to reduced N₂ pressure in the gas phase is negligible. For non-sulfated zirconia, only a broad feature at 2341 cm⁻¹ is observed and it does not undergo significant changes during *n*-butane exposure (not shown). In light of these observations it can be concluded that *n*-butane or its reaction products displace N₂ adsorbed on strongly acidic Lewis sites on the surface of sulfated zirconia materials.

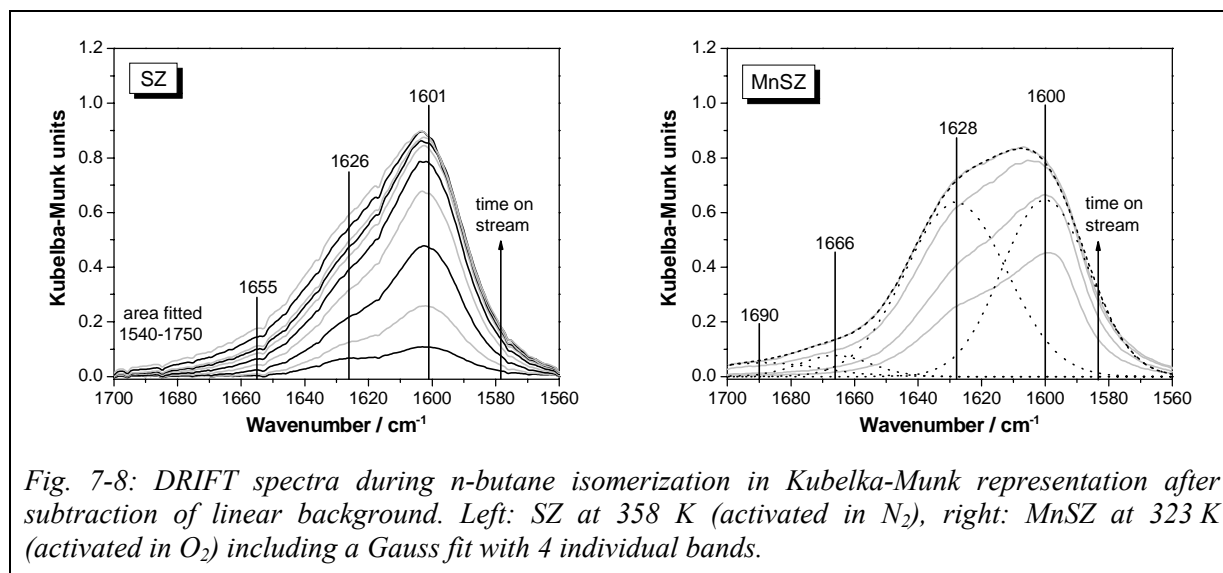


Fig. 7-8: DRIFT spectra during *n*-butane isomerization in Kubelka-Munk representation after subtraction of linear background. Left: SZ at 358 K (activated in N₂), right: MnSZ at 323 K (activated in O₂) including a Gauss fit with 4 individual bands.

Further distinct changes occur in the region 1760–1540 cm⁻¹. Two small bands at about 1600 and 1625 cm⁻¹ are present in this region already after activation. These bands increase somewhat with time also in the absence of butane because water is present as a trace contamination in the system and adsorbs on the catalyst. During *n*-butane isomerization, several intense bands develop rapidly with time on stream, shown for SZ and MnSZ in Fig. 7-8 after conversion to Kubelka Munk units and subtraction of a linear background. Bands in this region can arise from the deformation vibration of water, which in the gas phase water is observed at 1595 cm⁻¹ but is shifted to higher wavenumbers when water is hydrogen-bonded to surface atoms or other water molecules. Alternatively, C=C stretching vibrations can absorb within this range. A band simultaneously growing at 5200 cm⁻¹ is a combination mode of OH stretching and bending vibration and indicates formation of water; however, contributions from other species cannot be excluded on the basis of the obtained spectra. The broad feature between 1760 and 1540 cm⁻¹ was fit with up to four Gauss curves (see example Fig. 7-8, right). Band positions were at 1720–1685, 1680–1655, 1635–1620, and 1605–1598 cm⁻¹. An area of zero sometimes resulted for the bands at 1720–1685 and 1680–1655 cm⁻¹, depending on the constraints applied during the fitting procedure. All bands grew with time on stream, and when the full width at half maximum was fixed (e.g. to 27 cm⁻¹), scatter was reduced and the increase was monotonous. The areas of the bands in the range

1690–1625 cm^{-1} increased first steeply for about 2 h and then more slowly. The band at 1600 cm^{-1} increased during the induction period and then ceased growing, which can also be recognized in the spectra in Fig. 7-8. This species is thus clearly associated with the induction period. It has often been hypothesized that the induction period is due to “buildup of olefins on the catalyst surface”.⁹⁴ Although the time-on-stream evolution of the species here suggests it could be such a postulated intermediate, there is no indication yet for it not being water and thus a side-product of an initiation reaction. The frequency is very close to that of gaseous water, consistent with isolated water molecules; with increasing time on stream and surface coverage these water molecules will associate with other water or hydrocarbon molecules and the frequency will change, meaning the band at 1600 cm^{-1} may stop growing or even shrink.

Assuming that each molecule of water or of any other species is equivalent to the formation of one surface intermediate from *n*-butane, the band areas can be taken as a measure of the number (concentration) of these active surface species. If the formed surface species act as active sites for many reaction cycles in a catalytic manner, the rate of isomerization will be proportional to the concentration, i.e. the total band area increase relative to the starting value. It has also been proposed that during the initial phase of high activity of promoted catalysts, processes are stoichiometric rather than catalytic.⁸⁸ If each intermediate reacts just once, the rate of isomerization would be proportional to the differential increase in surface species, i.e. to the incremental band area.

It was attempted to correlate the rate of isobutane formation (during the induction period of increasing activity) to the area of individual bands or the sum of areas of several bands. There was definitely no correlation between rate and incremental area increase for any of the bands. As all bands increase with time on stream and the rate also increases during the induction period, correlations with linear segments were almost always obtained, and the linear correlation extended through most of the data points from the induction period for the two large bands. The band(s) at high frequency were very small and the areas extracted from the fits not considered reliable. It was not possible to make an assessment as to which individual bands were connected to the rate and which not. If the bands arose from differently associated water species, all of them would indicate formation of an active surface species and the sum would reflect the total number. The best correlation with the rate was obtained when all bands in the range 1760–1540 cm^{-1} were considered. Because the baseline is not straight over this range (see Fig. 7-3, middle) the minima (in Kubelka-Munk representation) on either side of the group of bands were used as integration limits. The area prior to reaction was subtracted, i.e. the isomerization rate was plotted vs. the area increase. Such correlations are shown in

Fig. 7-9 (left) for SZ and MnSZ. For SZ (358 K and 1 kPa *n*-butane) the conversion was low and the rate data, which scattered somewhat (see Fig. 7-2), were smoothed for this analysis. A linear correlation results in the case of SZ, consistent with observations by Li et al.¹²⁴ At 378 K and 5 kPa *n*-butane, a steeper slope resulted (roughly 10 times as steep, not shown). For MnSZ, the rate of isomerization also increased with the area of the feature in the IR spectra but the data show deviations from linearity, and linear regressions do not necessarily pass through the origin. Possible reasons might be the following: Seemingly small initial rates may be caused by hindered product desorption at the low reaction temperature, or a delay of the gas phase analysis relative to the events in the DRIFTS cell, which becomes evident only when the performance changes rapidly. Towards the end of the induction period, the rate may already be reduced by deactivation because in contrast to SZ, MnSZ deactivates. All these arguments are valid also in case of FeSZ, which changes performance even faster than MnSZ. Indeed, rate and IR data seemed uncorrelated in case of FeSZ. However, in the transmission IR cell FeSZ had to be pressed to a wafer (see Chapter 6.1), which led to a lower activity due to the mechanical stress exerted on it (see Chapter 5.1). Here a similar correlation as for the DRIFT spectra of MnSZ was found for the absorbance of FeSZ in the range 1760–1540 cm^{-1} (Fig. 7-9, right).

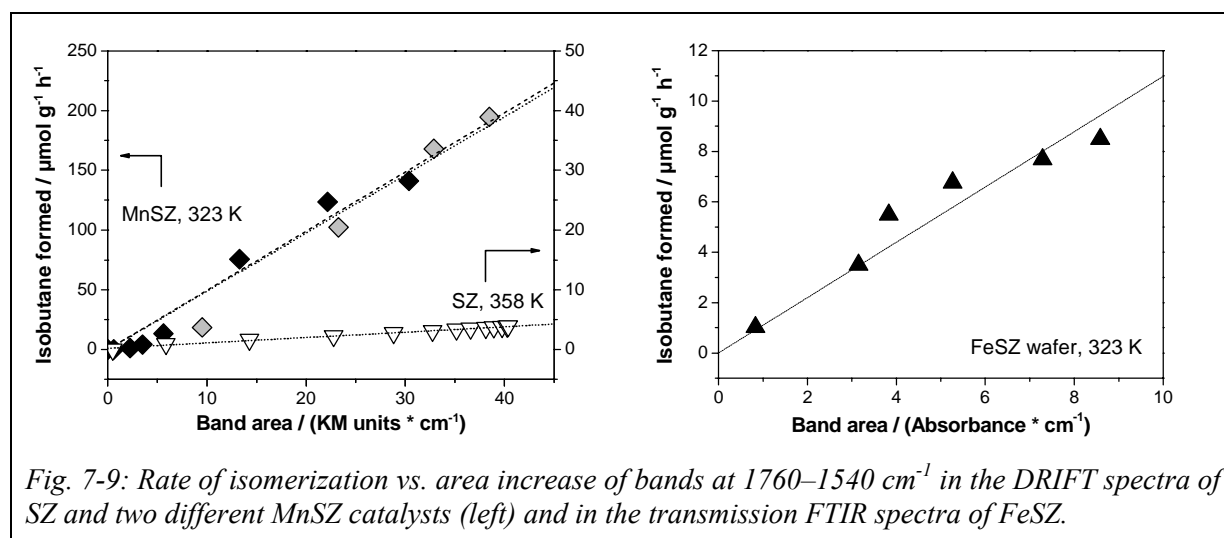


Fig. 7-9: Rate of isomerization vs. area increase of bands at 1760–1540 cm^{-1} in the DRIFT spectra of SZ and two different MnSZ catalysts (left) and in the transmission FTIR spectra of FeSZ.

A linear correlation of the isomerization rate to the amount of water is consistent with the hypothesis of an ODH initiation reaction. However, water is only one out of three products of ODH. There is so far no proof of an adsorbed butene or a species formed from it unless one or more of the bands arise from C=C vibrations. Reduction of a catalyst component is also not evident, whereby probably only reduction of sulfate and not of zirconium or a promoter may be detectable by IR spectroscopy. Furthermore, it cannot be distinguished, whether water is

formed by ODH or in a secondary reaction after protonation of the alkane, i.e. through oxidation of the hydrogen *in statu nascendi* from decay of an alkanium ion.

There is a considerable difference between SZ and MnSZ in the slopes (Fig. 7-9, left). Assuming equal extinction coefficients of the same bands for the two catalysts, a faster turnover per active surface species is observed for the promoted catalyst. The reaction temperature is lower for the promoted catalyst but this should cause a flatter slope: The isomerization rate should be lower at lower temperature, and more of the formed water should accumulate on the surface (and not desorb) than at higher temperature. Hence, the difference between the two catalysts may in reality be even larger. The result demonstrates that independent of the initiation reaction, promoted catalysts exhibit a faster intrinsic isomerization rate. The total amounts of water formed on either of the catalysts in the two experiments shown in Fig. 7-9 (left) are comparable, indicating no significant difference in the number of sites capable of initiation. Considering also the observations of the Mn valence, which does not change in any particular way during the induction period,¹¹⁰ the role of the promoters seems to be acceleration of the isomerization cycle.

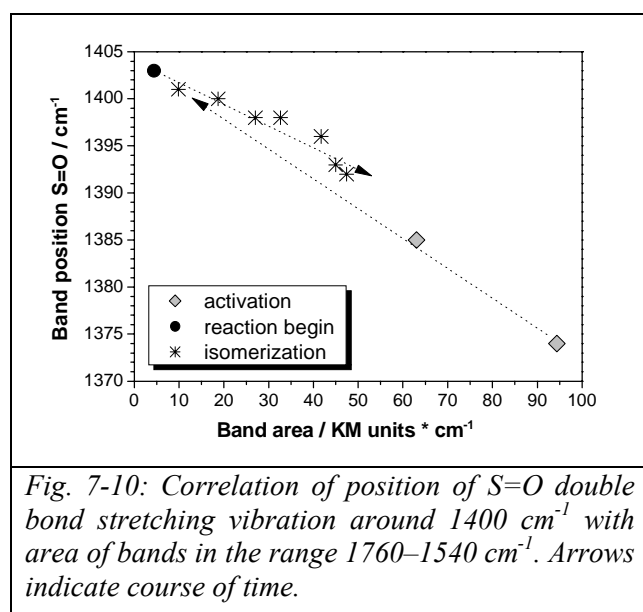


Fig. 7-10: Correlation of position of S=O double bond stretching vibration around 1400 cm⁻¹ with area of bands in the range 1760–1540 cm⁻¹. Arrows indicate course of time.

The position of one of the S=O vibrations changed during the course of the reaction, indicating modifications to structure or environment of the sulfate. This band, in the literature located at 1400–1370 cm⁻¹ depending on sample and pretreatment, is known to shift upon adsorption of polar molecules, e.g. pyridine or CO cause shifts of up to -81²³⁴ or -31 cm⁻¹,⁴⁵ respectively. Here, this band had shifted upwards during pretreatment, i.e. dehydration of the catalyst, and shifted

downward during reaction. In Fig. 7-10 the shift of the S=O double bond stretching vibration is plotted vs. the area of the bands in the range 1760–1540 cm⁻¹ for the SZ catalyst. There seems to be a linear correlation, although the change of the S=O band position for SZ is small and the slopes are shallow. One interpretation of the almost identical slope for the activation and for the reaction branch is that the shift during reaction is only caused by water and not by any other surface species, such as a hydrocarbon deposit. However, the effect of the very polar water molecule may overpower the effect of a second species. For promoted SZ, the

shift of the S=O band is about 1.5 larger than for SZ at equal total area of the water bands (not shown), which is further evidence for a more reactive sulfate in presence of Mn and Fe as discussed in Chapter 6. Reasons for this difference between SZ and promoted SZ could be variations in the extinction coefficient for the adsorbed water species, a more easily polarizable sulfate species on the surface of the promoted catalysts, or both.

7.3.4 Regeneration

Several authors have reported that the activity of SZ^{135,141,149} and of promoted SZ¹⁰² catalysts can be fully regenerated by heating in air to 723 K or in O₂ at 753 K. Regeneration in O₂ at 723 K “essentially reproduces” the DRIFT spectrum of freshly activated SZ,¹³⁸ also the Raman spectrum is identical to that of a fresh catalyst after reactivation at 753 K in O₂.¹³⁵ Irreversible changes to the SZ were reported after reaction of longer hydrocarbons such as hexane at a relatively high reaction temperature of 473 K.¹³⁶ Formation of H₂S during reaction of *n*-butane at 523 K was reported by Ng and Horvát.¹³³ Furthermore, Risch and Wolf claimed that to recover the original activity of SZ, treatment in oxygen must be followed by rehydration.²²⁷ Also for promoted SZ, regeneration may fail, e.g. Coelho et al. could not recover the high initial activity.⁹⁸ Morterra et al. reported that an initial activation of Fe- and Mn-promoted SZ in He produces a material as active as unpromoted SZ, and even subsequent oxidizing treatments cannot generate a highly active catalyst.¹⁰² Here, it was possible to completely re-establish the IR spectrum and the catalytic activity of MnSZ through treatment at 773 K in O₂. Even when the catalyst was first activated in N₂ and then regenerated in O₂ the same state as after activation or repeated regeneration in O₂ was reached, as evidenced through spectra and performance. Obviously, neither of the treatments at 773 K nor the isomerization reaction at 323 K causes irreversible changes to the material. One potential explanation for the discrepancy in comparison to Morterra’s results is the difference in composition; his catalyst contained additionally Fe.

The spectrum of the deactivated MnSZ is dominated by bands of adsorbed water. On this broad background, very weak bands of hydrocarbon species are visible in the CH stretching vibration region. After a regeneration attempt in N₂, pronounced bands of hydrocarbon deposits are detected. Two bands at 1533 and 1465 cm⁻¹ indicate conjugated C=C stretching and CH bending (position not specific for unsaturated or saturated species) vibrations. Therefore, small amounts of hydrocarbons must have remained on the surface after reaction, although the system was purged for 1 h in N₂ before heating for regeneration, and these species undergo dehydrogenation to unsaturated compounds. According to the literature,

removal of coke through heating in inert gas is possible,¹¹⁸ but according to Li and Gonzalez is accompanied by SO₂ evolution.¹³⁸ The reflectance in the region of the fundamental sulfur-oxygen vibrations is so low that changes in sulfate content may not lead to a measurable change in intensity. But the sulfur-oxygen overtones and combination modes are almost congruent in the spectra of the activated and the “regenerated” MnSZ (Fig. 7-7, left). Hence, there is no evidence for significant sulfur loss during the treatment in N₂. This result seemingly contrasts Li’s and Gonzalez’ observation of SO₂ evolution upon heating the deactivated catalysts in N₂,¹³⁸ but they had conducted the isomerization at 473 K using 10 kPa *n*-butane, and presumably more and different coke species formed than under the mild reaction conditions used here. In light of the presented observations and the literature data, it appears that SZ catalysts are irreversibly damaged when exposed to trace amounts of hydrocarbons—even contaminations in a feed delivery system—at too high a temperature.

The fact that MnSZ “regenerated” in N₂ is completely inactive although the sulfate pattern in the IR spectrum equals that of activated MnSZ merits some consideration. As sulfate is a prerequisite for isomerization activity, it is assumed that it is part of the active site. It has been proposed that only 20 % of the sulfate are involved in adsorption of the reactant, and only 2 % acted as reaction sites.¹⁴³ A change of a small fraction (2 %) of sulfate species would be difficult to discern because slight changes in the DRIFT spectra can arise from small variations in treatment (compare Fig. 7-5, left and right). In other words, the poisoning by the deposits is not reflected in the spectral signature of the sulfate either because the number of sites blocked is too small, or these sites are not directly connected to the sulfate.

7.4 Conclusions

After activation of sulfated zirconia and Fe- or Mn-promoted sulfated zirconia, the surface is still partially hydrated with an estimated water content of 60–125 μmol·g⁻¹. Strong Lewis acid sites capable of adsorbing N₂ at temperatures up to 358 K are present.

Experiments with activation in N₂ or O₂ demonstrate that the state of the surface functional groups (hydroxyl and sulfate) of MnSZ is independent of the atmosphere while the reaction profile is not. Complete regeneration of the catalytic and spectroscopic properties can be achieved in O₂. In N₂, the spectral signature of the hydroxyl and sulfate groups is recovered but the material is rendered inactive. Both these observations indicate that solely from the state of the functional groups it is impossible to predict catalytic activity.

Spectroscopic evidence is presented for the accumulation of certain species on the surface during the induction period in *n*-butane isomerization. Several bands are observed between

1760–1540 and at 5200 cm^{-1} , indicating adsorbed water, potentially a product of oxidative dehydrogenation (ODH) of butane to butene, from which the active carbenium ion-like intermediates are easily formed, and water, but maybe additional other species. At early times on stream, before maximum conversion is reached, the rate of isomerization is proportional to area of the bands in the region 1760–1540 cm^{-1} . Hence, the absorbing species must be active intermediates or side products of the reaction producing the intermediates. Assuming that the area increase is solely caused by water formation due to ODH, the number of water molecules is equivalent to the number of carbenium ions species formed via ODH, and the turnover frequency per such site can be calculated from the data in Fig. 7-9 (left). On the bases of a initial water content of 60–125 $\mu\text{mol g}^{-1}$, the turnover frequency amounts to 10^{-6} s^{-1} for SZ and to 10^{-4} s^{-1} for MnSZ. The rate during the induction period depends on two factors: the number of active surface species formed and the intrinsic turnover per such species. The presence of manganese enhances this intrinsic turnover frequency.

8. Conclusions and Outlook

The object of this thesis was to reveal influences of handling and storage on the structure and activity of sulfated zirconia-based catalysts, and to elucidate the mode of operation of these catalysts in *n*-butane isomerization focusing on the role of the promoters iron and manganese.

8.1 Prerequisites for Successful Structure–Activity Correlations

Although sulfated zirconia (SZ) has been investigated intensively, no convincing structure–activity relationship has evolved so far (see Chapter 2). Unnoticed structural changes are a possible reason for this lack in information, and in our laboratory hints existed that sulfated zirconia-based materials undergo phase changes when being ground and lose activity in *n*-butane isomerization with time of storage. In this work, a systematic investigation of these phenomena revealed that both the handling and the storage conditions influence structure and activity of sulfated zirconia catalysts, which renders their investigation difficult (see Chapter 5).

Zirconia, even if stabilized by sulfate and promoters in cationic form, is sensitive to mechanical stress (see Chapter 5.1). Treatments like milling or pressing lead to appearance or an increase of the fraction of the monoclinic phase in the catalysts. Concomitantly with the structural changes, the *n*-butane isomerization activity of SZ-based catalysts is reduced. Pressing, milling, or grinding is common practice for many experiments to produce a wafer or pellet, to obtain particles of a certain size, or to mix samples with standards or diluents. The sensitivity towards mechanical stress explains why a fundamental structure–activity relationship for sulfated zirconia catalysts is missing so far, since data obtained in experiments involving different sample handling procedures reflect the properties of partially different materials.

Without changing the surface area, the storage conditions (temperature, oxygen and water partial pressure) do influence the performance of sulfated zirconia catalysts (see Chapter 5.2). In order to enhance the throughput and allow simultaneous tests of catalysts aged under three different atmospheres (laboratory cupboard, glovebox, and “tropical” conditions), an apparatus was constructed that enables performance of three parallel catalytic reactor tests on laboratory scale without loss of product analysis information (see Chapter 4). For unpromoted SZ, a partial transformation to monoclinic zirconia is observed within two months for samples stored under tropical conditions (water saturated at 313 K) and within half a year for samples stored in the water and oxygen depleted atmosphere of a glovebox. For manganese-promoted

SZ, no phase change was observed with aging time, but the catalytic rate decreased dramatically upon storage in the glovebox. The changes in butane isomerization activity of unpromoted and promoted SZ can be explained by differences in the degree of hydration and oxidation state of the Mn and Zr cations. Storage of the catalysts in a laboratory cupboard proved to be the best way to minimize structural changes and to preserve the catalytic performance of the fresh catalysts.

To obtain a valid correlation between structure and activity, it must be guaranteed that the material used for the catalytic test is the same as during characterization. Due to the sensitivity of SZ catalysts towards mechanical stress and time of storage, there are only two possibilities to do so: Either the catalysts have to be handled in the same way for all experiments, which in turn have to be performed within a minimum time interval to analyze catalysts of the same age, or characterization has to be performed *in situ* on the operating catalysts. This finding is vital for successful investigation of sulfated zirconia catalysts.

8.2 Initial Step in Skeletal Isomerization of *n*-Butane

The skeletal isomerization of *n*-butane is believed to propagate via carbenium ion intermediates, but it is unclear how they are generated. Discussion is ongoing about the initial step of isomerization, i.e. the activation of *n*-butane, which has been proposed to be acid catalyzed as the isomerization itself—proceeding either via protonation and subsequent H₂ liberation (Brønsted acidity) or via hydride abstraction (Lewis acidity)—or to involve a redox reaction, in which butane is oxidatively or non-oxidatively dehydrogenated to butene under formation of water or H₂ (see Chapter 2.5). The promoters manganese and iron were not found to increase the acid strength of the catalyst, and as a hint for oxidative dehydrogenation (ODH) a higher activity after activation in oxidizing atmosphere than after activation in inert gas has been presented in case of promoted catalysts containing both Fe and Mn (see Chapter 2.4).

Many observations made in this thesis point towards occurrence of ODH as initial step in the skeletal isomerization of *n*-butane. By adsorption of hydrogen and the reactant, it could be shown that Mn and Fe promoters neither augment the hydride abstraction ability of the catalyst nor improve its ability to activate *n*-butane via protonation (see Chapter 6.2). Both these mechanisms might play a role, but the effect of the promoters on the reaction rate must be related to a different, e.g. a redox, functionality of the catalyst, which points towards the responsibility of more than a single type of sites for activity.

The mode of operation of the catalysts was elucidated investigating the catalysts by *in situ* IR spectroscopy in transmission (see Chapter 6.1) and diffuse reflectance (see Chapter 7). All bands in the IR spectra obtained after activation of sulfated zirconia and promoted sulfated zirconia have been assigned with help of DFT results from the literature. SZ is containing an extra type of OH groups vibrating at 3489 cm^{-1} that is missing on the promoted catalysts, but the influence of the promoters on the structure of the sulfate is marginal and the IR spectra are all dominated by the pattern of pyrosulfate, $\text{S}_2\text{O}_7^{2-}$ (see Chapter 3.4).

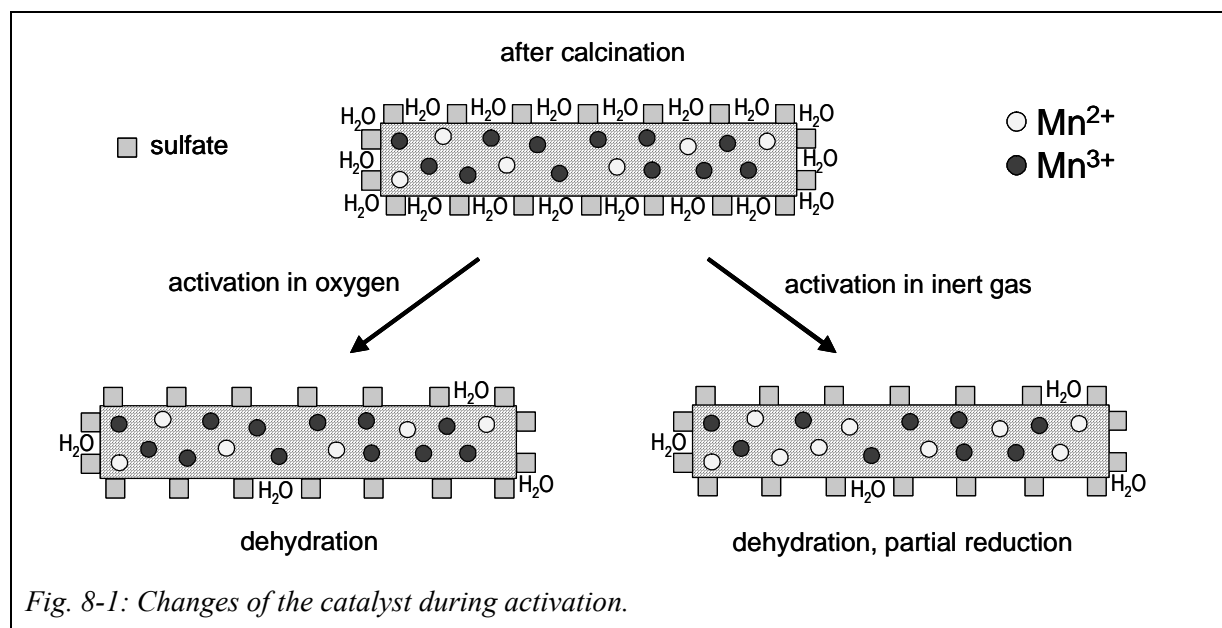


Fig. 8-1: Changes of the catalyst during activation.

During activation the state of the hydroxyl groups and the sulfate on manganese-promoted SZ is independent of the activation atmosphere while the catalytic performance is not: The material is, indeed, slightly more active after heating in oxidizing than in inert atmosphere (see Chapter 7). Results obtained in our group by X-ray absorption spectroscopy show a linear correlation between the maximum rate and the average valence of manganese after activation, which is lower after activation in helium (2.55) than after activation in 50 vol% oxygen (2.70), but no correlation of the average Mn valence with the reaction profile,¹⁴⁸ which is characterized by an induction period until maximum conversion is reached followed by a partial deactivation. Thus, the positive influence of an oxidizing activation atmosphere leads to the assumption that only Mn³⁺ has a promoting effect but not Mn²⁺. The main process during the heat-treatment is dehydration; about 95 % of the adsorbed water are removed, but due to the low reaction temperatures ($< 373\text{ K}$) the surface is still partially hydrated with an estimated water content of $60\text{--}125\ \mu\text{mol}\cdot\text{g}^{-1}$ before it is contacted with the reactant (see Chapter 7). In Fig. 8-1, the processes during activation are summarized.

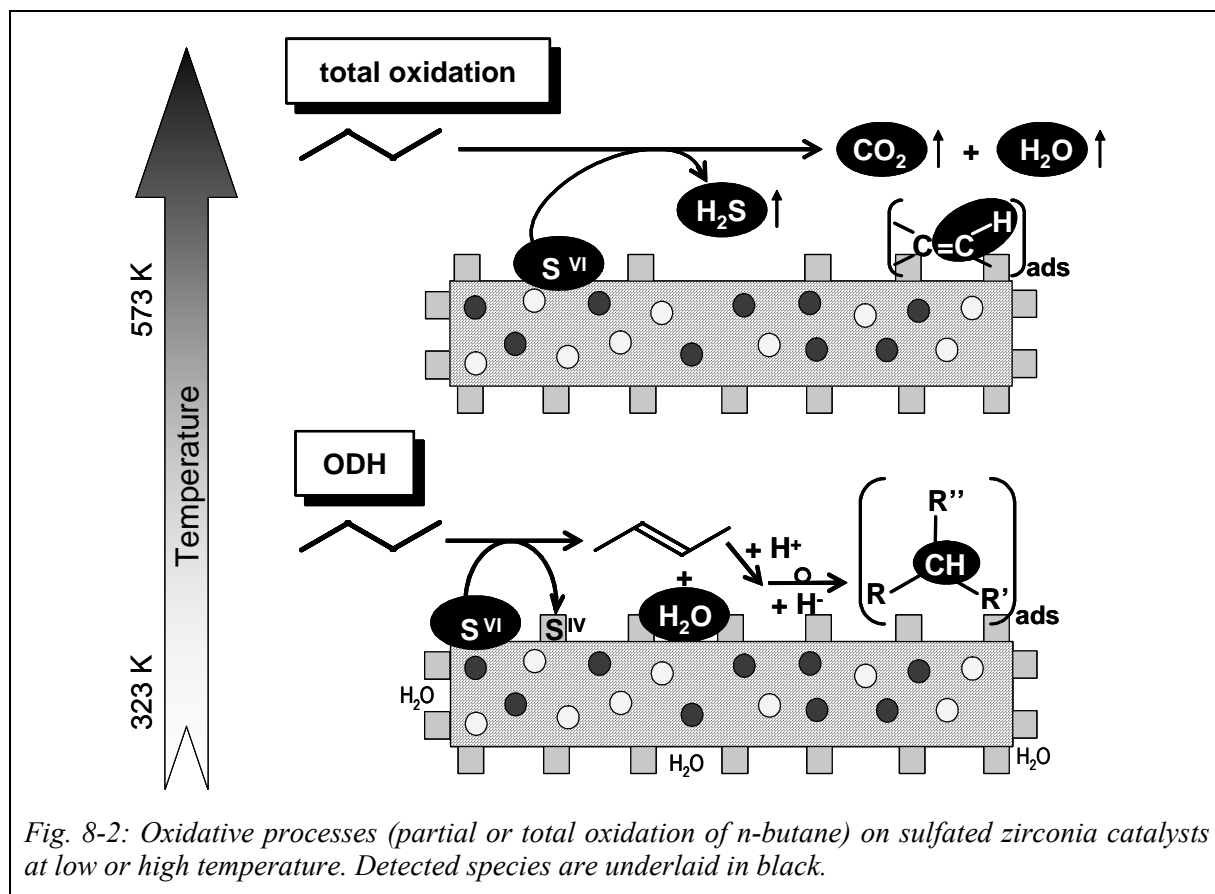


Fig. 8-2: Oxidative processes (partial or total oxidation of *n*-butane) on sulfated zirconia catalysts at low or high temperature. Detected species are underlined in black.

During the induction period, water is accumulated on the surface of SZ, MnSZ, and FeSZ and the rate of *n*-butane isomerization is proportional to the area of the water deformation bands in the region 1760–1540 cm⁻¹ until maximum conversion is reached (see Chapter 7). This behavior would be expected, if *n*-butane was activated via ODH leading to butene and water. The water is blocking Lewis acid sites as shown by quasi *in situ* CO adsorption performed on iron-promoted SZ after *n*-butane isomerization that was stopped at different states of activity (see Chapter 6.1). Formation of water via ODH requires reduction of a catalyst component, i.e. Zr⁴⁺, sulfate, or the promoter cations. For MnSZ activated in helium, no change in the oxidation state of the promoter could be detected with time on stream,¹⁴⁸ which is contradicting a stoichiometric reduction. But the promoters increase the oxidizing power of SZ (see Chapter 6.2). At a temperature where SZ is inert, MnSZ oxidizes hydrogen to water. A concomitant decrease in the amount of sulfate vibrations indicates sulfate to be the oxidizing agent, whose reactivity is enhanced in the presence of manganese. In a batch experiment at high temperature (573 K), it could be shown that SZ is capable to oxidize butane partially to unsaturated hydrocarbons as well as totally to CO₂ and water under total reduction of sulfate to H₂S. A loss of sulfate at low temperatures can be excluded, since complete regeneration of the functional groups and the catalytic properties of MnSZ after

n-butane isomerization at 323 K is possible in oxygen. Treatment in O₂ is not only reoxidizing the catalyst but also responsible for the removal of hydrocarbonaceous deposits, which upon heating in inert gas produce unsaturated surface species absorbing at 1532 and 1465 cm⁻¹ that destroy the catalytic activity (see Chapter 7). During *n*-butane isomerization at lower temperatures (323–378 K), water and species with methyne groups were detected on the surface. A partial oxidation of butane to butene and water accompanied by a partial reduction of sulfate to sulfite, which is still connected to the catalyst, is thus conceivable (see Fig. 8-2).

The catalytic performance of MnSZ and FeSZ is in the same order of magnitude and the rate is often higher for FeSZ. The surface area is always larger for Fe-promoted SZ (ca. 135 m² g⁻¹ compared to ca. 110 m² g⁻¹ in MnSZ), which might be due to the better incorporation of Mn into the zirconia lattice compared with Fe. The turnover frequency per carbenium ion generated via ODH is 10⁻⁴ s⁻¹ for MnSZ and 10⁻⁶ s⁻¹ for unpromoted SZ. The rate during the induction period of *n*-butane isomerization depends on two factors: the number of active surface species formed and the intrinsic turnover per such species. The presence of manganese enhances the intrinsic turnover frequency (see Chapter 7), which could be due to a change from monomolecular to bimolecular mechanism induced by the faster formation and, thus, higher density of active sites in promoted catalysts. So far it has been believed that promoters such as iron or manganese facilitate the reaction initiation; here an effect of a promoter on the isomerization itself is proven.

8.3 Outlook

In this thesis, it was shown that the active sites are generated by and presumably located at the surface terminations of defects in the crystal structure, which are caused by metal ions of lower valence than Zr⁴⁺ during preparation and healed up e.g. by mechanical or hydrothermal treatment. The catalytic power is, thus, an extrinsic property of the structure of the solid SZ catalysts. Furthermore, ODH was proven to play a role in the initiation of the skeletal isomerization of *n*-butane and the weakening of sulfate bands during this process was demonstrated. To obtain evidence that reduction of sulfate is responsible for the partial oxidation of butane, in a complementary experiment the occurrence of sulfite has to be investigated. Vibrations of absorbed SO₂, expected to occur below 1200 cm⁻¹, were not detected in our IR spectroscopic set-up due to the poor reflecting power of the catalysts. Thus, *in situ* experiments should be carried out with diluted catalysts, whereby the diluent has to be inert towards reactant and catalyst, even at high temperatures (up to 773 K) during activation.

Despite a partial deactivation, sulfated zirconia-based catalysts possess a stable long-term activity (> 120 h). Since ODH causes a reduction of the catalyst, this reaction is limited to a certain time range until all oxidized species are consumed. It has to be investigated, whether the number of cycles per active site is large enough to explain the long-term activity or if non-oxidative initiation reactions play a major role in this state of catalytic performance.

During the course of this thesis, the following two interesting observations were made: SZ and promoted SZ contain strong Lewis sites that are capable of adsorbing nitrogen at temperatures up to 358 K (see Chapter 7). Their number is reduced upon milling, but it is unclear whether and how they influence the catalytic activity. All catalysts contain a thermally very stable sulfate species (1–5 % of total sulfate that amounts to about $560 \mu\text{mol}\cdot\text{g}^{-1}$, i.e. 4 wt% SO_3) that endures temperatures above 1200 K before decomposition. In the presence of manganese or iron, the stability of this sulfate fraction is decreased (see Chapter 3.3). The location of this species as well as its importance for the catalytic activity has not yet been understood. Both observations deserve further investigation.

9. Experimental

9.1 Materials

The materials that were used for preparation, characterization and catalytic tests are listed in the following table which contains information about their producers and their purity.

Tab. 9-1: Producers and purity of the used materials

material	source	purity
Mn(NO ₃) ₂ · 4H ₂ O	Merck	≥ 98.5 %
Fe(NO ₃) ₃ · 9H ₂ O	Merck	≥ 99 %
ZrO(OH) ₂ · aq (XZO 632/03), Batch: 95/256/01	MEL Chemicals	70–80 wt% ZrO ₂
sulfated ZrO(OH) ₂ · aq (XZO 682/01), Batch: 92/184/01	MEL Chemicals	5–6 wt% SO ₃
KBr	Aldrich, Merck	≥ 99 %
O ₂	Linde, Westfalen	5.0 (≥ 99.999 %)
Helium	Westfalen	5.0 (≥ 99.999 %)
H ₂	Linde, Westfalen	5.0 (≥ 99.999 %)
synthetic air	Linde, Westfalen	hydrocarbon-free
N ₂	Linde, Westfalen	5.0 (≥ 99.999 %)
5 vol% <i>n</i> -butane in N ₂	Linde	3.5 (≥ 99.95 %)
CO	Messer Griesheim	4.7 (≥ 99.997 %)

9.2 Preparation

Pure zirconia (“Z”): 45.0 g ZrO(OH)₂·aq (“ZH”) are dried for 21 h at 383 K in a drying oven and cooled to room temperature in a desiccator to obtain 35.2 g dried ZH (21.6 % weight loss). About 19 g of it are calcined in a quartz boat of 17.1 ml volume at 823 K to receive about 16 g ZrO₂ (Z: BK12/#0203, BK64/#0205)^{ix}.

Sulfated zirconia (“SZ”): 45.0 g sulfated ZrO(OH)₂·aq (“SZH”, contains 74 wt% SZ) are dried for 21 h at 383 K in a drying oven and cooled to room temperature in a desiccator to obtain 37.2 g dried SZH (17.7 % weight loss). About 23 g of it are calcined in a quartz boat of 17.1 ml volume at 823 K to receive about 20 g SZ (BK10/#0202, BK67/#0210, BK88/#0669, BK89/#0931, BK90/#1837).

Promoted SZ: Samples promoted with 0.5 or 2.0 wt% iron or manganese (“0.5FeSZ”, “2.0FeSZ”, “0.5MnSZ”, “2.0MnSZ”) are prepared according to the “incipient wetness” method: 0.020 or 0.005 equivalents (eq.) of the metal nitrate are dissolved in 4 ml deionized water (see Tab. 9-2). The solution is added drop wise and under vigorous stirring to 10.9 g dried SZH (1 eq., corresponding to 10 g SZ). The received powder is dried at least 24 h at

room temperature before calcination at 823 K (for comparison with SZ) or 923 K (for most active catalyst). About 25 g (three batches) are needed to fill the quartz boat of 17.1 ml volume (0.5FeSZ: BK87/#0666, 2.0FeSZ: BK7/#0201, 0.5MnSZ: BK69/#0212, 2.0MnSZ: BK3/#0200, BK68/#0211, BK79/#0213, BK85/#0667, BK86/#0668).

Tab. 9-2: Amount of metal nitrate per 4 ml water to reach the desired metal content

metal content / wt%	FeSZ $\text{Fe}(\text{NO}_3)_3 \cdot 9\text{H}_2\text{O} / \text{g}$	MnSZ $\text{Mn}(\text{NO}_3)_2 \cdot 4\text{H}_2\text{O} / \text{g}$
0.5	0.36	0.22
2.0	1.45	0.90

9.3 Calcination

All samples were calcined in a quartz boat of 17.1 ml volume, which was placed into a quartz tube ($d_{\text{in}} = 29$ mm) and with this centrally in the isothermal zone of a tubular furnace (*Heraeus*, RO 4/25) with PID control. The sample bed temperature could be monitored by a sheathed thermocouple with 0.5 mm diameter (*Thermocoax*) positioned in the middle of the bed. Under a flow of 200 ml/min synthetic air purged through the quartz tube, the samples were heated with a ramp of 3 K/min to 823 K (ZH, SZH) or 923 K (promoted SZH), held there for three hours, and then cooled to room temperature, whereby the nominal ramp of 3 K/min could not be maintained at lower temperatures. As reference a 2.0MnSZH sample was calcined at the lower temperature.

9.4 BET Surface Analysis

Surface areas were determined by nitrogen adsorption according to the method of Brunauer, Emmett, and Teller using a *Quantasorb Junior*, an *Autosorb-1*, or an *Autosorb-6* apparatus. Prior to the measurements, the samples were outgassed *in vacuo* at 473 K for 16 h. The BET surface area was calculated either by a three point (*Quantasorb Junior*) or a multipoint analysis (*Autosorb*). The *Autosorb* software package included a tool for determination of the pore size distribution according to the BJH method by Barrett, Joyner, and Halenda.

^{ix} Sample number (BK) and AC database entry number (#) of the batches used in this thesis.

9.5 Thermogravimetry (TG) and Differential Scanning Calorimetry (DSC)

TG and DSC analyses were performed in a STA 499 C instrument (*Netzsch*) with on-line MS (*Pfeiffer*, QMS 200) and OmniStar® software. Samples were heated in 20 ml/min Ar flow to 1373 K, held at this temperature for 30 minutes, and then cooled to 473 K. The nominal heating and cooling rate was 10 K/min.

9.6 X-Ray Diffraction (XRD) and X-Ray Absorption Spectroscopy (XAS)

X-ray diffractograms were recorded using STOE-STADI-P diffractometers either in Debye-Scherrer geometry with Cu K α radiation, primary Ge monochromator, and linear position-sensitive detector (PSD, internal resolution $2\Theta = 0.01^\circ$), or in reflection (Bragg-Brentano) geometry with Cu K α radiation, secondary Si (111) monochromator, and scintillation counter. The loose powders were mixed 1:1 by weight with sieved α -Al₂O₃ (through gentle shaking) and embedded in X-ray amorphous grease (transmission mode) or filled in a cup (reflection mode); pressed samples were mounted as wafers. PowderCell v 2.4 was used to fit the diffractograms with patterns calculated from single crystal data (see Chapter 3.2.2).

X-ray absorption spectra (XAS) on the Mn or Fe K-edge were taken in fluorescence mode at the Hamburg Synchrotron Radiation Laboratory (HASYLAB) beamline E4. All spectra were energy calibrated by comparison with the spectrum of a simultaneously measured metal foil. The first inflection point in this reference spectrum was set to the Mn (6539 keV) or Fe (7112 eV) K-edge.

9.7 Pressing and Milling

The pressing experiments were conducted using flat-surfaced stainless steel tools and a manually operated hydraulic press (*Perkin-Elmer* or *Ernst Hammerschmidt*). Milling was performed in a vibrating mill (*Perkin-Elmer*) using 1.5 ml stainless steel capsules, a single ball ($d = 3$ mm), and, usually, 300 mg of sample. The maximum interval was 30 s; longer milling times were achieved by consecutive intervals.

9.8 Infrared Spectroscopy in Transmission and in Diffuse Reflectance

The IR spectra were recorded using three different spectrometers in different cells and set-ups, one designed for Fourier transform IR spectroscopy in transmission (A) and two for diffuse reflectance (B and C).

A) *In situ* and CO adsorption FTIR spectra in transmission were recorded with a PE 2000 spectrometer (*Perkin–Elmer*) using Spectrum™ spectroscopy software. The spectrometer was equipped with a home-made high temperature cell (“HTZ”, $T_{\max} = 623$ K, electrical heating) having two CaF_2 windows and a DTGS (deuterated triglycine sulfate) detector. Powders were pressed into self-supporting wafers (20 s at 250 MPa) with a specific mass of 24–32 mg cm^{-2} . For activation they were transferred into a home-made oven ($T_{\max} = 823$ K). The whole system could be evacuated by a turbomolecular pump (*Pfeiffer, Balzers*); CO was dosed via a variable leak valve (*Varian*). Spectra were converted into decadic absorbance.

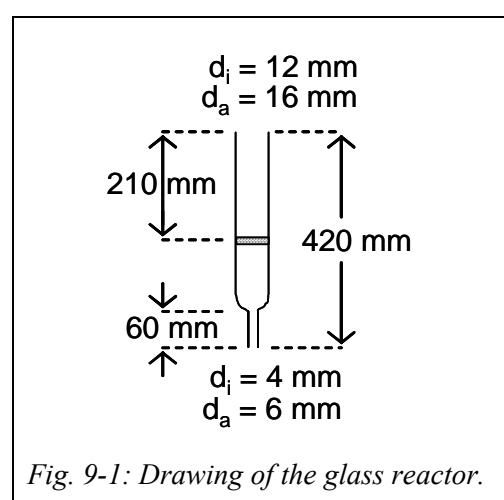
B) DRIFT spectra of hydrogen and *n*-butane adsorption and reaction were recorded with a Nicolet “Impact 410” FTIR spectrometer (4 cm^{-1} resolution) equipped with an MCT (mercury cadmium telluride) detector using OMNIC™ spectroscopy software. A further development of the diffuse reflectance attachment described by Kazansky et al.,²³⁵ which needs only two mirrors to focus the IR beam onto the sample, was arranged in the beam path. Prior to the vacuum pretreatment for activation of the catalysts (see p. 61), the powders were pressed at 100 hPa for 2 s and sieved into fractions of 0.2–0.5 or 0.5–1.0 mm. Low temperature spectra were recorded in an all-quartz cell that was immersed in a quartz dewar filled with liquid nitrogen. For room temperature measurements, a section of the quartz cell equipped with CaF_2 window was used. Samples were placed directly at the window, hence the beam path through the gas phase was limited to the void space within the catalyst bed, and gas phase contributions were minimized. CaF_2 powder was used to generate the background spectra. All presented spectra were recorded at room temperature except for the hydrogen adsorption experiments at 77 K. The samples were contacted with hydrogen at 77 K, room temperature and 473 K, with *n*-butane at room temperature and in steps up to a maximum of 573 K. These experiments were performed using one sample in a series of experiments with increasing temperature and intermittent cooling for the measurement; fresh samples were used when the gas type was changed. For all spectra, the reflectance with respect to CaF_2 was converted into Kubelka–Munk units, setting the reflectance at 5000 cm^{-1} to a value of 0.9.

C) DRIFT spectra during *n*-butane isomerization were recorded with a Bruker IFS 66 FTIR spectrometer (1 or 2 cm^{-1} resolution) equipped with a commercial *in situ* cell (*Graseby Specac*, Environmental Chamber, $T_{\max} = 773$ K, $p_{\max} = 3.6$ MPa, estimated dead volume of 100 ml) with a chemically resistant ZnSe window, a diffuse-reflectance attachment (*Graseby Specac*, “The Selector”), and an MCT detector using OPUS™ spectroscopy software. The spectrometer was purged with purified air. The catalyst powder was placed in a 2.5-mm-tall gold cup ($d_{\text{out}} = 8.5$ mm, $d_{\text{in}} = 7.2$ mm) that was heated electrically from below. There was no

flow through the bed; gas exchange occurred by convection and diffusion. The top part of the bed was analyzed with IR radiation. Spectra of KBr under N_2 purging were used as a reference. The parameters for spectrum acquisition and calculation were the following: 100 scans, single-sided fast return interferogram, and Blackman–Harris 3-term apodization function. For correlation of band intensities with concentration the spectra were converted into Kubelka–Munk units.

9.9 Catalytic tests

Isomerization of *n*-butane to isobutane was conducted at atmospheric pressure either in a single tubular glass reactor ($d_{in} = 12$ mm, see Fig. 9-1), a three-channel fixed bed reactor (see Chapter 4), or *in situ* in the DRIFTS cell or HTZ (see Chapter 9.8). Analysis was performed



with on-line gas chromatography (*Varian*) either by a GC 3800 with a SilicaPLOT capillary column (*Chrompack*, $d_{in} = 0.32$ mm, length 60 m, film thickness 4 μ m) and flame ionization detection, or a Micro-GC 4900 (see Chapter 4.4.3). All gases used for activation and reaction flow through filters (*Swagelok*, 2 μ m) to remove particulate matter. Nitrogen, helium, and oxygen were further purified with Oxysorb® (only N_2 and He) and Hydrosorb® cartridges (*Messer Griesheim*).

For activation, the catalysts were heated in flowing nitrogen or oxygen with 25–29 $K \cdot \text{min}^{-1}$ to 723 K (DRIFTS cell: 773 K), held at this temperature for 30 min, and then cooled to reaction temperature. Isomerization was performed at 358 K, 373 K, or 378 K for SZ and 323 K for promoted SZ feeding a 1 vol% *n*-butane in nitrogen mixture. In Tab. 9-3, the catalysts' masses as well as the flow rates are listed for the different test set-ups.

Tab. 9-3: Amount of catalyst tested and gas flow during activation or reaction

test set-up	mass of catalyst	flow during activation	flow during reaction
single reactor	500 mg	48 ml/min	80 ml/min
three-channel reactor	200 mg	40 ml/min	25 ml/min
DRIFTS cell	ca. 160 mg	48 ml/min	30 ml/min
HTZ	ca. 40 mg	40 ml/min	30 ml/min

The amount of isobutane in the *n*-butane mixture, the only detectable impurity, was subtracted from the isobutane concentration in the effluent stream. Conversion was calculated

as conversion to isobutane. For a 1 vol% butane feed, the rate of isobutane formation in $\mu\text{mol g}^{-1} \text{h}^{-1}$ was obtained from the produced isobutane concentration (c_{i-C_4}) in ppm, the flow velocity of the feed (w_{feed}) in ml min^{-1} , the mass of catalyst (m_{cat}) in g and the molar volume of gas (V_{mol}), which is $24.667 \text{ l mol}^{-1}$ at room temperature, with the following equation:

$$rate = \frac{c_{i-C_4} \cdot 0.001 \cdot w_{feed} \cdot 60}{V_{mol} \cdot m_{cat}} \quad \text{Eq. 9-1}$$

10. Literature

1. I. Chorkendorff, J.W. Niemantsverdriet, *Concepts of Modern Catalysis and Kinetics*, Wiley-VCH, Weinheim **2003**, pp. 1, 11.
2. G. Ertl, T. Gloyna, *Z. Phys. Chem.* **2003**, *217(10)*, 1207–1219.
3. Gabor A. Somorjai, *Introduction to surface chemistry and catalysis*, Wiley, New York et al. **1994**, p. 446.
4. V.C.F. Holm, G.C. Bailey, *US Patent 3032599*, **1962**.
5. P.J. Kuchar, R.D. Gillespie, C.D. Gosling, W.C. Martin, M.J. Cleveland, P.J. Bullen, *Hydrocarbon Eng.* **1999**, March, 50–57.
6. M. Hino, S. Kobayashi, K. Arata, *J. Am. Chem. Soc.* **1979**, *101(21)*, 6439–6441.
7. M. Hino, K. Arata, *J. Chem. Soc., Chem. Commun.* **1980**, (18), 851–852.
8. Jean D'Ans (auth.), Ellen Lax (auth.), Claudia Synowitz (ed.), *Taschenbuch für Chemiker und Physiker, 2: Organische Verbindungen*, 4th ed., Springer-Verlag, Berlin et al. **1983**, p. 1020.
9. F. Asinger, *Paraffins*, Pergamon Press, New York **1968**, pp. 696–697.
10. N.A. Cusher, in *Handbook of Petroleum Refining Processes*, R.A. Meyers (ed.), 3rd ed., McGraw-Hill, New York **2004**, Chapter 9, p. 7.
11. K. Arata, M. Hino, *Mater. Chem. Phys.* **1990**, *26(3–4)*, 213–237.
12. K. Tanabe, H. Hattori, T. Yamaguchi, *Crit. Rev. Surf. Chem.* **1990**, *1(1)*, 1–25.
13. T. Yamaguchi, *Appl. Catal.* **1990**, *61(1)*, 1–25.
14. K. Arata, *Appl. Catal. A* **1996**, *146(1)*, 3–32.
15. X. Song, A. Sayari, *Catal. Rev. – Sci. Eng.* **1996**, *38(3)*, 329–412.
16. A. Corma, *Curr. Opin. Solid State Mater. Sci.* **1997**, *2(1)*, 63–75.
17. C.X. Miao, Z. Gao, *Mater. Chem. Phys.* **1997**, *50(1)*, 15–19.
18. V. Adeeva, H.-Y. Liu, B.-Q. Xu, W.M.H. Sachtler, *Top. Catal.* **1998**, *6(1–4)*, 61–76.
19. Z. Hong, K.B. Fogash, J.A. Dumesic, *Catal. Today* **1999**, *51(2)*, 269–288.
20. H. Xu, X. Song, *Mater. Res. Bull.* **1999**, *34(4)*, 527–531.
21. G.D. Yadav, J.J. Nair, *Microporous Mesoporous Mater.* **1999**, *33(1–3)*, 1–48.
22. C. Morterra, G. Cerrato, F. Pinna, *Spectrochim. Acta Part A* **1999**, *55(1)*, 95–107.
23. J. Pasel, V. Speer, C. Albrecht, F. Richter, H. Papp, *Appl. Catal. B* **2000**, *25(2–3)*, 105–113.
24. A. Corma, H. García, *Chem. Rev.* **2003**, *103(11)*, 4307–4365.
25. T. Okuhara, *J. Jpn. Pet. Inst.* **2004**, *47(1)*, 1–10.
26. S. Hara, M. Miyayama, *Solid State Ionics* **2004**, *168(1–2)*, 111–116.

27. F.C. Jentoft, *Sulfated Zirconia Alkane Isomerization Catalysts: A Treatise*, Thesis (Habilitationsschrift), Humboldt-Universität Berlin, **2004**.
28. P. Li, I.W. Chen, J.E. Penner-Hahn, *Phys. Rev. B* **1993**, *48(14)*, 10063–10073.
29. A.F. Holleman, E. Wiberg, N. Wiberg, *Lehrbuch der Anorganischen Chemie*, 101th ed., Walter de Gruyter, Berlin, New York **1995**, pp. 571, 1416.
30. A.A.M. Ali, M.I. Zaki, *Thermochim. Acta* **2002**, *387(1)*, 29–38.
31. I.I. Štefanć, S. Musić, G. Štefanić, A. Gajović, *J. Mol. Struct.* **1999**, *480–481*, 621–625.
32. R.C. Garvie, *J. Phys. Chem.* **1965**, *69(4)*, 1238–1243.
33. R.C. Garvie, *J. Phys. Chem.* **1978**, *82(2)*, 218–224.
34. P. Bouvier, E. Djurado, G. Lucazeau, T. Le Bihan, *Phys. Rev. B* **2000**, *62(13)*, 8731–8737.
35. M.J. Torralvo, M.A. Alario, J. Soria, *J. Catal.* **1984**, *86(2)*, 473–476.
36. X. Bokhimi, A. Morales, O. Novaro, M. Portilla, T. López, F. Tzompantzi, R. Gómez, *J. Solid State Chem.* **1998**, *135(1)*, 28–35.
37. H.-C. Wang, K.-L. Lin, *J. Mater. Sci.* **1991**, *26(9)*, 2501–2506.
38. H.J. Stöcker, *Ann. Chim.* **1960**, *5*, 1459–1502.
39. F.C. Jentoft, A. Hahn, J. Kröhnert, G. Lorenz, R.E. Jentoft, T. Ressler, U. Wild, R. Schlögl, C. Häbner, K. Köhler, *J. Catal.* **2004**, *224(1)*, 124–137.
40. R. Srinivasan, R.A. Keogh, D.R. Milburn, B.H. Davis, *J. Catal.* **1995**, *153(1)*, 123–130.
41. F.R. Chen, G. Coudurier, J.-F. Joly, J.C. Vedrine, *J. Catal.* **1993**, *143(2)*, 616–626.
42. F. Lónyi, J. Valyon, *J. Therm. Anal.* **1996**, *46(1)*, 211–218.
43. C. Morterra, G. Cerrato, F. Pinna, M. Signoretto, *J. Catal.* **1995**, *157(1)*, 109–123.
44. W. Stichert, F. Schüth, *J. Catal.* **1998**, *174(2)*, 242–245.
45. W. Stichert, F. Schüth, S. Kuba, H. Knözinger, *J. Catal.* **2001**, *198(2)*, 277–285.
46. A.F. Bedilo, A.S. Ivanova, N.A. Pakhomov, A.M. Volodin, *J. Mol. Catal. A* **2000**, *158(1)*, 409–412.
47. C. Morterra, G. Cerrato, V. Bolis, *Catal. Today* **1993**, *17(3)*, 505–515.
48. M. Bensitel, O. Saur, J.-C. Lavalley, B.A. Morrow, *Mater. Chem. Phys.* **1988**, *19(1–2)*, 147–156.
49. J.M. Parera, *Catal. Today* **1992**, *15(3–4)*, 481–490.
50. K. Arata, *Adv. Catal.* **1990**, *37*, 165–211.
51. M. Signoretto, F. Pinna, G. Strukul, P. Chies, G. Cerrato, S. Di Ciero, C. Morterra, *J. Catal.* **1997**, *167(2)*, 522–532.
52. A. Clearfield, G.P.D. Serrette, A.H. Khazi-Syed, *Catal. Today* **1994**, *20(2)*, 295–312.
53. F. Babou, G. Coudurier, J.C. Vedrine, *J. Catal.* **1995**, *152(2)*, 341–349.

54. C. Morterra, G. Cerrato, F. Pinna, M. Signoretto, *J. Phys. Chem.* **1994**, *98*(47), 12373–12381.
55. L.M. Kustov, V.B. Kazansky, F. Figueras, D. Tichit, *J. Catal.* **1994**, *150*(1), 143–149.
56. D.A. Ward, E.I. Ko, *J. Catal.* **1994**, *150*(1), 18–33.
57. M. Waqif, J. Bachelier, O. Saur, J.-C. Lavalley, *J. Mol. Catal.* **1992**, *72*(1), 127–138.
58. V.V. Strelko, *Kinet. Catal.* **2003**, *44*(6), 834–839.
59. T. Riemer, D. Spielbauer, M. Hunger, G.A.H. Mekheimer, H. Knözinger, *J. Chem. Soc., Chem. Commun.* **1994**, (10), 1181–1182.
60. V. Bolis, G. Magnacca, G. Cerrato, C. Morterra, *Langmuir* **1997**, *13*(5), 888–894.
61. R.L. White, E.C. Sikabwe, M.A. Coelho, D.E. Resasco, *J. Catal.* **1995**, *157*(2), 755–758.
62. A. Hofmann, J. Sauer, *J. Phys. Chem. B* **2004**, *108*(38), 14652–14662.
63. G.A. Olah, Y. Halpern, J. Shen, Y.K. Mo, *J. Am. Chem. Soc.* **1973**, *95*(15), 4960–4970.
64. N.F. Hall, J.B. Conant, *J. Am. Chem. Soc.* **1927**, *49*(12), 3047–3061.
65. R.J. Gillespie, *Acc. Chem. Res.* **1968**, *1*(7), 202–209.
66. L.P. Hammett, A.J. Deyrup, *J. Am. Chem. Soc.* **1932**, *54*(7), 2721–2739.
67. G. Busca, *Phys. Chem. Chem. Phys.* **1999**, *1*(5), 723–736.
68. E.P. Parry, *J. Catal.* **1963**, *2*(5), 371–379.
69. T. Jin, T. Yamaguchi, K. Tanabe, *J. Phys. Chem.* **1986**, *90*(20), 4794–4796.
70. E.C. Sikabwe, M.A. Coelho, D.E. Resasco, R.L. White, *Catal. Lett.* **1995**, *34*(1–2), 23–30.
71. R. Srinivasan, R.A. Keogh, A. Ghenciu, D. Fărcașiu, B.H. Davis, *J. Catal.* **1996**, *158*(2), 502–510.
72. C. Morterra, G. Cerrato, *Phys. Chem. Chem. Phys.* **1999**, *1*(11), 2825–2831.
73. A.V. Lavrenov, V.P. Finevich, V.L. Kirilov, E.A. Paukshtis, V.K. Duplyakin, B.S. Bal'zhinimaev, *Petrol. Chem.* **2003**, *43*(5), 324–328.
74. V.S. Komarov, M.F. Sinilo, *Kinet. Catal.* **1988**, *29*(3), 605–609.
75. M. Bensitel, O. Saur, J.C. Lavalley, G. Mabilon, *Mater. Chem. Phys.* **1987**, *17*(3), 249–258.
76. D. Spielbauer, G.A.H. Mekheimer, M.I. Zaki, H. Knözinger, *Catal. Lett.* **1996**, *40*(1–2), 71–79.
77. V. Adeeva, J.W. de Haan, J. Jänchen, G.D. Lei, V. Schünemann, L.J.M. van de Ven, W.M.H. Sachtler, R.A. van Santen, *J. Catal.* **1995**, *151*(2), 364–372.
78. A. Ghenciu, D. Fărcașiu, *J. Mol. Catal. A* **1996**, *109*(3), 273–283.
79. M. Hino, K. Arata, *React. Kinet. Catal. Lett.* **2004**, *81*(2), 321–326.
80. A.R. Ramadan, N. Yacoub, J. Ragai, *J. Mater. Sci.* **2004**, *39*(4), 1383–1388.

81. Z. Gao, Y. Xia, W. Hua, C. Miao, *Top. Catal.* **1998**, *6(1-4)*, 101–106.
82. M. Perez-Luna, A. Cosultchi, J. Toledo-Antonio, E. Aree-Estrada, *Catal. Lett.* **2005**, *102(1-2)*, 33–38.
83. M. Signoretto, M.A. Stefano, F. Pinna, S. Polizzi, G. Cerrato, C. Morterra, *Microporous Mesoporous Mater.* **2005**, *81(1-3)*, 19–29.
84. S. Baba, Y. Shibata, T. Kawamura, H. Takaoka, T. Kimura, K. Kousaka, Y. Minato, N. Yokoyama, K. Lida, T. Imai, *Eur. Patent* EP0174836, **1986**.
85. F. Garin, D. Andriamasinoro, A. Abdulsamad, J. Sommer, *J. Catal.* **1991**, *131(1)*, 199–203.
86. K. Watanabe, T. Kawakami, K. Baba, N. Oshio, T. Kimura, *Catal. Surv. Asia* **2005**, *9(1)*, 17–24.
87. C.-Y. Hsu, C.R. Heimbuch, C.T. Armes, B.C. Gates, *J. Chem. Soc., Chem. Commun.* **1992**, (22), 1645–1646.
88. F.C. Lange, T.-K. Cheung, B.C. Gates, *Catal. Lett.* **1996**, *41(1-2)*, 95–99.
89. C.-H. Lin, C.-Y. Hsu, *J. Chem. Soc., Chem. Commun.* **1992**, (20), 1479–1480.
90. V. Adeeva, G.D. Lei, W.M.H. Sachtler, *Appl. Catal. A* **1994**, *118(1)*, L11–L15.
91. A. Jatia, C. Chang, J.D. MacLeod, T. Okubo, M.E. Davis, *Catal. Lett.* **1994**, *25(1-2)*, 21–28.
92. J.E. Táborá, R.J. Davis, *J. Chem. Soc., Faraday Trans.* **1995**, *91(12)*, 1825–1833.
93. T.-K. Cheung, J.L. d'Itri, B.C. Gates, *J. Catal.* **1995**, *151(2)*, 464–466.
94. M.A. Coelho, D.E. Resasco, E.C. Sikabwe, R.L. White, *Catal. Lett.* **1995**, *32(3-4)*, 253–262.
95. R. Srinivasan, R.A. Keogh, B.H. Davis, *Appl. Catal. A* **1995**, *130(2)*, 135–155.
96. X. Song, K.R. Reddy, A. Sayari, *J. Catal.* **1996**, *161(1)*, 206–210.
97. C. Miao, W. Hua, J. Chen, Z. Gao, *Catal. Lett.* **1996**, *37(3-4)*, 187–191.
98. M.A. Coelho, W.E. Alvarez, E.C. Sikabwe, R.L. White, D.E. Resasco, *Catal. Today* **1996**, *28(4)*, 415–429.
99. K.T. Wan, C.B. Khouw, M.E. Davis, *J. Catal.* **1996**, *158(1)*, 311–326.
100. M. Benaissa, J.G. Santiesteban, G. Diaz, M. José-Yacamán, *Surf. Sci.* **1996**, *364(2)*, L591–L594.
101. W.E. Alvarez, H. Liu, D.E. Resasco, *Appl. Catal. A* **1997**, *162(1-2)*, 103–119.
102. C. Morterra, G. Cerrato, S. Di Ciero, M. Signoretto, A. Minesso, F. Pinna, G. Strukul, *Catal. Lett.* **1997**, *49(1-2)*, 25–34.
103. A. Sayari, Y. Yang, X. Song, *J. Catal.* **1997**, *167(2)*, 346–353.

104. D.R. Milburn, R.A. Keogh, D.E. Sparks, B.H. Davis, *Appl. Surf. Sci.* **1998**, *126(1–2)*, 11–15.
105. S.X. Song, R.A. Kydd, *Catal. Lett.* **1998**, *51(1–2)*, 95–100.
106. M. Scheithauer, E. Bosch, U.A. Schubert, H. Knözinger, T.–K. Cheung, F.C. Jentoft, B.C. Gates, B. Tesche, *J. Catal.* **1998**, *177(1)*, 137–146.
107. T. Tanaka, T. Yamamoto, Y. Kohno, T. Yoshida, S. Yoshida, *Jpn. J. Appl. Phys. Part 1* **1999**, *38(Suppl. 1)*, 30–35.
108. T. Yamamoto, T. Tanaka, S. Takenaka, S. Yoshida, T. Onari, Y. Takahashi, T. Kosaka, S. Hasegawa, M. Kudo, *J. Phys. Chem. B* **1999**, *103(13)*, 2385–2393.
109. A. Sayari, Y. Yang, *J. Catal.* **1999**, *187(1)*, 186–190.
110. R.E. Jentoft, A. Hahn, F.C. Jentoft, T. Ressler, *J. Synchrotron Rad.* **2001**, *8(Part 2)*, 563–565.
111. E.A. García, E.H. Rueda, A.J. Rouco, *Appl. Catal. A* **2001**, *210(1–2)*, 363–370.
112. J.C. Yori, J.M. Parera, *Appl. Catal. A* **1996**, *147(1)*, 145–157.
113. T. Løften, N.S. Gnep, M. Guisnet, E.A. Blekkan, *Catal. Today* **2005**, *100(3–4)*, 397–401.
114. R.S. Drago, N. Kob, *J. Phys. Chem. B* **1997**, *101(17)*, 3360–3364.
115. C.D. Nentitzescu, I.P. Cantuniari, *Ber. Dtsch. Chem. Ges.* **1933**, *66(8)*, 1097–1100.
116. T.–K. Cheung, B.C. Gates, *Top. Catal.* **1998**, *6(1–4)*, 41–47.
117. E.A. Paukshtis, N.S. Kotsarenko, V.P. Shmachkova, *Catal. Lett.* **2000**, *69(3–4)*, 189–193.
118. C.R. Vera, C.L. Pieck, K. Shimizu, C.A. Querini, J.M. Parera, *J. Catal.* **1999**, *187(1)*, 39–49.
119. Z. Hong, K.B. Fogash, R.M. Watwe, B. Kim, B.I. Masqueda-Jiménez, M.A. Natal-Santiago, J.M. Hill, J.A. Dumesic, *J. Catal.* **1998**, *178(2)*, 489–498.
120. D.M. Brouwer, in: *Chemistry and Chemical Engineering of Catalytic Processes*, R. Prins (ed.), G.C.A. Schuit (ed.), Sijdhoff & Noordhof, Alphen a. d. Rijn **1980**, pp.137–160.
121. J.E. Tabora, R.J. Davis, *J. Am. Chem. Soc.* **1996**, *118(48)*, 12240–12241.
122. J.E. Tabora, R.J. Davis, *J. Catal.* **1996**, *162(1)*, 125–133.
123. S. Hammache, J.G. Goodwin Jr., *J. Catal.* **2003**, *218(2)*, 258–266.
124. X. Li, K. Nagaoka, L.J. Simon, R. Olindo, J.A. Lercher, A. Hofmann, J. Sauer, *J. Am. Chem. Soc.*, accepted.
125. J.M.M. Millet, M. Signoretto, P. Bonville, *Catal. Lett.* **2000**, *64(2–4)*, 135–140.

126. V.P. Shmachkova, N.S. Kotsarenko, E.A. Paukshtis, *Kinet. Catal.* **2004**, 45(4), 554–557.
127. X. Li, K. Nagaoka, L.J. Simon, R. Olindo, J.A. Lercher, *J. Catal.* **2005**, 232(2), 456–466.
128. V.N. Ipatieff, H. Pines, *J. Org. Chem.* **1936**, 1(5), 464–489.
129. H. Pines, *Kinet. Catal.* **1993**, 34(2), 335–338.
130. V. Adeeva, G.D. Lei, W.M.H. Sachtler, *Catal. Lett.* **1995**, 33(1–2), 135–143.
131. F. Garin, L. Seyfried, P. Girard, G. Maire, A. Abdulsamad, J. Sommer, *J. Catal.* **1995**, 151(1), 26–32.
132. T. Suzuki, T. Okuhara, *Chem. Lett.* **2000**, 29(5), 470–471.
133. F.T.T. Ng, N. Horvát, *Appl. Catal. A* **1995**, 123(2), L197–L203.
134. R.A. Comelli, C.R. Vera, J.M. Parera, *J. Catal.* **1995**, 151(1), 96–101.
135. D. Spielbauer, G.A.H. Mekhemer, E. Bosch, H. Knözinger, *Catal. Lett.* **1996**, 36(1–2), 59–68.
136. S.R. Vaudagna, R.A. Comelli, N.S. Figoli, *Catal. Lett.* **1997**, 47(3–4), 259–264.
137. S.R. Vaudagna, R.A. Comelli, S.A. Canavese, N.S. Figóli, *J. Catal.* **1997**, 169(1), 389–393.
138. B. Li, R.D. Gonzalez, *Appl. Catal. A* **1997**, 165(1–2), 291–300.
139. K.B. Fogash, Z. Hong, J.M. Kobe, J.A. Dumesic, *Appl. Catal. A* **1998**, 172(1), 107–116.
140. H. Knözinger, *Top. Catal.* **1998**, 6(1–4), 107–110.
141. B. Li, R.D. Gonzalez, *Appl. Catal. A* **1998**, 174(1–2), 109–119.
142. B. Li, R.D. Gonzalez, *Catal. Today* **1998**, 46(1), 55–67.
143. S.Y. Kim, J.G. Goodwin Jr., D. Galloway, *Catal. Today* **2000**, 63(1), 21–32.
144. R. Marcus, U. Diebold, R.D. Gonzalez, *Catal. Lett.* **2003**, 86(4), 151–156.
145. G. Resofszki, M. Muhler, S. Sprenger, U. Wild, Z. Paál, *Appl. Catal. A* **2003**, 240(1–2), 71–81.
146. C. Li, P.C. Stair, *Catal. Lett.* **1996**, 36(3–4), 119–123.
147. R.E. Jentoft, A.H.P. Hahn, F.C. Jentoft, T. Ressler, *Phys. Scr.* **2005**, T115, 794–797.
148. R.E. Jentoft, A.H.P. Hahn, F.C. Jentoft, T. Ressler, *Phys. Chem. Chem. Phys.* **2005**, 7(14), 2830–2838.
149. C. Morterra, G. Cerrato, F. Pinna, M. Signoretto, G. Strukul, *J. Catal.* **1994**, 149(1), 181–188.
150. L. Wöhler, *Kolloid Z.* **1926**, 38(2), 97–111.
151. Leopold Gmelin, *Handbuch der theoretischen Chemie, Band 2*, Varrentrapp, Frankfurt a.M. **1817**.

152. A. Hahn, T. Ressler, R.E. Jentoft, F.C. Jentoft, *Chem. Commun.* **2001**, (6), 537–538.
153. P.W. Atkins, *Physikalische Chemie*, 2nd corr. repr. of 1st ed., VCH, Weinheim et al. **1990**, p. 566.
154. W.H. Bragg, W.L. Bragg, *Proc. Roy. Soc. London, Ser. A* **1913**, 88(605), 428–438.
155. P. Scherrer, *Nachr. Ges. Wiss. Göttingen, Math.–Phys. Kl.* **1918**, (1), 98–100.
156. H.P. Klug, L.E. Alexander, *X-ray Diffraction Procedures: For Polycrystalline and Amorphous Materials*, 2nd ed., Wiley, New York et al. **1974**, pp. 656, 687–690.
157. G.K. Williamson, W.H. Hall, *Acta Metall.* **1953**, 1(1), 22–31.
158. A. Corma, A. Martínez, C. Martínez, *Appl. Catal. A* **1996**, 144 (1–2), 249–268.
159. W.F. Hemminger, H.K. Cammenga, *Methoden der Thermischen Analyse*, Springer-Verlag, Berlin et al. **1989**.
160. S. Chokkaram, R. Srinivasan, D.R. Milburn, B.H. Davis, *J. Colloid Interf. Sci.* **1994**, 165(1), 160–168.
161. Jean D'Ans (auth.), Ellen Lax (auth.), R. Blachnik (ed.), *Taschenbuch für Chemiker und Physiker, 3: Elemente, anorganische Verbindungen und Materialien, Minerale*, 4th ed., Springer, Berlin et al. **1998**, pp. 708–709.
162. X. Li, K. Nagaoka, J.A. Lercher, *J. Catal.* **2004**, 227(1), 130–137.
163. J.E. Stewart, *Infrared Spectroscopy: Experimental Methods and Techniques*, Marcel Dekker, New York **1970**, p. 2.
164. A. Fadini, F.–M. Schnepel, *Schwingungsspektroskopie: Methoden – Anwendungen*, Georg Thieme Verlag, Stuttgart, New York **1985**, p. 2.
165. U. Schiedt, H. Reinwein, *Z. Naturforschung* **1952**, 7b, 270–277.
166. M.M. Stimson, M.J. O'Donnell, *J. Am. Chem. Soc.* **1952**, 74(7), 1805–1808.
167. R.B. Barnes, R.C. Gore, E.F. Williams, S.G. Linsley, E.M. Petersen, *Anal. Chem.* **1947**, 19(9), 620–627.
168. N.B. Colthup, L.H. Daly, S.E. Wiberley, *Introduction to Infrared and Raman Spectroscopy*, 3rd ed., Academic Press San Diego et al. **1990**, pp. 88–89.
169. J.S. Ard, *Anal. Chem.* **1953**, 25(11), 1743–1744.
170. G. Kortüm, *Reflexionsspektroskopie: Grundlagen, Methodik, Anwendungen*, Springer-Verlag, Berlin et al. **1969**.
171. W.W. Wendlandt, H.G. Hecht, *Reflectance Spectroscopy*, Interscience Publ., New York et al. **1966**.
172. C. Morterra, G. Cerrato, M. Signoreto, *Catal. Lett.* **1996**, 41(1–2), 101–109.
173. R.J. Gillespie, E.A. Robinson, *Canad. J. Chem.* **1963**, 41(8), 2074–2085.

174. M. Benaïssa, J.G. Santiesteban, G. Díaz, C.D. Chang, M. José-Yacamán, *J. Catal.* **1996**, *161*(2), 694–703.
175. A.A. Tsyganenko, V.N. Filimonov, *J. Mol. Struct.* **1973**, *19*(2), 579–589.
176. T.P. Beebe, P. Gelin, J.T. Yates Jr., *Surf. Sci.* **1984**, *148*(2–3), 526–550.
177. W. Hertl, *Langmuir* **1989**, *5*(1), 96–100.
178. P.E. Hintze, H.G. Kjaergaard, V. Vaida, J.B. Burkholder, *J. Phys. Chem. A* **2003**, *107*(8), 1112–1118.
179. B.S. Klose, *In situ–Diffuse–Reflexions–Infrarotspektroskopie an sulfatierten Zirconiumdioxid–Katalysatoren für die n–Butanisomerisierung*, Thesis (Diplomarbeit), TU München, **2001**.
180. G. Herzberg, *Molecular Spectra and Molecular Structure, II. Infrared and Raman Spectra of Polyatomic Molecules*, 11th print, D. van Nostrand, New York et al. **1964**, p. 281.
181. J. Weidlein, U. Müller, K. Dehnicke, *Schwingungsspektroskopie. Eine Einführung*, 2nd ed., Thieme, Stuttgart, New York **1988**, pp. 27, 49, 51, 79, 87, 90.
182. A.A. Davydov, *Kinet. Catal.* **1979**, *20*(6), 1245–1250.
183. C. Markert, *Angew. Chem.* **2005**, *117*(15), 2220–2221.
184. J.G. Creer, P. Jackson, G. Pandey, G.G. Percival, D. Seddon, *Appl. Catal.* **1986**, *22*(1), 85–95.
185. J.M. Serra, A. Chica, A. Corma, *Appl. Catal. A* **2003**, *239*(1–2), 35–42.
186. A. Hagemeyer, B. Jandeleit, Y. Liu, D.M. Poojary, H.W. Turner, A.F. Volpe Jr, W.H. Weinberg, *Appl. Catal. A*, **2001**, *221*(1–2), 23–43.
187. H. Purnama, *Catalytic Study of Copper based Catalysts for Steam Reforming of Methanol*, Thesis (Dissertation), TU Berlin **2003**, pp. 45–47.
188. D.A. Ellis, S.A. Mabury, J.W. Martin, D.C.G. Mui, *Nature* **2001**, *412*(6844), 321–324.
189. S. Guan, L. Vanerden, R.C. Haushalter, X.P. Ziiou, J.X. Wang, R. Srinivasan, *WO9964160*, **1999**.
190. A. Keshavaraja, A.V. Ramaswamy, *Appl. Catal. B* **1996**, *8*(1), L1–L7.
191. E. Fernández López, V. Sánchez Escribano, C. Resini, J.M. Gallardo–Amores, G. Busca, *Appl. Catal. B* **2001**, *29*(4), 251–261.
192. J.E. Bailey, D. Lewis, Z.M. Librant, L.J. Porter, *Trans. J. Brit. Ceram. Soc.* **1972**, *71*(1), 25–30.
193. P.N. Kuznetsov, L.I. Kuznetsova, A.M. Zhyzhaev, G.L. Pashkov, V.V. Boldyrev, *Appl. Catal. A* **2002**, *227*(1–2), 299–307.
194. P.A. Agron, E.L. Fuller Jr., H.F. Holmes, *J. Colloid Interf. Sci.* **1975**, *52*(3), 553–561.

195. T. Ressler, S.L. Brock, J. Wong, S.L. Suib, *J. Phys. Chem. B* **1999**, *103*(31), 6407–6420.
196. B.S. Klose, F.C. Jentoft, R. Schlögl, *J. Catal.* **2005**, *233*(1), 68–80.
197. R. Srinivasan, D. Taulbee, B.H. Davis, *Catal. Lett.* **1991**, *9*(1–2), 1–7.
198. B.S. Klose, R.E. Jentoft, A. Hahn, T. Ressler, J. Kröhnert, S. Wrabetz, X. Yang, F.C. Jentoft, *J. Catal.* **2003**, *217*(2), 487–490.
199. E.D. Whitney, *Trans. Faraday Soc.* **1965**, *61*(65), 1991–2000.
200. M. Thiede, J. Melsheimer, *Rev. Sci. Instrum.* **2002**, *73*(2), 394–397.
201. R. Ahmad, *n-Butane and n-Pentane Isomerization over Sulfated Zirconia Catalysts Investigated by In Situ UV-vis-near-IR Diffuse Reflectance Spectroscopy*, Mensch & Buch Verlag, Berlin **2003**, p. 115.
202. H. Nishizawa, N. Yamasaky, K. Matsuoka, H. Mitsushio, *J. Am. Ceram. Soc.* **1982**, *65*(7), 343–346.
203. T. Sato, M. Shimada, *J. Am. Ceram. Soc.* **1985**, *68*(6), 356–359.
204. T. Sato, M. Shimada, *Am. Ceram. Soc. Bull.* **1985**, *64*(10), 1382–1384.
205. R.J. Madon, X. Liu, M. Sanchez–Castillo, J.A. Dumesic, talk at conference: *18th North American Catalysis Society Meeting*, June 1–6, **2003**, Cancun/Mexico, p. 17.
206. M.R. González, J.M. Kobe, K.B. Fogash, J.A. Dumesic, *J. Catal.* **1996**, *160*(2), 290–298.
207. S.X. Song, R.A. Kydd, *J. Chem. Soc., Faraday Trans.* **1998**, *94*(9), 1333–1338.
208. V. Bolis, C. Morterra, B. Fubini, P. Ugliengo, E. Garrone, *Langmuir* **1993**, *9*(6), 1521–1528.
209. Z.T. Feng, W.S. Postula, C. Erkey, C.V. Philip, A. Akgerman, R.G. Anthony, *J. Catal.* **1994**, *148*(1), 84–90.
210. F. Pinna, M. Signoreto, G. Strukul, G. Cerrato, C. Morterra, *Catal. Lett.* **1994**, *26*(3–4), 339–344.
211. E. Guglielminotti, *J. Phys. Chem.* **1994**, *98*(18), 4884–4891.
212. L.M. Kustov, V.Yu. Borovkov, V.B. Kazanskii, *Kinet. Catal.* **1984**, *25*(2), 393–398.
213. M. Sigl, S. Ernst, J. Weitkamp, H. Knözinger, *Catal. Lett.* **1997**, *45*(1–2), 27–33.
214. A.I. Serykh, V.B. Kazansky, *Phys. Chem. Chem. Phys.* **2004**, *6*(22), 5250–5255.
215. S. Bordiga, E. Garrone, C. Lamberti, A. Zecchina, C.O. Areán, V.B. Kazansky, L.M. Kustov, *J. Chem. Soc., Faraday Trans.* **1994**, *90*(21), 3367–3372.
216. X. Li, K. Nagaoka, L.J. Simon, J.A. Lercher, S. Wrabetz, F.C. Jentoft, C. Breitkopf, S. Matysik, H. Papp, *J. Catal.* **2005**, *230*(1), 214–225.

217. G. Herzberg, *Molecular Spectra and Molecular Structure: I. Spectra of Diatomic Molecules*, 2nd ed., Van Nostrand Reinhold, New York et al. **1950**, p. 123.
218. J. Kondo, K. Domen, K.-I. Maruya, T. Onishi, *Chem. Phys. Lett.* **1992**, *188*(5–6), 443–445.
219. V.B. Kazansky, A.I. Serykh, *Phys. Chem. Chem. Phys.* **2004**, *6*(13), 3760–3764.
220. X. Wang, L. Andrews, *J. Phys. Chem. A* **2003**, *107*(20), 4081–4091.
221. W.F. Edgell, G. Asato, W. Wilson, C. Angell, *J. Am. Chem. Soc.* **1959**, *81*(8), 2022–2023.
222. A.J. Hart–Davis, W.A.G. Graham, *J. Am. Chem. Soc.* **1971**, *93*(18), 4388–4393.
223. A.J. Tursi, E.R. Nixon, *J. Chem. Phys.* **1970**, *52*(3), 1521–1528.
224. D.A. Estrin, L. Paglieri, G. Corongiu, E. Clementi, *J. Phys. Chem.* **1996**, *100*(21), 8701–8711.
225. J. Kondo, Y. Sakata, K. Domen, K.-I. Maruya, T. Onishi, *J. Chem. Soc., Faraday Trans.* **1990**, *86*(2), 397–401.
226. D. Eder, R. Kramer, *Phys. Chem. Chem. Phys.* **2002**, *4*(5), 795–801.
227. M. Risch, E.E. Wolf, *Catal. Today* **2000**, *62*(2–3), 255–268.
228. I.V. Bobricheva, I.A. Stavitsky, V.K. Yermolaev, N.S. Kotsarenko, V.P. Shmachkova, D.I. Kochubey, *Catal. Lett.* **1998**, *56*(1), 23–27.
229. M.R. González, K.B. Fogash, J.M. Kobe, J.A. Dumesic, *Catal. Today* **1997**, *33*(1–3), 303–312.
230. R. Ahmad, J. Melsheimer, F.C. Jentoft, R. Schlögl, *J. Catal.* **2003**, *218*(2), 365–374.
231. R.A. Keogh, R. Srinivasan, B.H. Davis, *J. Catal.* **1995**, *151*(2), 292–299.
232. J.M. Kobe, M.R. González, K.B. Fogash, J.A. Dumesic, *J. Catal.* **1996**, *164*(2), 459–466.
233. K.M. Neyman, P. Strodel, S.P. Ruzankin, N. Schlensog, H. Knözinger, N. Rösch, *Catal. Lett.* **1995**, *31*(2–3), 273–285.
234. A. Patel, G. Coudurier, N. Essayem, J.C. Védrine, *J. Chem. Soc., Faraday Trans.* **1997**, *93*(2), 347–353.
235. V.B. Kazansky, V.Yu. Borovkov, H.G. Karge, *J. Chem. Soc., Faraday Trans.* **1997**, *93*(9), 1843–1848.

Curriculum Vitae

Personal Data

Name:	Barbara Susanne Klose
Date of birth:	June 21, 1977
Place of birth:	Munich, Germany
Parents:	Dr. Elfriede M. and Dr. Peter K. Klose
Nationality:	German

Education and Academic Career

since 2002	Dissertation at Fritz-Haber-Institute of the MPG, Berlin, Germany Title of thesis: "Skeletal Isomerization of Butane by Sulfated Zirconia Catalysts – A Branched Field" in inorganic chemistry under supervision of Prof. Dr. Robert Schlögl and Dr. Friederike C. Jentoft
09 – 10/2002 and 05 – 06/2004	Two visits to the Zelinsky Institute of Organic Chemistry in Moscow, Russia, for low temperature IR experiments in the group of Prof. Dr. Vladimir B. Kazansky
1996 – 2001	Study of chemistry at Technical University Munich (TUM) Diploma in chemistry ("Diplom-Chemikerin") in Dec. 2001; grade: 1.7* Diploma thesis entitled (in German) " <i>In situ</i> DRIFT spectroscopy on sulfated zirconia catalysts for <i>n</i> -butane isomerization" under supervision of Prof. Dr. Klaus Köhler (TUM) and Dr. Friederike C. Jentoft (Fritz-Haber-Institute, Berlin): test of DRIFTS cell for <i>in situ</i> IR experiments with on-line GC
04/2000	4-week internship at a chemical plant (SKW Trostberg AG)
1987 – 96	High school: Theresien-Gymnasium in Munich Languages: Latin, English, Ancient Greek, Italian Graduation ("Abitur") in June 1996; grade: 1.4**
08/1993 – 06/1994	10-month visit to the graduating class at Katedralskola in Uppsala, Sweden; grade: 4.3***
1983 – 87	Primary School: Grundschule an der Führichstraße in Munich

* on a scale from 1 (=very good) to 5 (= unsatisfactory)

** on a scale from 1 (=very good) to 6 (= unsatisfactory)

*** on a scale from 5 (=very good) to 1 (= unsatisfactory)

Articles

Structural and Active Site Characterization of Sulfated Zirconia Catalysts for Light Alkane Isomerization

M. Standke, C. Bretkopf, H. Papp, S. Wrabetz, B.S. Klose, X. Yang, R.E. Jentoft, F.C. Jentoft, X. Li, L.J. Simon, J.A. Lercher, in *Proceedings of the DGMK Conference "Chances for Innovative Processes at the Interface between Refining and Petrochemistry"*, G. Emig et al. (eds) DGMK, Hamburg **2002**, pp. 23–30.

In Situ Spectroscopic Study of Isomerization of Light Alkanes over Sulfated Zirconia Catalysts

X. Yang, R. Ahmad, J. Melsheimer, B.S. Klose, F.C. Jentoft, *ibid.*, pp. 217–224.

Mechanical stress induced activity and phase composition changes in sulfated zirconia catalysts

B.S. Klose, R.E. Jentoft, A. Hahn, T. Ressler, J. Kröhnert, S. Wrabetz, X. Yang, F.C. Jentoft, *J. Catal.* **2003**, *217*(2), 487–490.

Deactivation and Regeneration of Mn-Promoted Sulfated Zirconia Alkane Isomerization Catalysts: An In-Situ Spectroscopic Study

B.S. Klose, R.E. Jentoft, T. Ressler, P. Joshi, A. Trunschke, R. Schlögl, F.C. Jentoft, in *Proceedings of the DGMK Conference "C₄/C₅-Hydrocarbons: Routes to higher value-added products"*, S. Ernst et al. (eds), DGMK, Hamburg **2004**, pp. 23–30.

In situ diffuse reflectance IR spectroscopic investigation of promoted sulfated zirconia catalysts during n-butane isomerization

B.S. Klose, F.C. Jentoft, R. Schlögl, *J. Catal.* **2005**, *233*(1), 68–80.

Effect of Mn and Fe on the reactivity of sulfated zirconia towards H₂ and n-butane: A diffuse reflectance IR spectroscopic investigation

B.S. Klose, F.C. Jentoft, R. Schlögl, I.R. Subbotina, V.B. Kazansky, *Langmuir* **2005**, *21*(23), 10564–10572.

In Situ Spectroscopic Investigation of Activation, Start-Up & Deactivation of Promoted Sulfated Zirconia Catalysts

B.S. Klose, F.C. Jentoft, P. Joshi, A. Trunschke, R. Schlögl, I.R. Subbotina, V.B. Kazansky, *Catal. Today*, submitted.

Oral Conference Contributions

(speaker underlined)

Änderung von Aktivität & Phasenzusammensetzung beim Mahlen und Pressen von ZrO₂-Katalysatoren

B.S. Klose, A. Hahn, R.E. Jentoft, T. Ressler, F.C. Jentoft, R. Schlögl, *102. Hauptversammlung der Deutschen Bunsen-Gesellschaft für Physikalische Chemie*, May 29–31, **2003**, Kiel/Germany.

Role of Bulk Phase in Sulfated Zirconia Catalysts

F.C. Jentoft, B.S. Klose, A.H.P. Hahn, R.E. Jentoft, T. Ressler, R. Ahmad, J. Melsheimer, X. Yang, R. Schlögl, *North American Catalysis Society Meeting*, June 01–06, **2003**, Cancun/Mexico.

Deactivation and Regeneration of Mn-Promoted Sulfated Zirconia Alkane Isomerization Catalysts: An In-Situ Spectroscopic Study

B.S. Klose, R.E. Jentoft, T. Ressler, P. Joshi, A. Trunschke, R. Schlögl, F.C. Jentoft, *DGMK Conference*, October 13–15, **2004**, Munich/Germany.

In Situ Spectroscopic Analysis of Role of Manganese in Promoted Sulfated Zirconia for Initiation of Butane Isomerization

F.C. Jentoft, P. Joshi, B.S. Klose, R.E. Jentoft, T. Ressler, A. Trunschke, R. Schlögl, *XXXVIII. Jahrestreffen Deutscher Katalytiker*, March 16–18, **2005**, Weimar/Germany.

In Situ Diffuse Reflectance IR Spectroscopic Investigation of n-Butane Isomerization on Promoted Sulfated Zirconia Catalysts

B.S. Klose, F.C. Jentoft, R. Schlögl, *5th International Symposium On Acid Base Catalysis*, June 27 – July 01, **2005**, Puerto Vallarta/Mexico.

Posters

In situ-DRIFT-Spektroskopie an sulfatierten ZrO₂-Katalysatoren

B.S. Klose, F.C. Jentoft, XXXV. Jahrestreffen Deutscher Katalytiker, March 20–22, 2002, Weimar/Germany.

In Situ Spectroscopic Study of Isomerization of Light Alkanes over Sulfated Zirconia Catalysts

X. Yang, R. Ahmad, J. Melsheimer, B.S. Klose, F.C. Jentoft, DGMK Conference “Chances for Innovative Processes at the Interface between Refining and Petrochemistry”, October 09–11, 2002, Berlin/Germany.

Investigating Zirconia Catalysts = Handling Sensitive Materials

B.S. Klose, R.E. Jentoft, A. Hahn, T. Ressler, X. Yang, F.C. Jentoft, XXXVI. Jahrestreffen Deutscher Katalytiker, March 19–21, 2003, Weimar/Germany.

Active Site Characterization of Sulfated Zirconia Catalysts for n-Butane Isomerization

C. Breitkopf, H. Papp, S. Wrabetz, X. Yang, B.S. Klose, F.C. Jentoft, X. Li, J.A. Lercher, XXXVI. Jahrestreffen Deutscher Katalytiker, March 19–21, 2003, Weimar/Germany.

Effect of Mn Promoter on Sulfated ZrO₂ Studied by IR Spectroscopy

B.S. Klose, F.C. Jentoft, R. Schlögl, I. Subbotina, V.B. Kazansky, EuropaCat-VI, August 31 – September 04, 2003, Innsbruck/Austria.

Bulk Structural Characteristics of Sulfated Zirconia Catalysts

R.E. Jentoft, A.H.P. Hahn, B.S. Klose, F.C. Jentoft, T. Ressler, Thorsten, EuropaCat-VI, August 31 – September 04, 2003, Innsbruck/Austria.

Design of an Enhanced Throughput Catalytic Test System Capable of Rapid Heating and Cooling

B.S. Klose, F.C. Jentoft, R.E. Jentoft, B. Kubias, M. Swoboda, R. Schlögl, XXXVII. Jahrestreffen Deutscher Katalytiker, March 17–19, 2004, Weimar/Germany.

In Situ DRIFT and UV-vis Spectroscopic Investigation of Mn-Promoted Sulfated Zirconia during Alkane Isomerization

F.C. Jentoft, B.S. Klose, A. Trunschke, R. Schlögl, 3rd International Taylor Conference, September 05–08, 2004, Belfast/Northern Ireland.

Interaction between Promoters Mn/Fe, Sulfate, and Zirconia in Accordingly Composed Alkane Isomerization Catalysts

F.C. Jentoft, A. Hahn, U. Wild, B.S. Klose, R.E. Jentoft, T. Ressler, R. Schlögl, C. Häfner, K. Köhler, 13th International Congress on Catalysis, July 11–16, 2004, Paris/France.

Dynamic Phenomena on the Surface of Sulfated Zirconia: Understanding IR-Spectra with the Help of DFT Calculations

B.S. Klose, F.C. Jentoft, R. Schlögl, A. Hofmann, J. Sauer, XXXVIII. Jahrestreffen Deutscher Katalytiker, March 16–18, 2005, Weimar/Germany.

Initiation of Alkane Isomerization on Sulfated Zirconia Catalysts Studied by In Situ X-ray Absorption, UV-vis and IR Spectroscopy

F.C. Jentoft, B.S. Klose, R.E. Jentoft, T. Ressler, P. Joshi, C. Chan Thaw, A. Trunschke, R. Schlögl, 19th North American Catalysis Society Meeting, May 22–27, 2005, Philadelphia/USA.

Influence of Storage Atmosphere on Properties and Performance of Sulfated Zirconia Isomerization Catalysts

B.S. Klose, F.C. Jentoft, R. Schlögl, EuropaCat-VII, August 28 – September 01, 2005, Sofia/Bulgaria.